UNIVERSITY OF BIRMINGHAM

Sonoelectrochemical Production of Hydrogen via Alkaline Water Electrolysis

By

Salman Hassan Zadeh

Thesis prepared for the degree of Masters of Research in
Hydrogen, Fuel cells and Their Applications

Department of Chemical Engineering
School of Engineering and Physical Sciences
University Of Birmingham

July 2012

Acknowledgement

Praise belongs to the creator and the foremost is the acknowledgement of him.
I would like to start by thanking my supervisors Dr. Bushra Al-Duri and Dr. Bruno Pollet for their supervision and advice during this project.

I wish to offer my appreciation and gratitude to my family especially my father for their help and support throughout this project without which the completion of this work wouldn't have been possible.

Finally it's a pleasure for me to thank Professor Mahmoud Salari and Dr. Sarah Horswell for their guidance during this program, I am also grateful to Prof. Fryer, Prof. Kevin Kendall, Daniel Symes, Gaurav Gupta, Oliver Curnick, Dr. Surbhi Sharma, friends and fellow researchers at Hydrogen and Fuel Cell Research facility at the University of Birmingham for their help in the course of this task.

Table of Contents:

Table of Figures

Table of Tables

CDROM Contents

Abstract

Alkaline water electrolysis is a promising technology to produce clean and pure hydrogen. This technology coupled with the ultrasound results in an enhanced rate of hydrogen production. The recent technologies in the area of electrolysis are the application of solar energy using photovoltaic cells to supply electricity, steam electrolysis, PEM electrolysis, the application of magnetic field and high temperature solid oxide electrolysis cell. The literature studies indicate an improved mass transfer and 10%-25% energy saving using the ultrasound.

This work continues the previous research done in this area by investigating the effect of the ultrasound on a conventional water electrolysis cell along with other parameters subject of alteration such as electrode active surface area, concentration and temperature. The hydrogen production was measured using a digital hydrogen flowmeter; the average production efficiency and energy efficiency of the electrolysis cell were 72% and 14.5% respectively. It was calculated that the ultrasound increased the production efficiency by 6% and energy efficiency by 1.3%. The act of the ultrasound resulted in bubble removal from the surface of the electrode and the solution therefore prepared the electrode surface for the electrochemical reactions thus enhanced the hydrogen generation.

The current generation was enhanced by about 70% when the electrode active surface area was increased by about 45%, the hydrogen production rate however was not improved in an orderly fashion as a result of this increase in the electrode surface area. This increase is resulted from a larger electrode surface area available for the reaction, which refers to more active sites. The lowest ohmic resistance in our cell was obtained at 15M experiment, which was about 1.5 Ω at 3.3V applied potential. This was slightly higher than 0.8 Ω mentioned for a very recent work carried out in an advanced alkaline electrolysis cell, which benefited from a hydrophilic separator between the electrodes using a 28% KOH electrolyte solution. The average low ohmic resistance in our study for low concentration experiments (0.1M) was about 14Ω at 30V.

Chapter 1: Introduction

1.1. Introduction

With ever-increasing global demand concerning fossil fuels and the significant consequences of their use, the quest for clean and sustainable energy resources is essential while the highest demand still belongs to the oil, natural gas and coal according to Shell and BP [1] [2].

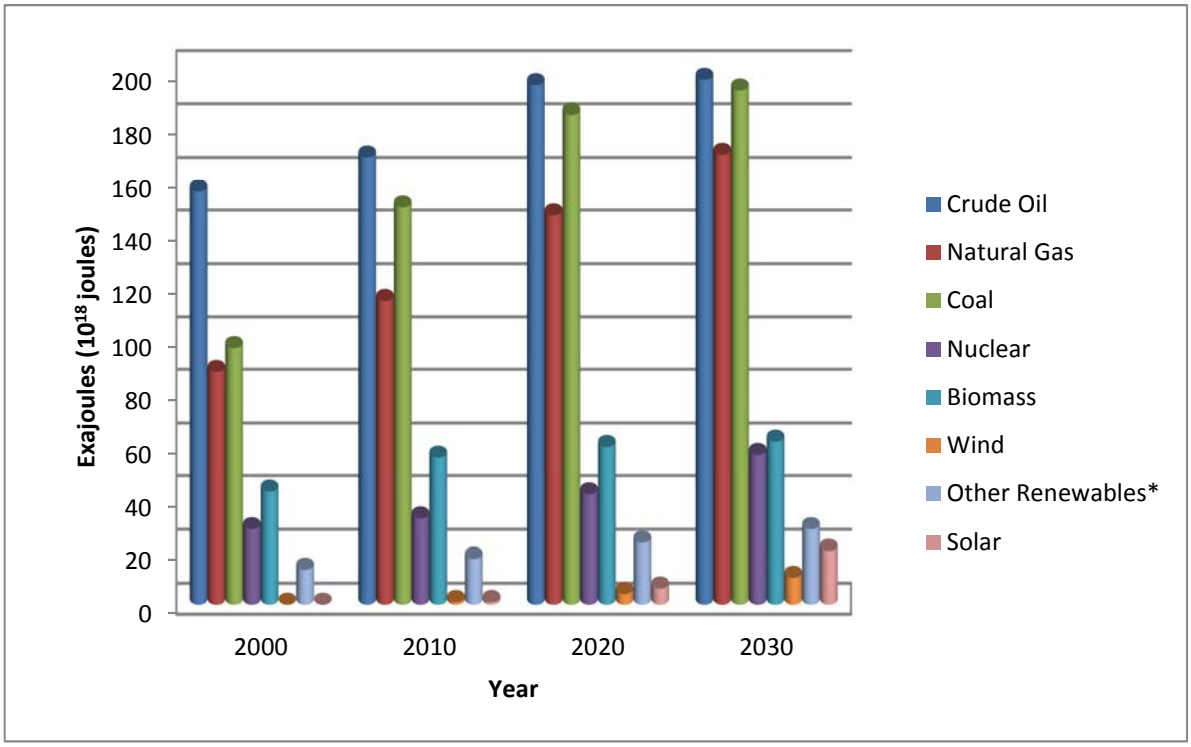

Figure 1: World primary energy demand, data obtained from Shell. *Other Renewables includes tidal, geothermal, hydroelectric and waste [1].

In the figure 1 above it is shown that crude oil, natural gas and coal have the highest values of energy demanded per year decade by decade whilst renewables grow each year in demand but still very low compared to the fossil fuel based resources.

The Hydrogen when introduced as a fuel could be used as a source of energy in variety of applications from fuel cells, rockets and space industry to domestic applications such as pumping and heating. The majority of hydrogen currently comes from steam reforming of natural gas and partial oxidation of hydrocarbons as other technologies are less cost effective and efficient (see more in 2.1.3).

Hydrogen as a fuel could be a sustainable solution to the world energy crisis if produced through a renewable based technology. The majority of hydrogen production technologies including coal gasification,

biomass processing and else are not either sustainable or do they produce hydrogen in the amount required [3]. This leaves us with any technology through which the electricity is produced from renewables, which can then power an electrolyser to produce hydrogen. Solar and wind technology due to their great potential could help supply the future hydrogen production sustainable and renewable [4] [5].

The water electrolysis, as a technology to generate hydrogen, is responsible for about 4-5% of hydrogen production in the world and this practise in the presence of ultrasound has gained the interest of researchers and good deal of attention has been paid towards the method since the introduction of ultrasound improves the mass transfer and energy transfer consequently the rate of hydrogen production [6].
The recent technologies in field of water electrolysis include photo-electrolysis or photovoltaic (PV) electrolysis, high temperature and pressure electrolysis, steam electrolysis, bio-catalysed electrolysis and the application of sonobioreactor to produce hydrogen from organic electrolyte [6].

The early studies related to gas generation involving electrolysis and the ultrasound (sonoelectrochemisty) were performed during 1930-1940 where the effect of 280 kHz or 1200 kHz ultrasonic field on the deposition potential of hydrogen or chlorine was investigated [7] [8]. In 1992 Franco Cataldo et al [9] were among the first to electrolyse the aqueous solution of NaCl or HCl applying 30 kHz ultrasonic field and compared the results to the silent conditions. The main observation was a very strong degassing effect of ultrasonic waves and enhanced coalescence of gas bubbles hence an increase in the production of chlorine gas under sonication [9]. There have been numerous experiments with different cell configurations, various electrodes and electrolytes as of the primary works in the sonoelectrochemistry among which the immersion of ultrasonic tip and electrodes are the most broadly used configuration.

The use of bioreactor has also been mentioned as one of the promising techniques in the literature with a maximum increase in the hydrogen production of up to 118% when methane was used as sparge gas compared to the experiment without sparging. The ultra-sonication is reported to have caused localised pressure drop and formation of cavitation bubbles [10].
In a recent work, advanced alkaline water electrolysis has been practised using gas diffusion electrodes, a hydrophilic separator (Celgard or ZrO_2) and 28% KOH electrolyte solution. The authors reported a better performance in comparison to PEM electrolyser, low resistance (0.8 ohm cm^2) and lower capital cost using nickel based catalyst with catalyst cost of 10$/kW [11].

This research project was done with an emphasis to investigate the effect of ultrasound on the generation of hydrogen production, albeit other parameters were altered such as electrode surface area, temperature and concentration of the electrolyte and material of electrodes and electrolytes. The results under the ultrasonic field were then compared to that of silent conditions for further analysis.

1.2. Aims and objectives

The aim of this research was to evaluate the success of producing hydrogen with and without an ultrasonic field and also explicate the influence of ultrasound on the generation of hydrogen. In this study the effects of other parameters on the hydrogen production were considered among which, the electrode active surface area was an important one. Other factors include electrolyte concentration, temperature and also electrode configuration.

The main objective of this research project is to provide the academic grounds validating the hydrogen production via alkaline water electrolysis under silent and sonicated conditions and quantifying the amount of hydrogen produced.

The specific objectives of this work are as follow:

- To study the effect of ultrasound on the production of hydrogen and compare the results with silent conditions.
- To examine the influence of electrode active surface area on the current and hydrogen generation.
- To see the effect of concentration and temperature on hydrogen production
- To find the hydrogen production efficiency and energy efficiency for the electrolytic cell

Chapter 2: Background and Literature Review

2.1 Hydrogen

2.1.1. Overview

The word hydrogen contains two parts; hydro meaning water in Greek and genes is translated as forming. Hydrogen is an element with the atomic number 1 and atomic weight of 1.00794. Cavendish in 1776 prepared hydrogen but at the time it was still not recognised until it was named by Lavoisier.
Hydrogen on earth can mainly be found in arrangement with oxygen in water however it is also available in organic materials such as coal, petroleum and living plants. Hydrogen exists as a free element in atmosphere in such a low degree that the value is less than 1 ppm by the volume. It is known as the lightest among all gases and is widely used to produce methanol, other applications are hydrocracking, hydrodealkylation, hydrodesulfurization, production of hydrochloric acid, welding purposes, rocket fuel, reduction of metallic ores, filling balloons and more. In the US, production of hydrogen is said to equal an amount of 3 billion cubic feet per year [12] however this amount is reported by the US department of energy in 2006 to be around 9 million tons per annum [13], globally though, the annual production of hydrogen in 2004 reached some 50 million tons with a 10%-increase year by year. The economic value of hydrogen produced per year in the globe was around $135 billion as of 2005 [14].

Hydrogen can be prepared by the following methods; decomposition of certain hydrocarbons using heat treatment, action of steam on heated carbon, electrolysis of water, displacement from acid using specified metals, action of potassium or sodium on aluminium and other techniques [12].

Hydrogen consists of three isotopes named as protium, deuterium and tritium; deuterium was discovered by Urey in 1932 which, has an atomic weight of 2 and present in natural hydrogen as low as 0.015%.
Clean hydrogen could be employed as a reducing agent in chemical processes, refinery, metallurgy and also used as a good replacement for natural gas, gasoline and etc. Hydrogen as a fuel has a few barriers on its way towards the establishment of hydrogen economy such as high costs in comparison to other fuels, high capital investment and also public approval [12]. On the other hand, the renewable-based techniques of hydrogen production such as solar photovoltaic electrolysis of water and photo-electrochemical decomposition of water would not be capable to reduce the cost of hydrogen production appreciably as they themselves are expensive processes while fossil fuels benefits from factors including availability, low costs, easy transport and storage [15].

It can be seen in figure 2 below; the hydrogen energy path from primary resources of energy to hydrogen energy itself where its distribution, storage and end use are depicted; this could be a good representative path for a sustainable hydrogen economy.

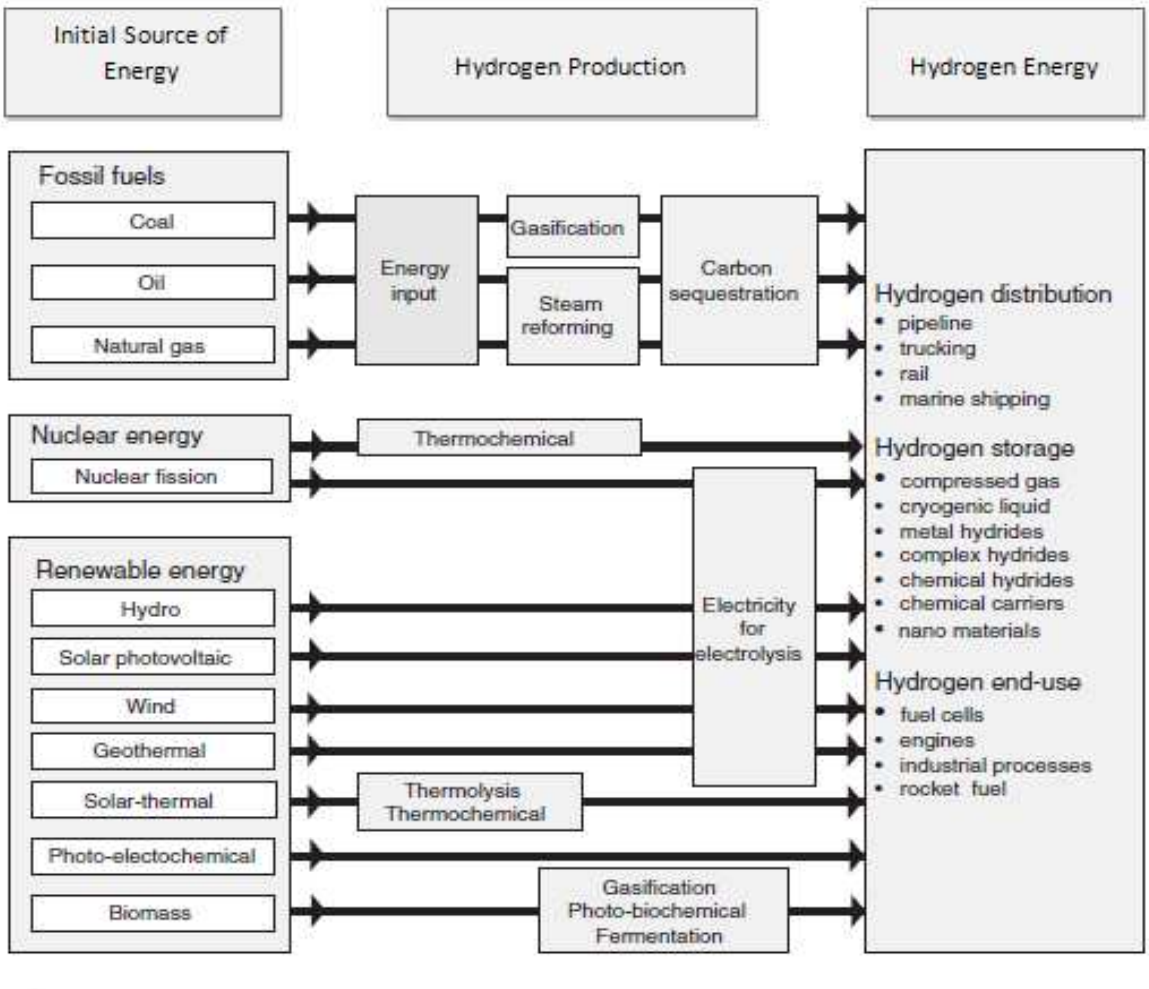

Figure 2 [16]**:** Primary Resources of energy to Hydrogen.

2.1.2. Hydrogen as a fuel

Hydrogen as a fuel is a top quality energy carrier (calorific value: 141,790 Kj/Kg) which, has the advantages of extremely low emissions and high efficiency. Hydrogen fuel can be used for a variety of application as briefly mentioned in the previous section and also for power generation, transportation and heating as well as a fuel replacement. Hydrogen as a fuel owns properties including flammability over extensive range of concentrations and temperatures plus considerable combustion efficiency, even though this combustibility is a useful property for a fuel, it yet raises some technical obstacles for production, storage and transportation

of hydrogen such as safety issues. Hydrogen liberates energy in an explosive manner when mixed with oxygen giving pure water as by-product [14]. In figure 3 the use of hydrogen energy in diverse areas is shown.

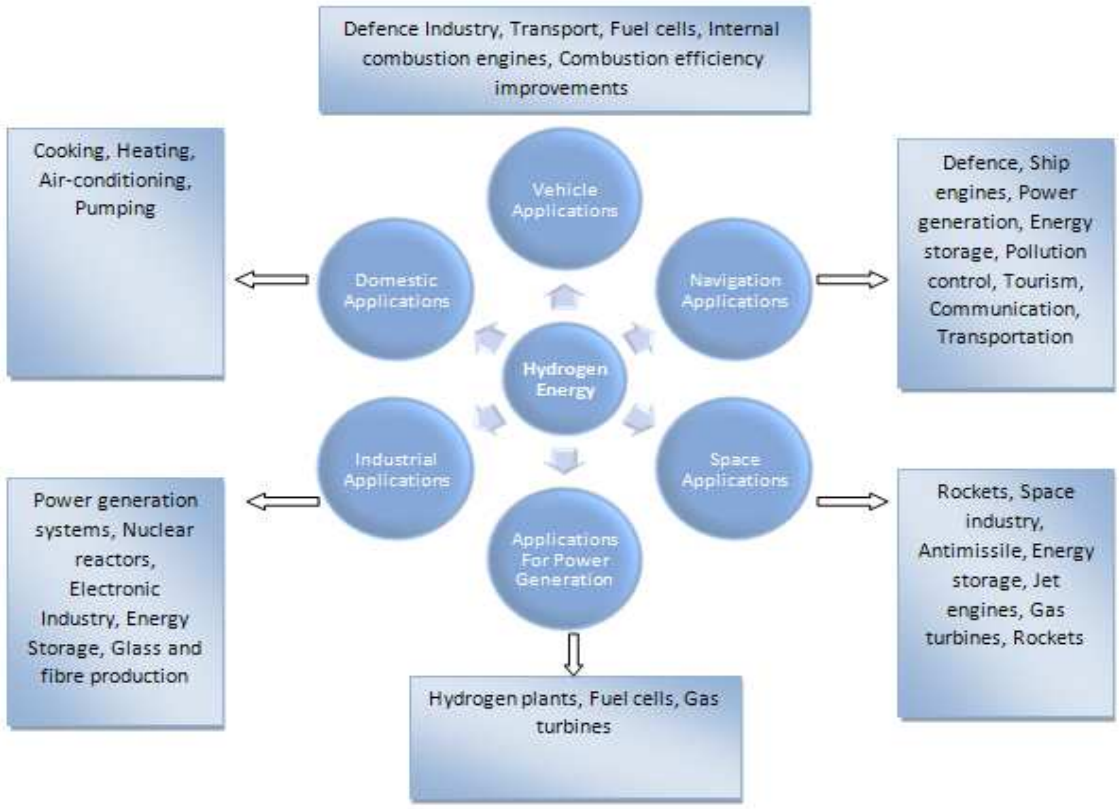

Figure 3 [14]**:** Hydrogen Energy applicable areas.

2.1.2.1. Energy content

Hydrogen benefits from the highest energy content per unit mass of any fuel while suffers from low volumetric density, which creates the storage problem specifically for on-board storage tanks used in vehicles. Hydrogen on a weight basis has almost triple the amount of the energy content of gasoline (140.40 MJ/kg Vs. 48.6 MJ/kg) whilst on a volume basis the ratio is different (8491 MJ/m^3 for liquid hydrogen Vs. 31150 MJ/m^3 for gasoline) [14].

Hydrogen due to its electrochemical property can be used in a fuel cell, for instance in H_2/O_2 cells with 50%-60% efficiency and lifetime of nearly 3000-5000 hours for light-duty vehicles [17], the current output could give a range of 440-1720A/m^2 of the electrode surface. This could yield a power output within the range of 50 to 2500 W for different fuel cells [14](See more in section 2.2 on fuel cells).

2.1.3. Hydrogen Production

There is a wide range of technologies available to produce hydrogen from which some are preferred due to factors such as cost, environmental issues, sustainability and etc.
The US department of energy categorised current technologies into three sections including thermal processes, electrolytic processes and photovoltaic processes [18].

The majority of hydrogen produced in the world comes from the natural gas using steam-reforming technology, as for the rest, partial oxidation process of oil and coal is responsible for it. From 45-50 Mt of hydrogen produced in the world per year about 20% belongs to the USA however this requires an increase by 2040 to 65 Mt for the USA only, The US Department of Energy reported. US alone by 2040 will have 300 million light-duty vehicles, which require hydrogen if powered by fuel cells. In order to cope with such an enormous increase from 9-10 Mt at present to 65 Mt in 2040, the construction of about 700 large steam-reformer plants is required where each plant in average can produce 0.1 Mt of hydrogen annually. This may push fossil fuel industry to the limits (as the majority of hydrogen currently comes from natural gas and coal); also the establishment and engagement of a new energy industry based on renewable may be needed, which is a difficult task per se.
Currently about 4-5% of hydrogen is produced via electrolysis globally, the reason to such a low figure is the high cost of this process especially on industrial scale. Electrolysis is used for hydrogen production in large scale when it is either economically justified or hydrogen is a by-product of another process such as Chlor-Alkali manufacturing process for the production of chlorine and caustic soda [19]. Industrial water electrolysers are designed to produce 244,440 $\mathrm{Nm}^3/\mathrm{year}$(Normal cubic metre) with an energy efficiency of 61% [6].

Some of the hydrogen production technologies are listed below [19]:

- Reforming of Natural Gas
- Partial Oxidation of Hydrocarbons
- Plasma, Sorbet-Enhanced and Autothermal Reforming
- Gasification Technology including Fluidised-Bed, Moving-Bed and Entrained-flow Gasifiers
- Water Electrolysis
- Combined Cycle Processes
- Biomass processing
- Thermo-Chemical Hydrogen Production

2.1.3.1. Reforming of Natural gas

In this technique steam is used to reform natural gas in order to produce hydrogen in industry. The chemical equation is as follows:

$$CH_4 + H_2O(gas) \rightarrow CO + 3H_2 \quad (1)$$

In the above process (equation 1) methane reacts with steam in the presence of a nickel-based catalyst at 900°C and elevated pressures. The mixture gas $(CO + 3H_2)$ is known as synthesis gas or syngas. The steam reaction absorbs heat making it endothermic, which requires a large amount of heat, that is to say 252 KJ per mole of methane under STP conditions ; temperature of 298.15K and pressure of 101.325kPa.
This reaction may be carried out in autothermal reformer or allothermal reformer, which refers to the heat supplied as either external or internal respectively by inserting oxygen or air to the reaction mixture.
An alternative method to produce hydrogen could be partial oxidation where oxygen or air is added to the gaseous mixture hence some of methane exothermically and internally is oxidised [20]:

$$2CH_4 + O_2 \rightarrow 2CO + 4H_2 \quad (2)$$

Solar-thermal reforming is another kind of reforming, researches have been carried out to see if it is possible to provide the required heat for the steam reforming of natural gas, landfill and coal-bed methane using solar energy. Solar-thermal reforming while benefiting from reduced CO_2 emissions and high thermal efficiency, also offers a syngas contained with nearly 25% solar energy. The only drawback to this method is that this cannot be functional at nights unless the conventional steam reforming is used combined with the solar technology [20].

2.1.3.2. Partial Oxidation of Hydrocarbons

The process of oxidation is an alternative to reforming of natural gas. This process also applies to the gasification of coal and an extensive range of liquid hydrocarbons. The process can be termed as the general reaction below:

$$2C_mH_n + mO_2 \rightarrow 2mCO + nH_2 \quad (3)$$

The partial oxidation technique has a weakness in comparison to the steam reforming and that is the amount of hydrogen molecules produced per molecule of methane, which is 2 molecules as opposed to three produced in steam reforming before water gas shift reaction. In this technique, feedstock such as light hydrocarbons are used for catalytic process at 600-900°C and non-catalytic process includes heavy residual oils and coal as feedstock with temperature range of 1100-1500°C [21].

2.1.3.3. Plasma, Sorbent-Enhanced and Autothermal Reforming

Plasma reforming is a technique developed to produce hydrogen through direct thermolysis or thermocatalytic cracking of methane or other hydrocarbons. Thermal plasma technology is operated at temperatures between 3000-10000°C while thermocatalytic cracking is carried out at considerably lower temperature than direct thermolysis. The by-product of both processes is soot, that is easier to capture and also the energy needed per mole of methane is less than steam reforming process however plasma reforming is a massive consumer of electricity as the plasma is created by an electric arc at the aforementioned elevated temperature ranges. Thermocatalytic decomposition though endures catalyst deactivation when carbon builds up in the process while there is no such problem in direct thermolysis because of high temperature existing in the process, which does not necessitate any catalyst.

Sorbent-enhanced reforming usually yields a product including 90% hydrogen, 10% unreacted methane, small fraction of carbon dioxide and footprints of carbon monoxide, the temperature in this method is reduced to 400-500°C thanks to the combination of methane steam reforming with its consequent shift reaction into a single step and simultaneous decrease in temperature from original 900°C to the reduced value of around 500°C as mentioned above. The lowered temperature in this process allows less expenditure on materials of construction and also as this procedure is a transformed process into a single step; it does not need gas-separation stages. Sorbent-enhanced reforming is still at R&D phase and needs development.

Autothermal reforming is another technology from series of reforming pathways, which is in fact the combination of best properties of partial oxidation and steam reforming processes. The pressure can reach up to 10 MPa and temperature range of 950-1100°C. This method needs no indirect heat exchanger or external heat output and its efficiency can climb up to 80-90% since all of the heat created in the partial oxidation is used to power steam reforming and this efficiency is higher than partial oxidation systems. Partial oxidation and steam reforming reaction are done simultaneously, all this results in more compact, lower-capital cost and easier system [22].

2.1.3.4. Gasification Technology

Gasification technology involves three major designs namely as fluidized bed (The Winkler) gasifier, moving bed (The Lurgi) gasifier, and entrained flow (the GE) gasifier [23]. Gasification is referred to as the conversion of solid materials into combustible gases at temperatures exceeding 700°C when an oxygen carrier is present. The partial combustion of solid or consequential syngas supplies the required energy for thermochemical conversion. Using the gasification technology almost any kind of fossil fuel can be processed to produce hydrogen.

The coal is a typical material used for gasification and its production in the world is expected to rise to 3779 Mtoe by 2030, most of which will be used for electricity generation [24]. Below in figure 4, there is a schematic diagram of the gasification processes where different types including entrained flow gasifier can be seen in which the most aggressive type of gasification occurs. The oxidizing gas and pulverized coal flow in the same direction in this process where the operating temperature is greater than 1400°C and pressures of up to 2-3 MPa is observed [24]. The produced syngas could be further processed in order to obtain hydrogen gas.

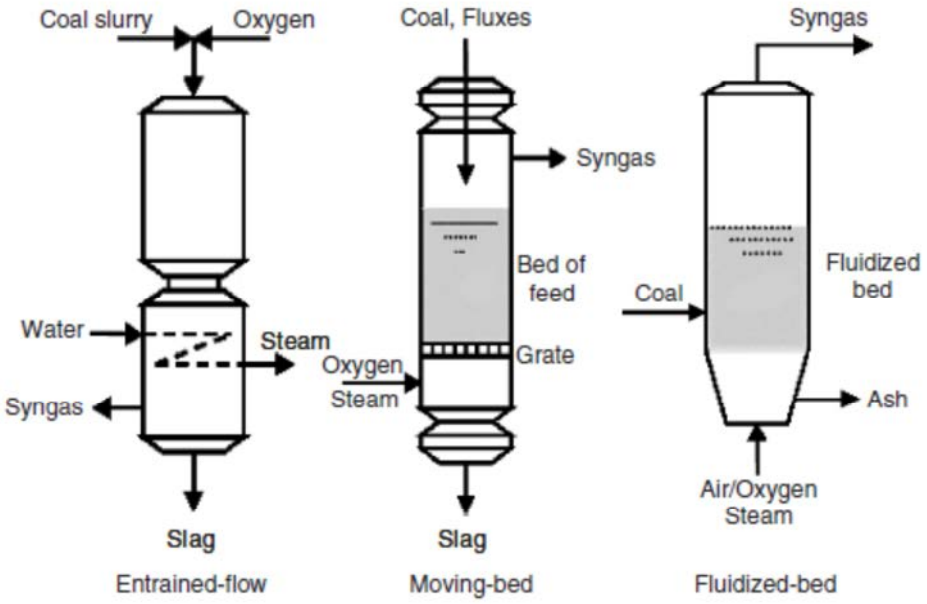

Figure 4 [24]: The gasifier designs.

In figure 4 the moving bed gasifier shown bears a resemblance to a blast furnace. The pressure in this gasifier reaches to about 3MPa while the temperature at top of the bed is usually 450°C and at the bottom nearly 2000°C. The residence time in moving-bed gasifier is between 30 minutes to 1 hour.
The fluidized bed gasifier is operated in such a way that keeps the solid particles suspended in upward position using an upward-flow gas. The suspended coal particles in this method react with risen oxygen-enriched gas at 950-1100°C and 2-3 MPa of pressure. There is homogeneous temperature distribution throughout the gasifier, which is resulted from high grades of back-mixing. The rate of heat and mass transfer between solid and gas in this system is high [24].

2.1.3.5. Hydrogen from water

In section 2.3 and 2.6, electrolysis and its applications are explained thoroughly, in this section various technologies in the realm of hydrogen production from water are introduced.
The first technique is water electrolysis with solar energy, which includes photovoltaic cells, solar-thermal process, photo-biochemical cells and photo-electrochemical cells.
Photo-electrochemical cells themselves consist of three subsections as follows:

- Tandem Cells
- Direct Hydrogen Production
- Dye-Sensitized Solar Cells

The other method is thermochemical hydrogen production, which includes the following [25]:

- Sulfur-Ammonia Cycle
- Sulfur-Iodine Cycle
- Westinghouse Cycle
- Metal Oxide Cycles

Photovoltaic cells are the most commonly used for conversion of solar energy to electricity, high costs of solar cells (photovoltaic cells) make this technology applicable to small scale at present [25] however large scale solar plants are operated currently in different regions such as Mojave Desert in California [26].
In PV technology, the photovoltaic cells are illuminated when the photons strike a PV cell and direct current is generated from the semiconductors. The cells are made of semiconductor materials, which have electrons bonded weakly at an energy level. The energy required to break this bond to let the electrons move freely is provided by photons in the sunlight. This puts the electron at a new energy level known as the conduction band; here electricity can be conducted through the material [27] [28].
Thermolysis is another process in which a substance is decomposed through the application of heat, when this heat is provided directly by sun, the practice is known as thermal-solar process. High temperature of about 3000°K is required to separate water molecules into hydrogen and oxygen through thermal decomposition [29]. In figure 5 water-splitting process using solar energy is schematically shown.

Photo-electrochemical cells are capable of breaking down water molecules using photo-electrochemical reactions occurring in the cell. The electrodes are light-sensitive and direct current of electricity can be produced, which then helps electrolyse water using PV cells [25].

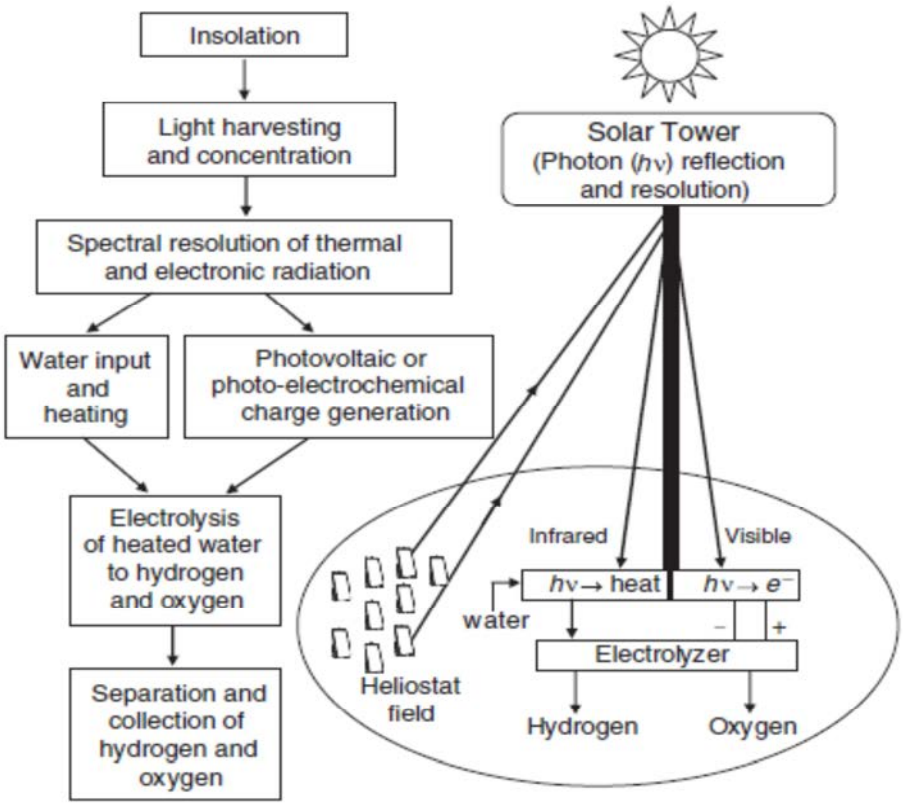

Figure 5 [25]: Enhanced solar-water splitting technology.

2.1.3.6. Combined Cycle Processes (CCP)

CCP technology is classified into two groups namely as Natural Gas Combined Cycle (NGCC) and Integrated Gasification Combined Cycle (IGCC). NGCC employs natural gas as the fuel while IGCC uses syngas or syngas-derived gas. Combined cycle plant burns fuel (liquid or gas) to produce electricity [30].
In a Combined Cycle Gas Generator (CCGG), high-temperature gas turbine is joined to a generator where the gas is burnt. The flue gas (exhaust gas) coming off the turbine is utilized to move up the steam and this steam hence is conveyed to a conventional steam turbine then a generator. Similar procedure is applied in an IGCC plant to generate electricity from coal [24].

2.1.3.7. Hydrogen from Biomass

Hydrogen can be produced from both wet and dry biomass stocks; dry biomass comes in the form of wood chips and straw while wet biomass typically includes silage, liquid manure and sewage. Anaerobic digestion at ambient temperature is used to treat wet biomass, which yields biogas containing methane, carbon

dioxide and monoxide and a small amount of hydrogen. The biogas can be further processed using a biogas scrubber to separate the gases for allocated purposes.
Dry biomass can also be used as feedstock for Combined Heat and Power (CHP) systems [31]. Biomass is mainly converted to hydrogen and other gases through gasification and pyrolysis. The gasification techniques available include supercritical conversion of biomass, direct solar gasification, biomass-derived synthesis gas conversion and etc. [32].

Wet biomass can be supercritically gasified in the presence of $Ni/\gamma Al_2O_3$ and $Ni/CeO_2\text{-}\gamma Al_2O_3$ catalysts to produce hydrogen. Ni-based catalysts serve best by recognising the high gasification efficiency of biomass when water reaches near its critical temperature. This process is carried out in an autoclave reactor at temperature and pressure of 673K and 24.5 MPa respectively with 9.09 wt. % concentration of glucose. Coking and carbon deposition in this method are the main problems, which cause deactivation of catalyst [33]. Supercritical gasification of biomass can also be operated in a fluidised bed reactor at 923K and 30MPa, in this way the problem of reactor plugging could be prevented, the produced gas through this experimental process is H_2, CO, CH_4, CO_2 and traces of C_2H_6, C_2H_4 [34].

2.1.3.8. Thermo-chemical Hydrogen Production

Thermo-chemical water decomposition has been recognised as a promising technology for the future of hydrogen production, which at the moment is an essential industrial service [35]. The idea is to break down water molecules at moderate high temperature of less than 1000°C because water molecules are stable and require elevated temperature to be broken thermally. The water in this method is reacted with one or more chemical substances that are later regenerated using a chain of cyclic thermochemical reactions. Various cycles may be used in thermo-chemical hydrogen production as mentioned in 2.1.3.5 [25].

2.1.3.9. Nuclear Hydrogen Production

Nuclear hydrogen production methods use water as the only feedstock, which means there would be no carbon emission. The efficiency of these processes (nuclear heat to hydrogen product) starts at 25% using available light water reactors rising up to 38% when using more efficient reactors. The application of high temperature reactors coupled with steam electrolysis, thermochemical process or a hybrid process will increase the efficiency up to 45-50%. Chemical reforming could be used along with a nuclear reactor's heat to decrease the use of biomass feedstock or fossil fuel consequently resulting in the reduction of CO_2 emissions. In table 1 below hydrogen production by the use of nuclear reactors is shown including various parameters involved [36].

Table 1 [36]: Nuclear Hydrogen Production; Techniques and parameters.

	Neutron Spectrum	**Typical sizes MWt/MWe**	**Coolant**	**Reactor outlet Coolant Temperature (°C)**	**Method of Electricity Generation**	**Fuel Cycles**	**Hydrogen Production Pathway**
Heavy water Reactor	Thermal	2000-3200 MWt 700-1100 MWe	Heavy Water	310-319	Steam Turbine	Natural UO_2, Low enriched UO_2	Water Electrolysis
Light water reactor	Thermal	2000-4800 MWt 600-1700 MWe	Light Water	280-325	Steam Turbine	UO_2, U-Pu MOX	Water Electrolysis
Supercritical water reactor	Thermal or Fast	1600-2540 MWt 700-1150 MWe	Light Water	430-625	Steam Turbine	UO_2, Th/U, U-Pu MOX	Water Electrolysis, M-T Thermochemical
High Temperature Gas Reactors	Thermal	100-600 MWt 45-300 MWe	Helium	750-950	Steam Turbine, Gas turbine	UO_2, Th/U, U-Pu, MOX, U-TRU, PuO_2	Water Electrolysis, Steam Electrolysis, Thermochemical, Chemical Reforming
Gas-fast Reactors	Fast	600-2400 MWt 280-1100 MWe	Helium	850	Steam Turbine, Gas turbine	U-TRU, U-Pu MOX	Water Electrolysis, Steam Electrolysis, Thermochemical, Chemical Reforming
Liquid metal Fast Reactors	Fast	45-3000 MWt 20-1100 MWe	Sodium, Lead, Lead Bismuth	500-800	Steam Turbine, SCO_2turbine	U-Pu MOX, U-Pu Nitrides, MOX w/TRU	Water Electrolysis, M-T Thermochemical, M-T Methane Reform
Molten Salt Reactors	Thermal	900-2400 MWt 400-1200 MWe	Salts, Li_2BeF_4 $NaF-ZrF_4$ and etc	750-1000	Steam Turbine, SCO_2turbine	Th/U, UO_2	Water Electrolysis, Steam Electrolysis, Thermochemical, Chemical Reforming

2.1.4. Hydrogen Storage and Distribution

2.1.4.1. Hydrogen Storage; a literature survey

Conventionally hydrogen can be stored in the form of compressed gas or alternatively as a cryogenic liquid. Liquefaction and compression of hydrogen gas requires a considerable amount of energy. The storage of hydrogen as a result of low density creates significant financial and technological challenges. Hydrogen can be stored in gaseous form in a vessel with average pressure of 30 MPa, which is the pressure that most gases are kept in a cylinder. Hydrogen however has been recently stored under pressures of 700 bar and higher and this calls for a meticulous look at the material of construction for the vessel. Aluminium alloys and austenitic stainless steel are appropriate choices for hydrogen storage purposes since the hydrogen is prone to adsorb and dissociate at the surface of materials causing embrittlement and diffusion [37].

In 1898 J.Dewar was the first person who liquefied hydrogen. The density of liquefied gases is noticeably greater as opposed to compressed gases thus complicated storage systems are required for liquefied gases as well as special needs for handling, between 20-30% of hydrogen's energy content is used for its liquefaction. Hydrogen during the liquefaction procedure is compressed to around 30 bar then cooled down to 80K using liquid nitrogen [38] [39].
Hydrogen liquefaction by magnetic refrigeration is an example in which ultra-cold temperatures of 1K is achievable with maximum liquefaction power of 25.3 W, this technique makes use of magnetocaloric effect meaning that the temperature of magnetic material goes up by magnetising and down by demagnetising. The magnetic refrigerant used in this method was a ceramic polycrystalline known as dysprosium gadolinium aluminium garnet (DGAG) [40].

Physisorption in porous materials is yet another mechanism to store hydrogen in which hydrogen is accumulated in molecular form. Hydrogen is trapped inside the molecular structure so that it won't dissociate on the surface of solid substance [41]. The examples of materials are microporous adsorbents such as silicon dioxide, zeolites and activated carbon [42].

At present hydrogen storage in solid-state materials has been inspected where a great deal of thoughts is given to the subject. The materials investigated include metallic, complex and destabilized hydrides, doped-carbon based nanostructures and metal organic frameworks [43] [44].

Another method of hydrogen storage is hybrid storage, which requires cooling down pure hydrogen to below its freezing point at -259°C where liquid and solid hydrogen known as slush is obtained benefiting from higher energy density. Supercritical storage of hydrogen in a cryogenic tank is also a technique currently under consideration [38] [39].

In 2003 Nobuhiko Takeichi et al reported the potential of a unique hybrid storage mechanism for hydrogen, merging an aluminium-carbon fiber reinforced plastic (Al‑CFRP) composite vessel and hydrogen storage alloy. The calculations were done for a storage system enabling to store 5kg of hydrogen at pressure of nearly 35 MPa. This storage technique as concluded in their work could be ideal for on-board storage in fuel cell vehicles since using the proposed hybrid vessels, the volume and weight of the storage system can be determined by altering the volume fraction of the hydrogen storage alloy in the vessel [45].

A concept design was also proposed by Indranil Ghosh et al for vehicle applications in which cryosorption storage of hydrogen gas in activated carbon was propounded. The design includes three 0.33m in 1.4m φ stainless steel storages allowing the storage capacity of 3.1 kg with both adsorption and desorption occurring adiabatically. A temperature range of 77K can be reached simply by liquid nitrogen (LN_2) at atmospheric pressure [46].

One of the main technologies to store hydrogen on a commercial level is high pressure gaseous hydrogen storage known as $HPGH_2$, which has been adopted by the majority of hydrogen refuelling stations globally [47]. Hydrogen storage for vehicular designs requires light weight $HPGH_2$ vessels, the US Department of Energy (DOE) in 2003 stated the range of the gravimetric and volumetric density of on-board hydrogen storage systems should be no less than 6 wt% H_2 and 60 kgH_2/m^3 in respective order to allow a driving range greater than 500 km on a single tank. Considering the new fuel cell vehicles introduced with different costs, designs and performance, the mentioned range is required to be no less than 5.5 wt% H_2 and 40 kgH_2/m^3 respectively by 2015 [48].

For stationary hydrogen storage systems at present there are mainly two types known as seamless hydrogen storage vessel and multifunctional layered stationary (MLS) hydrogen storage vessel [47]. The first type is constructed from high-strength seamless tubes with maximum permitted pressure of 65 MPa and the volume of 0.411 m^3, which requires assembly of many vessels for high storage [49].
The seamless method suffers from hydrogen embrittlement at high operating pressures [50] but with the 2nd technique (MLS) developed by Zheng et al. featuring a flat steel ribbon wound cylinder and two double-layered hemispherical heads, the embrittlement problem is tackled [51]. The hydrogen using the 2nd method could be stored with a volume of 2.5 m^3 at a pressure of 77 MPa [47].

2.1.4.2. Hydrogen Distribution

There are three main options to distribute hydrogen:

- Pipeline and tube trailers
- Marine and on-road transportation such as ships, barges, trucks and railway
- High energy density carriers such as ethanol and methanol

Hydrogen (in the form of gas or mixture of hydrogen and natural gas) can be transported using pipeline and tube trailers while liquefied hydrogen, since requires cryogenic tanks, could be delivered by means of ships, trucks and railway where careful handling and monitoring is more achievable.
Methanol and ethanol or other fuels could be used to transport hydrogen where hydrogen can be reformed at the destination for further use. The investigations however demonstrated that hydrogen transportation using pipelines is the most cost effective and energy-efficient method for large quantities of hydrogen over long distances [52].

2.1.5. Transportation via Hydrogen Fuel

In late 1920s hydrogen was used in airships when the burning of hydrogen in the internal combustion engine was experienced for the first time. In 1930s some 1000 vehicles renovated their internal combustion system to Erren's duo system, a German engineer who discovered if hydrogen is fed directly to the combustion chamber at raised pressure instead of carburettor, the pre-ignition, backfire and knock (problems attributed to low ignition energy of hydrogen in comparison to petrol) are tackled. Aircrafts and space shuttles also use forms of hydrogen as fuel, in mid 1950s, a customised American B57 twin-jet bomber flew numerous experimental missions with one engine functioning on LH_2 [53]. Later on though, it was clear that engines running on pure hydrogen were favoured from the viewpoint of air pollution in contrast to the dual systems.

Introducing hydrogen as a fuel into the transportation system requires a policy or an approach varying from the method of transportation and geographic consideration to the technological improvements in the vehicle design. The hydrogen as a fuel could be initially applied to the heavy-duty cargo mode vehicles and eventually makes its way towards light-duty vehicles; in this approach the transfer of technology and subsidiary industries could be maturely and efficiently achieved and also a group of associated skills and practises could be developed [54].

2.2. Fuel Cells

Fuel cell is an electrochemical device, which directly converts energy from a chemical reaction to electricity and heat while by-producing clean water in the process. The electricity is generated from a fuel and oxidant such as hydrogen and oxygen respectively [55] [56]. In figure 6 a diagrammatic depiction of a fuel cell is demonstrated where ion conduction stream and the product/reactant routes throughout the cell are shown.

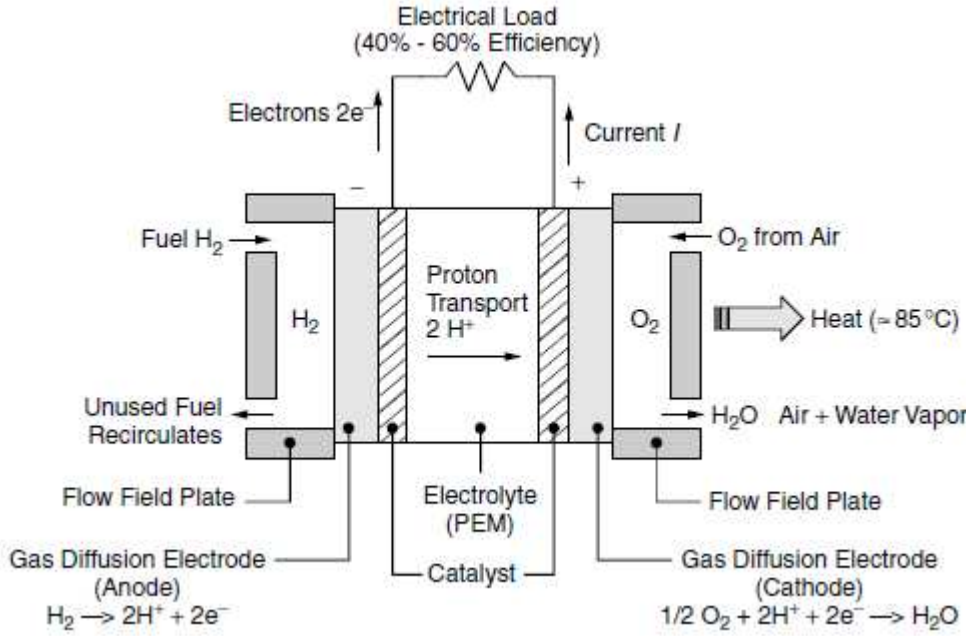

Figure 6 [57]: A diagrammatic representation of an individual fuel cell, a common configuration.

2.2.1. Fundamentals

In essence a fuel cell functions like a battery however contrary to the batteries, a fuel cell requires no recharging considering the fuel and oxidant are supplied. The basic structure of most fuel cells contains an electrolyte layer linked with a porous anode and cathode on either side [58]. In figure 6 the electrolyte is made up of a thin membrane capable to conduct positive ions while filtering away electrons or neutral gases. The fuel (hydrogen) and the oxidiser (oxygen), both directed by flow field plates at both sides of the cell, are introduced to the cell, one enters to a side of the cell and the other goes into the opposite side of the cell. The incoming hydrogen gas is prone to dissociate into electrons and proton as: $\mathrm{H_2} \leftrightarrow 2\mathrm{H^+} + 2\mathrm{e^-}$ It is favourable to coat the electrodes or membrane with catalyst to promote the above-mentioned dissociation, which therefore helps force the reaction to the right as the hydrogen gas liberates proton in the vicinity of the anode, there will be a concentration difference across the membrane between two electrodes, which causes the protons to travel through the membrane without electrons. This event gives

positive charge to the cathode with respect to anode. The left-behind electrons are then attracted towards positively charged cathode but since they cannot move through the membrane, they are to take another path. The electrons will take another route if an external circuit is created between electrodes. This flow of electrons through the exterior circuit brings energy to the load, as the electrons move from anode to the cathode, the current (I) direction, which is conventionally opposite to that of electrons, is from cathode to anode [57].

A single cell as shown in figure 6 produces 0.5V and 1V under normal operating conditions and open circuit conditions in respective order. Cell stacks are introduced to increase the voltage, to do this, gas flow plates within the stack are designed in such way to be bipolar meaning that they transport both hydrogen and oxygen used by neighbouring cells as shown in figure 7 [57].

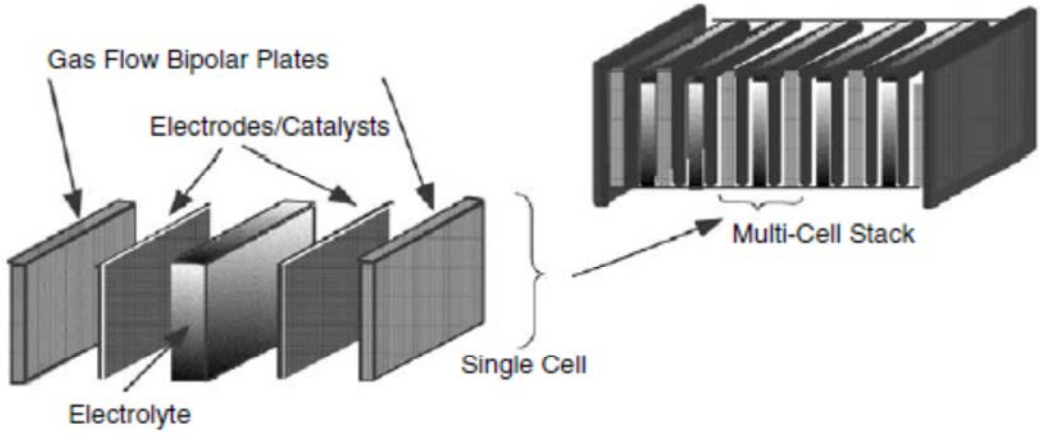

Figure 7 [59]: A multicell stack.

2.2.2. Thermodynamic considerations

Thermodynamics as we are familiar with is the science of energy conversion from one form to another, which entails objectives such as heat generation or work to be done. This could be implemented in forms of electrical or mechanical energies. The energy is supplied from a fuel resource within which the energy is encapsulated in a chemical form and can be released via chemical reactions using devices such as heat engines and fuel cells and then converted to electricity or heat. The heat and electricity can be converted to work using devices such as turbine and electrical circuit or an electromagnetic device (i.e. a motor) respectively [60].The anode and cathode half-cell reactions for the fuel cell represented in figure 6 are as follows:

Anode: $\mathrm{H_2} \rightarrow 2\mathrm{H^+} + 2\mathrm{e^-}$ (4)

Cathode: $\frac{1}{2}\mathrm{O_2} + 2\mathrm{H^+} + 2\mathrm{e^-} \rightarrow \mathrm{H_2O}$ (5)

When the half reactions are combined, the outcome is the reaction for combustion of hydrogen as we have:

$$H_2 + \frac{1}{2}O_2 \rightarrow H_2O + \text{Heat} \qquad (6)$$

The reaction shown in equation 6 happens spontaneously as it is exothermic therefore it releases heat. Hydrogen and oxygen in the above reaction readily react to form water while generating a certain amount of energy, which is used by fuel cell to distribute electrical energy to its load. In order to find the amount of energy released in the reaction and also the amount converted to electrical energy, three thermodynamic quantities need to be understood: entropy, enthalpy and free energy [59].

2.2.2.1. Entropy

Entropy is "A thermodynamic function defined such that when a small quantity of heat dQ is received by a system at temperature T, the entropy of the system is increased by dQ /T, provided that no irreversible change takes place in the system'' [61]. The concept of entropy is better appreciated when come across engineering processes as it is a rather complicated property, which is hard to define physically. The second law of thermodynamics guides towards the definition of entropy.

Time and again the 2nd law of thermodynamics leads to the terms that include inequalities, for instance a reversible heat engine is more efficient than an irreversible one running between the same two thermal energy sinks [62]. Entropy "can be described as a measure of molecular disorder, or molecular randomness" [63], as a system becomes more disordered the positions of the molecules become less predictable and the entropy increases [62]. Entropy in a fuel cell helps understand how much energy is directly converted to electricity while another thermodynamic property known as enthalpy could be used to know what amount of energy is released in a fuel cell. In addition to that entropy assists in developing the maximum efficiency of a fuel cell [64]. Additional information on the entropy can be found on page 2, Appendix I in the CD provided.

2.2.2.2. Enthalpy

The enthalpy of a material is characterised as the product of its pressure P, Volume V and the sum of its internal energy (U), which can be written as: $\text{Enthalpy } H = U + PV$ and usually has the unit of KJ of energy per mole of substance [59]. In some textbooks the term E is commonly used instead of U representing the energy. Enthalpy is in particular useful for constant pressure processes [61]. The internal energy (U) of a substance is defined as inclusive sum of kinetic energies of molecules and also energies related to intermolecular forces between molecules and atoms inside the molecules and atoms. This is referred to as microscopic properties. In other words enthalpy is considered as a scale of energy that it takes to constitute a matter from its component parts [59].

Enthalpy of formation is known to be the enthalpy change for the reaction when a substance formation is from its constituent elements [61] or it is the difference between the enthalpy of a substance and the enthalpies of its elements. The maximum possible fuel efficiency could be determined using the absolute entropy S°, enthalpy and Gibbs free energy G° [59].

2.2.2.3. Gibbs Free Energy

In a chemical reaction like the one occurring in a fuel cell, the chemical energy liberated can be considered as having two fractions; one as entropy-free, named free energy (ΔG), which can directly be converted to mechanical or electrical work and the 2nd part that must appear as heat (Q). The free energy (G) is the difference between the enthalpy (H) produced by the chemical reaction and the heat that needs to be released; $Q = T\Delta S$, this is to be consistent with the 2nd law.

The Gibbs free energy is associated with the maximum possible entropy-free mechanical or electrical yield from a chemical reaction and can be found by subtracting the sum of Gibbs free energies of reactants and products:

$$\Delta G = \sum G_{Products} - \sum G_{Reactants} \quad (7)$$

It can be inferred from equation 7 that the maximum possible efficiency is the fraction of Gibbs free energy to enthalpy change (ΔH) in the chemical reaction [65]:

$$\eta_{Max} = \frac{\Delta G}{\Delta H} \quad (8)$$

2.2.3. Type of fuel cells

Fuel cells can be categorised according to temperature, pressure or simply type of fuel or oxidant they use however for the sake of practicality fuel cells are now classified by the type of electrolyte they use. The types mentioned and frequently used in publications are as follows: Alkaline Fuel Cell (AFC), Phosphoric Acid Fuel Cell (PAFC), Molten Carbonate Fuel Cell (MCFC), Solid Oxide Fuel Cell (SOFC), Proton Exchange Membrane Fuel Cell (PEMFC) and Direct Methanol Fuel Cell (DMFC). Zinc Air Fuel Cell (ZAFC), Protonic Ceramic Fuel Cell (PCFC) and microbial Fuel Cell (MFC) are other types of fuel cells [66] [67]. In table 2 below a brief illustration of the types of fuel cells and their key properties can be found.

Table 2: Type of Fuel Cells and their applications [66], [67].

Fuel Cell System	Area of purpose	Efficiency (cell)	Electrolyte	Temperature range
Alkaline Fuel Cell (AFC)	Space and traction applications	50-60%	30-50% KOH	60-90°C
Solid Oxide Fuel Cell (SOFC)	Power generation	55-65%	Yttrium-stabilized Zirkondioxide (ZrO_2/Y_2O_3)	800-1000°C
Polymer Electrolyte Fuel Cell (PEFC)	Traction and space applications	50-60%	Polymer membrane (Nafion, Dow)	50-80°C
Phosphoric Acid Fuel Cell (PAFC)	Mostly dispersed power applications (50-500KW, 1MW, 5MW, 11MW)	55%	Concentrated phosphoric acid	160-220°C
Molten Carbonate Fuel Cell (MCFC)	Power generation	60-65%	Molten Carbonate melts (Li_2CO_3/Na_2CO_3)	620-660°C
Direct Methanol Fuel Cell (DMFC)	Small scale and military applications	40%	Polymer membrane	120-190°F≈49-90°C
Zinc Air Fuel Cell (ZAFC) [68]	-	-	Ceramic	700°C
Protonic Ceramic Fuel Cell (PCFC)	Power generation	-	Solid electrolyte (Ceramic)	N/A
Microbial Fuel Cell (MFC)	Wastewater treatment and medical applications	50%	-	20-40°C
Proton Exchange Membrane Fuel Cell (PEMFC)	Transport, portable and immobile applications	40-60%	Polymer Membrane	20-80°C

2.3. Electrolysis

Electrolysis can be referred to as the dissociation of ions of a solution by passing a direct current through the electrodes, which results in generation of positively and negatively charged ions. The electric current is used to make a chemical reaction (at the electrode), which does not occur under normal circumstances. Electrolysis in other words is the decomposition of a material caused by passing a DC between two electrodes submerged in a sample solution [69] . More technically referring to the electrolysis, this process entails passing a current through a cell to chemically change the electrolyte through detachment of ions where the cell potential is negative. This means that the electricity causes a chemical reaction to occur, which would otherwise be non-spontaneous. Oxygen and Hydrogen readily react to produce water where energy is released (in a fuel cell for instance), the reverse process however requires input energy and can be done through electrolysis. The reactions at the anode and cathode are [70]:

Anode: $2H_2O \longrightarrow O_2 + 4H^+ + 4e^-$ $E^\circ = -1.23V$

Cathode: $4\,H_2O + 4e^- \longrightarrow 2H_2 + 4OH^-$ $E^\circ = -0.83V$

Total Reaction: $6H_2O \longrightarrow 2H_2 + O_2 + 4(H^+ + OH^-)$ or $2H_2O \longrightarrow 2H_2 + O_2$ $E^\circ = -2.07V$

It must be noted that the potentials mentioned above are assumption for when the molar concentrations of H^+ and OH^- are one. In figure 8 a representative electrolytic cell is shown.

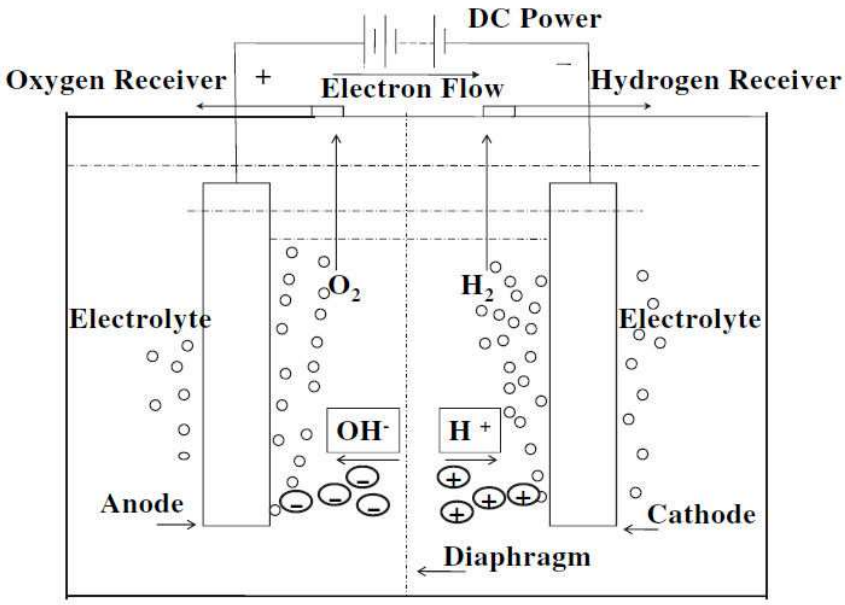

Figure 8 [6]: Schematic presentation of basic water electrolysis.

Here are anode and cathode reactions written differently:

At the Anode: $H_2O(l) \Leftrightarrow 2H^+ + \frac{1}{2}O_2 + 2e \qquad E^\circ_{Anode}(25°C) = 1.23V$

At the Cathode: $2H^+ + 2e \Leftrightarrow H_2 \qquad E^\circ_{Cathode}(25°C) = 0V$

The Net Reaction: $H_2O(l) \Leftrightarrow H_2 + \frac{1}{2}O_2 \qquad E^\circ_{Cell}(25°C) = 1.23V$

There is a minimum potential requirement before water molecules decompose, which is determined by chemical potential of gases or liquids at each electrode. The current in an electrolysis process is directly proportional to hydrogen production rate, which is itself enhanced by increased applied potential. The electricity consumption in an electrolysis process depends on the potential used in order to produce reasonable amount of hydrogen. In electrolysis the overall Gibbs free energy (ΔG) between products and reactants, is affected by change in potential and current, which are themselves function of temperature and concentration. The electrolysis potential (E) can be found using Nernst equation in terms of mole of electrons transferred (n), Faraday constant (F) and change in Gibbs free energy [71]. The equation is:

$$\mathbf{E = \frac{\Delta G}{nF}} \qquad (9)$$

In water electrolysis at potentials greater than 1.48V, thermoneutral voltage relates to the High Heating Value (HHV) of hydrogen (142 MJ/kg H_2) [equivalent to the enthalpy of water decomposition ($286\ KJ/mole, H_2O$)] while the minimum work (voltage) necessary for water decomposition at 1 atm and 300K is $237\ Kj/mole,\ H_2O$ or 1.23V corresponding to the hydrogen production rate of $32.6\ kWh/kg$. Water electrolysis for current electrolysers is an exothermic process generating in excess of $7\ kWh/kg$, H_2 [71].

In water electrolysis the activation overpotentials of cathode and anode are usually different to one another, which demonstrate their distinctive catalytic activities while these activities do not decide the ratio of electrochemical reaction rate on cathode to anode but this ratio is determined by the stoichiometric ratio only. The reason behind this may be that in an electrolytic process the electric current passing through the anode is always identical to that of cathode.

The hydrogen and oxygen production rates may be represented with the equations below in respective order [72]:

$$N_{H_2} = \frac{JA}{2F},\ N_{O_2} = \frac{JA}{4F}$$

Where N_{H_2} and N_{O_2} are the hydrogen and oxygen producing rates (mol. S^{-1}), J is the current density (A cm^{-2}), A is surface area cm^2 and F is Faraday's constant (96485 C mol^{-1})

A basic electrolyser includes cathode, anode and an electrolyte and the direction of electron movement is from anode to cathode considering that the oxidation takes place in anode and reduction in cathode. The water electrolysis is said to be divided into the three methods within each the conduction of one ionic species occur across the electrolyte [73]:

- Liquid Alkaline Electrolytes in which hydroxide (OH^-) is transferred (classic alkaline electrolysis cell)
- Proton Exchange membranes in which protons (H^+) are transported (PEM electrolysis)
- Ceramic Solid Oxide membranes in which Oxygen ions (O^{-2}) are conduced (Steam electrolysis)

The PEM electrolysis uses very pure water in the process. Potassium hydroxide, which is usually used in alkaline water electrolysis, is replaced by a proton conducting polymer membrane hence the problem of corrosion is tackled. In this type of electrolysis, hydrated protons are directed through the polymer electrolyte (such as perfluorosulfonic acid polymer). Active notable metal catalysts are required for this electrolysis in order to achieve high exchange current densities at room temperature [71].

Steam electrolysis on the other hand employs solid oxide electrolytes such as doped ZrO_2. In technique electrode reactions, unlike other electrolysis approaches, happens between gas phase reactants and crystalline ionic solids. The temperature range at which the reactions occur is between 1000 and 1200K. The steam electrolysis is rather in rudimentary stages of development compared to alkaline water electrolysis and PEM electrolysis and there is great potential for improvement [71].

In 1800 Shortly after Alessandro Volta invented the voltaic cell, Nicholson and Carlisle discovered electrolysis but since the knowledge of the time was limited, it took about 100 years for scientists to introduce the first industrial electrolyser. In the meantime the foundations for water electrolysis have been improved throughout the understanding of thermodynamic (enthalpy, entropy) and other fundamental electrochemical terms such as potential, overpotenial and decomposition voltage.

Today the majority of industrial electrolysers operate with the energy requirement of $4.5 - 5\ \mathrm{kWh/m^3}\ \mathrm{H_2}$ [74], [75] and can produce hydrogen with the efficiency of about 73% [76] and energy efficiency of between 40-60%.The Industrial water electrolysers are considered to produce 244,440 $\mathrm{Nm^3/year}$ [6].

2.3.1. Commercial use of Electrolysis

The most popular commercial electrolytic processes are:

- Production of aluminium
- Electro-refining of metals
- Metal plating
- Electrolysis of sodium chloride

Sodium metal is largely produced through the electrolysis of molten sodium chloride. In order to produce sodium, CaCl2 is mixed with NaCl to decrease the high melting point of sodium chloride down to 600° C, which was originally 800°C. In figure 9 the electrolysis of this mixture in a Downs cell is shown [70].

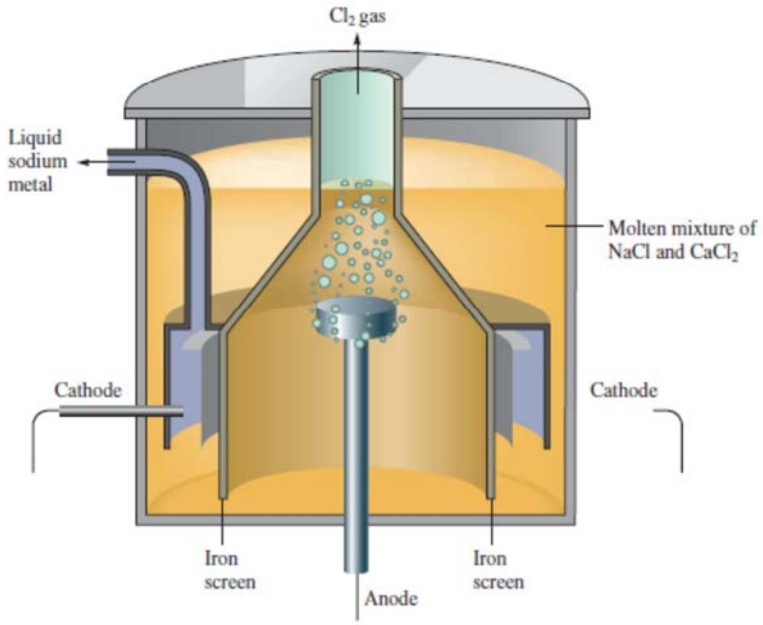

Figure 9 [70]: Downs Cell.

Anode Reaction $2Cl^- \rightarrow Cl_2 + 2e^-$

Cathode Reaction $Na^+ + e^- \rightarrow Na$

Metal Plating is another useful application to protect the readily corroded metals by coating a thin film of corrosion-resistant metal. The examples are silver plating of a spoon, tin coating of steel cans (known as tin cans) and chrome plating of steel car bumpers. An item can be plated when used as the cathode in a tank within which there are ions of plating metal.

Purification of metals can also be made through the electrolysis when there is aqueous copper sulphate as the electrolyte, thin slips of ultrapure copper as cathode and impure copper is cast into large slabs where they act as anodes for an electrolytic cell. This is an example of metal electrorefining.
In this procedure (metal electro-refining) an electric current is applied between the impure metal sample and a cathode as both are submerged in a solution within which exist the cations of the metal. Metal is then stripped off the impure sample and placed in pure form on the cathode [77]. Iron and Zinc can also be oxidised from impure anode [70].

Hydrogen can be produced as a by-product via hall-Heroult cell. This cell is used to produce aluminium worldwide. Aluminium is the 3rd most plentiful element on earth and can be found in nature in its oxide form known as bauxite [70]. This process is schematically shown in figure 10.

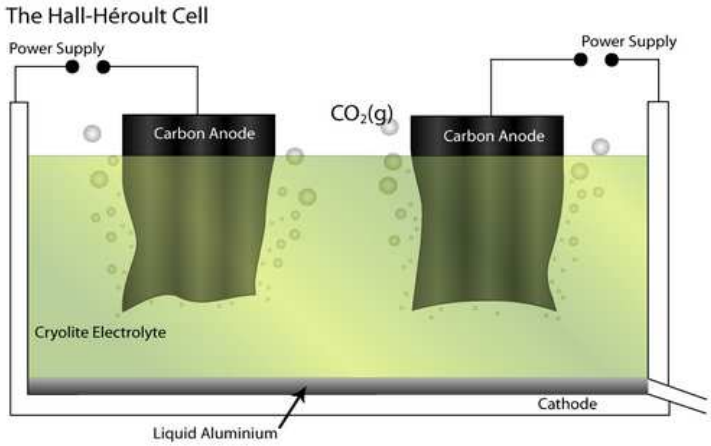

Figure 10 [78]**:** The Hall-Heroult Cell.

This is a process in which the conversion of alumina to aluminium occurs through electrolytic reduction in a molten bath of natural and synthetic cryolite. The energy consumption per ton of produced aluminium is 13-17 MWh [79]. Cryolite is a monoclinic mineral with the chemistry of $\mathrm{Na_3AlF_6}$ known as sodium aluminium fluoride [80].

In this section the electrolysis was defined and the principles were explained in brief along with the commercial use of electrolysis. The Nernst equation (equation 9 on page 31) was introduced with which the potential of an electrolysis cell can be calculated, this is a key equation in the electrolysis and electrochemistry. In the next section the principles of electrochemistry are discussed and Nernst equation will be explained in more details. The important electrochemical topics such as decomposition potential and overpotential are also talked over in addition to the methods to calculate these potentials.

2.4. Electrochemistry

The know-how of interconversion of electrical and chemical energies came to utilisation around mid-19th century. Chemical energy is converted to electricity through batteries, fuel cells and corrosion processes while the reverse, proceeds in electrolysis, electroplating and etc. The basic foundations (voltage, current, capacitance, concentration and etc.) for electrochemical phenomena were explicated through empirical observations by Michael Faraday and other European scientists before electron was discovered in 1893 and development of chemical thermodynamics in 1923. Potentiometry and polarography were introduced in 1920 and 1930 respectively. They are related to electrochemical phenomena and use of this phenomenon for molecule analysis and thermodynamic characterisation. Relationships that portray the two mentioned techniques are directly rooted from solution thermodynamics. As for polarography there is a further reliance on the diffusion of ionic species in solution. The latter is the foundation of conductivity measurements.
The quantitative relationships allowed applying electrochemistry to the comprehensive range of chemical species and processes in the solution phase [81].
Electrochemistry includes chemical facts correlated to charge separation and consequently charge transfer. The occurrence of this charge transfer could be homogenous in solution or heterogeneous on the electrode surface [82].
Electrochemistry is a division of chemistry corresponding to the electric current, potentials and chemical reactions with some reactions being spontaneous and electricity-productive just as batteries while others need electricity to develop such as electrolysis [83]. In 1800 Alessandro Volta devised the first battery called Voltaic pile, which was made of copper and zinc disks separated by paper bathed with acid solutions. The development towards today's electrochemistry was made feasible through the discovery of a sustainable source of electrical current. Michael Faraday definitively described concepts such as anode, cathode, electrolyte, electrode and ion before 1835, which made electrochemistry practically definable. The idea of negative and positive mathematical symbols on charges is accredited to Benjamin Franklin while earlier on Charles-François de Cisternay speculated the existence of only two kinds of electrical charges [84].

2.4.1. Principles of Electrochemistry

2.4.1.1. Nernst Equation

Nernst equation is used in electrochemistry to establish the equilibrium potential of a cell engaged with a reversible system applicable at the surface of the electrode. Let's consider a simple redox reaction:

$$O + ne^- \rightleftharpoons R$$

The Nernst equations are therefore:

$$E = E^{o\prime} + \frac{RT}{nF}\ln\frac{C^*_O}{C^*_R} \qquad (10)$$

$$E = E^{o} + \frac{RT}{nF}\ln\frac{a_O}{a_R} \qquad (11)$$

Where E^0(V) is the standard potential, $E^{0'}$ is the formal potential, C^*(mol L^{-1}) is the bulk concentration for the specified element, subscripts O and R refer to oxidised and reduced species, a (mol L^{-1}) is the activity, R is the universal gas constant ($JK^{-1}mol^{-1}$) and F is Faraday's constant (C/mol). The value of formal potential depends on the properties of supporting electrolyte and solvent [85]. A reduction example could be considered at which reduction reaction occurs for a platinum solution (pt^{2+}) and solid platinum electrode with the molar concentration of 1mM. We thus have:

$$Pt^{2+} + 2e^- \rightleftharpoons Pt$$

The voltage drop over the above system can now be calculated through the Nernst equation, as can be seen above the reduced product is a solid with unit activity; the activity for very dilute solution (1mM), which is the same as the concentration, hence using equation 11:

$E = 1.188V + \frac{RT}{2F}\ln\frac{0.001}{1} = 1.099V$ The SEP (Standard Electrode Potential) for platinum is 1.188 and the temperature is 25°C. The half-reaction voltage is 1.1V [85].

In an electrochemical system, the electrochemical reaction at one electrode occurs if the reaction proceeds at the other electrode, this is to say that a half reaction cannot occur on its own and there is always a reducer and oxidiser (i.e. electron donor and electron acceptor respectively). It is possible to measure potential difference between different half cells with respect to reference electrodes [86].

The half-cell potentials may be calculated with respect to a standard reference half-cell (standard hydrogen electrode or SHE) that is given the arbitrary value of 0.0V. The standard potential (E^0) is defined as a potential of a half cell at unit activity with respect to the standard hydrogen electrode. This activity of a half cell depends on concentration and temperature. The relations between E and E^0 can be found using Nernst equation where E may be related to the standard potential [86].

For a half cell reaction $aOx + ne^- \rightleftharpoons bRed$
Therefore Nernst equation can be written as below, which is the same as equation 10 and 11:

$$\mathbf{E = E^0 - \left[2.302\frac{RT}{nF}\right]\log_{10}\frac{[Red]^b}{[Ox]^a}} \qquad (12)$$

Where F is faraday constant, T is temperature in Kelvin, n is number of moles and R is gas constant, the symbol 'Red' denotes reduced and Ox stands for oxidised species.

2.4.1.2. Electrode Reactions

The reaction between electrodes and the solution is subject to occurrence at the interfacial area between electrode and electrolyte where charge distribution is different than that of bulk. Electrode reactions are known to be heterogeneous, at each electrode charge transfer and its difficulty can be characterised by capacitance and resistance respectively. The electrode can perform the role of a sink (for oxidation) of electrons transferred to or from species in solution and a source (for reduction).

In equation $\mathrm{A} + \mathrm{ne}^- \rightarrow \mathrm{B}$, A and B are oxidised and reduced species respectively, on the other hand the electrode can contribute to the electrode reaction as in dissolution of metal X we have:

$$\mathrm{X} \rightarrow \mathrm{X}^{\mathrm{n}+} + \mathrm{ne}^-$$

There should always be consistency between the energies of electron orbitals where transfer takes place in the donor and acceptor, in the electrode this level is the highest filled orbital. This is known as a Fermi energy level in a metal symbolised as E_F, this is different in soluble kinds and it is the orbital of valence electron to be received or given, therefore the following points can be concluded accordingly: [82]

1. Before the occurrence of electron transfer for a reduction reaction, there is a minimum energy requirement for the transferable electrons from the electrode. This corresponds to a suitably negative potential in volts.
2. For an oxidation reaction, there is a maximum energy threshold for the lowest unoccupied level in the electrode in order to accept electrons from the species in solution. This corresponds to adequately positive potential in volts.

The external control of potential values is possible through which the extent and direction of electrode reaction can be managed reasonably [82].

2.4.1.2.1 Kinetics and Thermodynamics

The electrode reactions by convention are half reactions articulated as reductions with which is correlated a standard electrode potential E^0, which is measured in relation to the normal hydrogen electrode (NHE). The Nernst Equation can relate standard electrode potential to the potential E at equilibrium for half-reactions.

$$\mathrm{E} = \mathrm{E}^{\ominus} - \frac{\mathrm{RT}}{\mathrm{nF}} \sum \mathrm{v_i} \ln \mathrm{a_i} \qquad (13)$$

Where a_i is activity, which is equal to 1 with all species for dilute solutions only, v_i is the stoichiometric numbers negative for oxidised species or reagents and positive for reduced species or products.

The propensity for the reaction to happen is given by equation 14 relative to the normal hydrogen electrode reference under standard conditions [82].

$$\Delta G^{\ominus} = -nFE^{\ominus} \qquad (14)$$

The Nernst Equation can be written in terms of concentration where we have $a_i = \gamma_i c_i$

$$E = E^{\ominus\prime} - \frac{RT}{nF}\sum v_i \ln c_i \qquad (15)$$

Where $E^{\ominus\prime}$ is the formal potential depending on the medium and γ_i the activity coefficient of species i.

The formal potential depends on the medium because it is inclusive of the term E and also logarithmic activity coefficient terms. The Nernst equation is applicable when there is equilibrium at the electrode surface between oxidised and reduced species engaged in an electrode reaction.

This electrode reaction is consequently known as a reversible one as it complies with the condition of thermodynamic reversibility. The mass transport of the species from the bulk determines their concentration at the interface, which is typically defined as mass transfer coefficient (k_d). A reaction is reversible when the rate of electrode reaction is significantly faster than that of mass transport. This rate or kinetics is standardised by a rate constant; k_0 which is when $E^0 = E^{0'}$, therefore for a reversible reaction we have $K_0 >> k_d$.

On the contrary for the opposite case, an irreversible reaction, the electrode reaction cannot be reversed. In this case a strong kinetic obstacle must be conquered. This could be done by use of an extra potential known as overpotential, for this we have $K_0 << k_d$.

There is the 3rd case known as quasi-reversible reaction whose behaviour is transitional between reversible and irreversible reactions. The overpotential in this case has a small value and with the aid of this additional potential reaction can be reversed. The rate constant for an electrode reaction depends on the potential and can be written for oxidation and reduction reactions as follow:

$$K_c = K_0 \exp[-\alpha_c nF(\frac{E-E^{0\prime}}{RT})] \qquad (16)$$

$$K_a = K_0 \exp[\alpha_a nF(\frac{E-E^{0\prime}}{RT})] \qquad (17)$$

Equation 16 is for reduction and equation 17 is designed for oxidation. In the above equations α_c and $\propto_a$ are cathodic and anodic charge transfer coefficients, which also act as a measure for the activation barrier. Another way to illustrate the rate of electrode reaction is in the course of the current exchange (I_0), which is defined as the scale or extent of the partial current at the anode or cathode at the equilibrium potential (E_{Eq}). Empirically speaking, the rates of electrode reactions are determined as the current passed to which

they are directly relative. In equations above R is gas constant, E is the cell potential, $E^{0'}$ is the formal potential, n is number of moles transferred and T is temperature in kelvin.

2.4.2. Electrochemical Terms

2.4.2.1. Decomposition Potential

Decomposition voltage (E_D) is expressed as 'The minimum potential difference, which must be applied between two electrodes before the currents flows and decomposition happens'. The values of decomposition voltages can be determined using a graph of current vs. cell voltage, this graph provides the decomposition curve, which then leads to the calculation of decomposition voltages.

Experimentally this value may be calculated finding the equation of the line for a graph of current versus voltage when y=0 the value of x in the equation equals to the decomposition potential. This means the extrapolation of 2nd branch of graph back to zero current [87]. For instance the decomposition potential for 0.1M KOH experiment in the presence of the ultrasound and electrode active length of 10 cm is as follows (The relevant graph can be found in the appendix V, page 121 on figure 4):

Finding the equation of the line (current- voltage graph) for this experiment, which is $y = 54.2x - 96$, the value of x gives us the decomposition potential when y=0, therefore $E_D = 1.77\text{volts}$

The overpotential of a system may be calculated via equation below;

$$\eta = E_D - E_{Rev}^{Cell} \qquad (18)$$

Where η is the overpotential in volts, E_D is the decomposition potential and E_{Rev}^{Cell} is the reversible potential with the value equals to 1.23 volts for pure water and can be found using Nernst equation (equations 10-12 on page 36) for different temperatures and concentrations [87] . While we have:

$$E_{Rev}^{Cell} = | E_{Rev,C} - E_{Rev,a} | \qquad (19)$$

Where $E_{Rev,C}$ and $E_{Rev,a}$ are the reversible potential of cathode and anode in respective order.

2.4.2.2. Overpotential

Overpotential [η (V)] is referred to as the divergence of electrode cell potential from its value at equilibrium, which can be negative or positive. The equations 18 and 19 introduced in 2.4.2.1 can be used to calculate overpotential [88]. Anode and cathode overpotentials can also be found separately from the equation 20 and 21 in this section.

The term polarisation is defined as a voltage loss or overpotential that is correlated to current density [89]. There are three main kinds of overpotential namely as activation, resistance (Ohmic) and concentrations overpotentials.

The activation overpotential is established based on the activation energy or Gibbs energy and is denoted by the symbol (η_a). This means that in order for an electrochemical reaction to advance, the activation overpotential, which is an energy barrier, must be overcome. This type of overpotential can have various values rooted from different types of electrode and also gases evolving on the electrodes [90]. For instance hydrogen and oxygen gas produced at the electrodes have the respective overpotential values of: -0.62V and +0.95V [91] [92].

Resistance overpotential or Ohmic polarisation is another type, which proposes that all materials except superconductors deliver resistance to charge transfer and this can be explained using Ohm's law. In an electrolytic process there are ionic and electronic resistivities that respectively manipulate oxide-ion transfer through the electrolyte and transport of electrons through the electrodes [93].

Concentration overpotential is another type explained and is a significant effect resulted from concentration variation in the locality of electrode surface caused by electrochemical reactions taking place in the neighbourhood. Concentration overpotential is denoted by symbol η_C [94].
In order to evaluate the overpotential of an electrolytic cell, there are two methods of decomposition voltage (sections 2.4.2.1 and 2.4.2.2) and discharge potential presented in section 2.4.2.3 [87].

2.4.2.2.1. Hydrogen and oxygen generation Overpotential

Hydrogen evolution reaction mechanism is in the following form including the formation of adsorbed hydrogen followed by either chemical desorption or electrochemical desorption [6]:

$H^+ + e^- \rightarrow H_{Ad}$

$2H_{Ad} \rightarrow H_2$ (Chemical Desorption)

$H^+ + e^- + H_{Ad} \rightarrow H_2$ (Electrochemical Desorption)

Where subscript 'Ad' denotes the adsorbed position.

The overpotential can also be calculated for hydrogen and oxygen separately using Tafel equation, the hydrogen overpotential can be found via:

$$\boldsymbol{\eta_{Cathode}} = \mathbf{2.3}\frac{\mathbf{RT}}{\boldsymbol{\alpha F}}\mathbf{log}\frac{\mathbf{i}}{\mathbf{i_0}} \quad (20)$$

Where i_0 is the exchange current density of reaction, R is the universal gas constant (8314 $JK^{-1}mol^{-1}$), T is temperature in kelvin, α is transit (transfer) coefficient (dimensionless), F (96,485 C/mole) faraday constant and i is the current (amperes).

The oxygen overpotential can also be found using the Tafel equation:

$$\boldsymbol{\eta_{Anode}} = \mathbf{2.3}\frac{\mathbf{RT}}{\mathbf{(1-\alpha)F}}\mathbf{log}\frac{\mathbf{i}}{\mathbf{i_0}} \quad (21)$$

Tafel equation is the linear relationship between the overpotential and logarithm of current density [6]. The logarithmic form of I (current) and potential make a linear relationship [82].Tafel equation in other word is a bridge that connects applied overpotential to the current i, which travels through the circuit. Here is Tafel equation [87]:

$$\eta = \frac{2.3RT}{\alpha F}\log i_0 - \frac{2.3RT}{\alpha F}\log i \quad (22)$$

Tafel equation then can be written in the form:

$$\eta = a + b\log i \quad (23)$$

In the equation 23 a and b are constant, which can be deduced from equation 22. Tafel plots (graph of $\log |i|$ vs η) are made up of a cathodic and anodic branch for negative and positive overpotentials respectively. In order to find out the transfer coefficient α, the slope of a linear area on the plot is considered to calculate reduction and oxidation slopes [87] [88]. Tafel equation however has restrictions for applicability, equation 23 can be applied if a number of assumptions are satisfied for a system including [95]:

- Negligible ohmic potential drop
- Uniform current density otherwise only point-to-point overpotetnial could be calculated
- Large overpotential for the reaction hence the following relation applies $|\eta/b| \geq 1$
- Suppression of the diffuse double layer by a large excess of supporting electrolyte.
- Small current density in contrast to the mass-transfer limited current density

The application of Tafel equation to an electrolytic system requires three-electrode electrolysis system and potentiostatic experiments to be done in order to find exchange current density (i_0). This way anode and cathode half-cell reactions can be studied independently and irrespective of one another.

2.4.2.3. Discharge Potential

In this technique an understanding of electrode reactions is required in a potentiostatic manner. Potentiostatic refers to a technique in which the electrode potential is kept constant, it is called potentiostatic Coulometry [96]. In order to find the anodic discharge potential (E_{da}) and cathodic discharge potential (E_{dc}), curves for the cathode and anode are plotted separately then extrapolated to give the values of E_{da} and E_{dc}.The sum of anode and cathode overpotential may be written as [87]:

Where E_{da} and E_{dc} are the decomposition potential of anode and cathode respectively.

$$\text{anode overpotential}(\eta_a) = E_{da} - E_{rev,a} \quad (24)$$

$$\text{cathode overpotential}(\eta_c) = E_{dc} - E_{rev,c} \quad (25)$$

Where $E_{rev,C}$ and $E_{rev,a}$ are the reversible potential of cathode and anode in respective order.

Therefore the overpotential of a system may be found via the following equations:

$$\eta = \eta_{Anode} + \eta_{Cathode} \quad (26)$$

Anode and cathode overpotentials may be calculated using equations 27 and 28 [87]:

$$\eta_{Anode} = \eta_{A,a} + \eta_{C,a} + \eta_{R,a} \quad (27)$$

$$\eta_{Cathode} = \eta_{A,c} + \eta_{C,c} + \eta_{R,c} \quad (28)$$

Where η is the overpotential, subscript A is the activation, C is the concentration and R is resistance whist subscripts a and c stand for anode and cathode respectively.

2.5. Ultrasound

2.5.1. Principles

Sound waves are defined as longitudinal pressure waves travelling through a substance. Ultrasound is a term applied to the sound waves above the frequency at which human ears are capable of hearing. Human hearing is ranged between 20 Hz to approximately 20 kHz. The ultrasonic band can be grouped into two sections including diagnostic ultrasound and power ultrasound where power ultrasound has a frequency range between 20 kHz and 1 MHz while diagnostic one goes above 1MHz [97]. In the figure provided below (figure 11) the spectrum of sound is demonstrated in a definitive diagram.

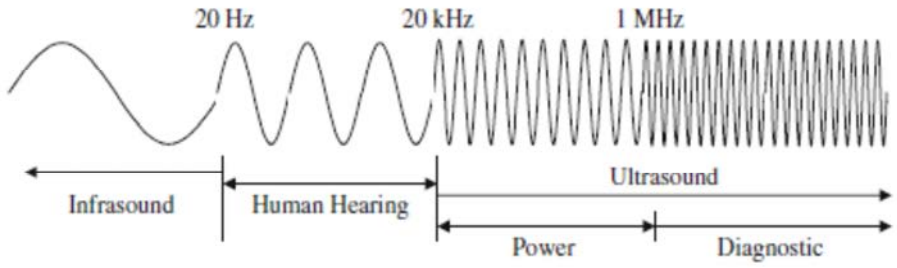

Figure 11 [97]: The classification of sound spectrum.

The ultrasound is a pressure wave with a high frequency, which generates spots of low and high pressures within a medium when moving through it. This pressure generally known as acoustic pressure depends on the energy input to the system. This sound wave creates steady streaming when going through viscous medium such as water hence scattering the energy in the form of viscous flow. The type of resultant flow is dependent on two factors;

First one is the shape of original acoustic wave and second factor is the occurrence of either following circumstances; reflection of pressure wave from the hard surfaces or its interaction with the system boundary [98]. It is noted that the ultrasound at higher frequency results in enhanced energy absorption thus larger acoustic streaming flow rates compared to the case where lower frequency is used for the same power intensity [97].

This streaming phenomenon and consequent pressure changes can be tolerated in mediums such as air as they are more compressible and elastic compared to the liquids, in liquids such as water though at sufficiently high pressures, the liquid can be ruptured affected by ultrasound leading to the formation of gas and vapour micro bubbles. These Microbubbles act as a relief valve of the tensile stresses built up by the pressure wave. This event would occur under high acoustic pressure variation of up to 3000 MPa nevertheless the formation of these micro bubbles could occur at moderately mild acoustic pressures that are because some gas cavities or nanobubbles exist in any liquid and this helps formation of microbubbles. The process of bubble development/creation is called cavitation. The created bubbles during the course of cavitation will expand first and then collapse, influenced by the sound fields creating a cycle of expansion/collapse in the form of a sinusoidal cycle. The expansion and collapse of the bubbles depend on the bubble size and also acoustic pressure as for some specific bubble sizes and acoustic pressures the expansion period is elongated and followed by an aggressive collapse known as the inertial cavitation. The cavitation is called stable or repetitive transient when this bubble oscillation can hold up to hundreds of acoustic cycles. Another type of cavitation occurs at low frequencies (20-100 kHz) and high amplitudes as the bubbles collapse in the period of only few acoustic cycles and the bubbles keep disintegrating to smaller bubbles, this type is referred to as unstable or transient cavitation [97].

2.5.2. Cavitation Microstreaming

There is another phenomenon known as cavitation microstreaming, which occurs when large bubbles are formed either through coalescence of small bubbles or growth of large bubbles during expansion phase. The process is called rectified diffusion, which takes place over a great number of acoustic cycles, since the interfacial area is great and mass transfer boundary layer is thinner throughout the bubble expansion rather than bubble collapse therefore more air is allowed into a bubble during the expansion phase while lesser air leaks out during the collapse period, which causes the growth of large bubbles. The large bubbles may even drift away from the sonication zone by the act of gravity. In addition to that, the pressure and velocity in the neighbouring fluid fluctuates as a result of bubbles bouncing up and down in an oscillatory movement and this is known as cavitation microstreaming. High pressures of up to 100MPa can be observed when a bubble collapses in the course of a transient or repetitive transient cavitation [97].

There is a great resistance to heat and mass transfer at fluid-fluid and fluid-solid boundary layer, this resistance could be overcome by focusing the distribution of acoustic energy in these regions. Ultrasound is very influential in enhancing the heat and mass transfer within a medium being under sonication [99] [100]. The ultrasound is less effective at high temperatures above ambient point [101] as raising up the external temperature increases the water vapour pressure within the bubbles being cavitated and this water vapour act as a pillow to mitigate the bubble collapse, which is why the ultrasonic field is less effectual [97].

There are chemical and physical effects involved with ultrasound at various frequencies. Chemical effects can be seen more dominantly than physical at frequencies between 200-500 kHz known as intermediate frequency and this is because the number of active bubbles formed is higher than low frequencies (20-100 kHz) however physical effects can still be spotted. The chemical effects contain the chemical changes in vapour phase, cavitation bubbles and the surrounding medium such as primary radical formation as a result of high temperature within a bubble at the instant of breakage, localised temperatures of up to 5000K and greater exist when a bubble collapses violently. The physical effects include the enhanced turbulence in the fluid at low frequencies, which strongly exist at the interfaces and system boundaries [97].

2.6. Electrolysis; a literature survey

Water electrolysis is a well-known technology and a process to produce pure hydrogen with minimal impact on the environment but still not a cost effective technique since it requires high energy to proceed. The energy requirement (electricity) for the water electrolysis has been mentioned in the literature [74], [75] $4.5 - 5\ \mathrm{kWh/m^3},\ \mathrm{H_2}$ for the majority of industrial electrolysers. The electricity is expensive in most countries and considering that the electricity has an average production efficiency of 30-40%, the overall efficiency of the electrolysers is usually below 40%. The solution is to lower the price or the electricity or alternatively reduce the energy requirement for this technique through the reduction of resistances in the process such as electrical and electrochemical, development of new electrode materials or refine cell geometry [74], [75].

Currently about 4-5% of hydrogen produced in the world is through water electrolysis, about 48% from steam methane reforming, oil reforming accounts for 30% and 18% belongs to coal gasification [102]. The reason to this low percentage (4-5%) is rather evident; large ohmic voltage losses and high overpotentials. These result in the elevated rate of energy consumption and the requirement for large electrode surface areas, which wholly make the production set-up, economically not reasonable. The overpotential however can be reduced utilising more active electrodes but there still exists the following problem; the majority of gas bubbles are adsorbed on the surfaces of electrode and membrane or distribute in the electrolyte throughout water electrolysis and this causes large ohmic voltage losses [103].

The rapid detachment of hydrogen and oxygen gas bubbles from the electrolytic system is rather a difficult task under normal gravity conditions, as the current density is raised ohmic voltage drop and bubble coverage are increased notably and this does not help the situation.
This separation of bubbles from the electrode surface, electrolyte and membrane is manipulated by interphase buoyancy expression Δρg. It suggests the carry-out of the experiment under super-gravitational field, which results in the increment of interphase slip velocity and convection flow velocity caused by high gravity acceleration field and consequently results in the intensification of multiphase separation.
As a result, the reduction of gas bubble coverage on the electrode surface can be observed, which would be beneficial for gas evolution reaction as there would be more active sites available, moreover the disengagement of gas bubbles from the electrolyte or membrane can be eased efficiently thus leading to the reduction of overpotential and ohmic voltage drop under super gravity field [103].

Alkaline water electrolysis is one of the popular techniques to easily produce hydrogen however there are challenges to be dealt with such as energy use, maintenance and cost, in this type of electrolysis, the

electrolyte is an alkaline solution, sodium or potassium hydroxide are dissolved in water to increase conductivity of solution. This is to say that ions with high mobility are applied thus transferring the electricity more readily. Potassium hydroxide is the most widely used material because it resists gigantic corrosion loss, the preferred type of electrodes used are nickel because of their reasonable price, high activity and also availability. The advance of this electrochemical reaction needs some requirements and that is to overcome a handful of barriers and this calls for adequate electrical energy supply. The barriers comprise the following [6]:

- Electrochemical reaction resistances
- Electrical resistances of the system
- Transport related resistances
- Availability of electrode surfaces

The electrical resistances can be found via Ohm's law R=V/I where V is the voltage that is applied only at the circuit and I is the current. Transport-related resistances are forms of physical resistances such as resistances to ionic transfer within the electrolyte solution or gas bubbles formation at the surface of electrodes and inside the bulk of electrolyte. In accordance with the Joule's law the two of mentioned resistances are the reasons for heat generation and transport phenomena hence inefficiency of the electrolysis. The energy lost in the process as a result of electrical and transport-related resistances is also referred to as Ohmic loss.

The electrochemical reaction resistances are resulted by the overpotentials needed to overcome activation energies of oxygen and hydrogen formation reactions on the cathode and anode surfaces, this nevertheless increases the overall cell potential [6].

Zeng et al [6] in their work have shown the overall resistances involved in an electrolytic process presented in the equation below:

$$\mathbf{R_{Total} = R_1 + R_2 + \cdots + R_8} \qquad (29)$$

Where R_1 is the external electrical circuit resistance including connections and wiring at anode. R_2 is anode resistance rooted from the overpotential of OER(Oxygen Evolution Reaction) on the surface of the anode. R_3 is resulted from oxygen gas bubbles accumulated on the surface of anode, which delays the contact between anode and the electrolyte. R_4 and R_5 are resistances enforced by the ions in the electrolyte and the membrane respectively. The resistance caused by partial coverage of cathode by hydrogen bubbles is R_6. R_7 is the resistance resulted from the overpotential for HER and finally R_8 is the electrical resistance of connections and wiring at the cathode [104].

Water electrolysis in the presence of an ultrasonic field is another area, which has been investigated by Sheng-De Li et al [105], the energy efficiency of water electrolysis was improved significantly in the presence of the ultrasound. This was done using two techniques of Linear Sweep Voltammetry (LSV) and galvanostatic polarisation; the measurements were done for cell voltage, energy consumption and efficiency of generated gas in the process of electrolysis utilising an alkaline solution.
The cell voltage was reduced considerably in the presence of ultrasound particularly at low electrolyte concentration and high current density. The efficiency of hydrogen gas generation showed an enhancement in the range of 5% to 18% at high current density in the presence of ultrasound while this efficiency for oxygen gas dropped, which was result of different characteristic behaviour of gas bubbles. It was concluded that the use of ultrasound as a powerful tool will improve the performance of an electrolytic cell. The LSV curves produced in the study showed that HER (Hydrogen Evolution Reaction) difference remained almost the same using ultrasonic field at various concentrations while OER was reduced with increasing electrolyte concentration. With increasing electrolyte concentration, cell voltage difference was reduced for both sonicated and unsonicated (silent) conditions under steady-state polarisation conditions [105] .

Steam electrolysis is yet another technique in the realm of the electrolysis. In the 1980s in a project known as HOTELLY, Donitz reported the use of electrolysis in the form of high temperature steam electrolysis, which was studied for hydrogen production employing solid oxide electrolysis cell (SOEC). This type of cell benefits from its intrinsic high efficiency and heat and electrical power supply by nuclear and solar energies for water electrolysis giving a green and high purity large-scale hydrogen production [106].

Another form of electrolysis has appeared as the practice of photo-electrolysis of water, which has been investigated broadly in the aspect of light to hydrogen fuel conversion. This investigation has so far been classified into two methods; use of semiconductor electrodes and utilisation of photovoltaic device (i.e. solar cell) as one of the components of whole electrolysis arrangement. TiO_2 used as semiconductor photoelectrodes is capable to decompose water with no external bias but the conversion efficiency is low (i.e.3.0%) due to their wide bandgap[1] , which takes in a limited amount of solar radiation however there is a drawback of photoelectrode dissolution for small bandgap semiconductor photoelectrode. Amorphous silicon solar cells have been studied for the systems utilising solar cell device where its bandgap matches with the solar spectrum well [107].

In another experimental set-up, Hexadecyl-trimethylammonium bromide (HTMAB) was used as a cationic surfactant to improve the water electrolysis on the carbon cloth electrode. This work was done to investigate the effect of this surfactant on the water electrolysis.

[1] An energy region in solid-state defining the electrical conductivity [180] of a solid.

The use of carbon-based electrodes and HTMAB surfactant had an opposite effect on the Oxygen Evolution Reaction (OER) and Hydrogen Evolution Reaction (HER). This is to say that the surfactant inhibited HER indicated as a small negative potential shift but enhanced OER, which showed as a large positive potential shift. The OER enhancement was caused mainly because of speeding up H_2O_2 production from water oxidation at a moderately negative potential. The improvement of OER after introduction of HTMAB was sufficiently large that makes up for the decrease of HER in water electrolysis. This surfactant however was introduced to other systems with different electrodes and the results were significantly different, which showed the effect of various electrodes in different electrolytes and their important characteristics in the electrolysis [76].

Jonathan Mbah et al in a study reduced the energy requirement for the decomposition of water molecules employing a solar chemical cell. They have decreased the equilibrium potential to 0.6V in practise utilising sulphur dioxide and anode tolerance materials. Silicon electrodes were used in this work on which was deposited ruthenium dioxide ($\mathrm{RuO_2}$). Sulphur dioxide ($\mathrm{SO_2}$) was used to scavenge the anode. Sulphur dioxide reacts with $\mathrm{H_2O}$ at the anode and is oxidised to sulphuric acid. The thermochemical free energy in this work was decreased six times its primary value from 56 to 9.18 kcal/mole [102].

In an electrochemical reactor using a Nafion 117 solid polymer electrolyte (SPE) with sulfonic acid groups, Ebru Önder Kiliç et al produced hydrogen with 99.999% purity with the use of Titanium oxide coated with iridium oxide as anode and carbon fibre with Pt catalyst as cathode. In this experiment formic acid was electrochemically decomposed. In this work hydrogen was produced at a rate of 3.2 mL/min at 25 mA cm^{-2} of current density and treatment time of 150 minutes [108].

P.K. Dubey et al reported a significant amount of hydrogen production in their work. They used 1.0 M NaOH as an electrolyte solution and anodic voltage of 1V (Vs. Standard Calomel Electrode) was employed. Multi-walled carbon nanotubes were used as anode, Platinum wire as counter electrode and saturated calomel electrode (SCE) as reference electrode. The reported amount of hydrogen for this type of anode was about $375\mathrm{lh^{-1}m^{-2}}$ for alkaline water at PH level of 14. The amount of hydrogen production for multi-walled carbon nanotube was double the amount produced for conventional graphitic carbon electrode (about 200 $\mathrm{lh^{-1}m^{-2}}$) while keeping the overpotential the same [109].

W.L. Guo et al have been able to generate hydrogen at a rate of 53 $\mu\mathrm{mol/hr}$ for 3.0 M HCOOH and 2.5 M NaOH solution at 8.0 $\mathrm{mA/cm^2}$ of current density. The hydrogen was produced via electrolysis of aqueous formic acid solutions. A further investigation was done to see the effect of concentrations of sodium hydroxide and formic acid on the cell potential. The initial cell potential of 0.30V was noted for the case in which the actual concentration of formic acid was greater $0.8 \times 10^{-9}\mathrm{M}$ [110].

PEM electrolysis as an alternative method for hydrogen production was studied by Frano Barbir from the renewable energy sources [111]. PEM electrolysers these days on industrial scale have production capacities of up to several thousands m^3/h using KOH or proton exchange membrane electrolyte. Potentials above thermoneutral (1.482V) are applied (as low as 1.6V) at the anode in order to split water into protons, electrons and oxygen. The protons travel through the membrane joining the electrons at the cathode to form hydrogen. The PEM electrolysers are mentioned to produce hydrogen up to 99.999% purity and are also simpler to deal with in comparison to the alkaline water electrolysis. Barbir's study showed that PEM electrolysers can be coupled with PV arrays/solar cells as an energy supply with coupling efficiency of above 93% [112] [111].

S. Siracusano et al in their work produced hydrogen at 270 lh^{-1} using a PEM electrolyser operating at 60A potential and 70°C with 876 W of electrical power. The overall cell stack efficiency of 73% and 85% were attained for low and high heating value of hydrogen, respectively [113].

Microbial electrolysis has been mentioned in the literature as a good alternative to conventional electrolysis, which also benefits from low energy requirement and concomitant treatment of waste water or biowaste. The microbial electrolysis cell (MEC) uses the microbes to decompose the organic matter at the anode and generate hydrogen at the cathode. Hongqiang Hu et al reported 2 $\mathrm{m}^3/\mathrm{day}/\mathrm{m}^3$ of hydrogen production at a current density of 12 A/m^2 for a nickel-based cathode (NiMO) at 0.6V potential. They also mentioned 240% energy efficiency based on electrical energy input at 0.4V potential applied [114].

Douglas F. Call et al in a work studied the effect of high surface area of stainless steel cathode on the generation of hydrogen in a microbial electrolysis cell. It was reported that using a stainless steel brush cathode with a specific surface area of 800 $\mathrm{m}^2/\mathrm{m}^3$ at 0.6V, hydrogen was generated at a rate of about 1.7 $\mathrm{m}^3, \mathrm{H}_2/\mathrm{m}^3, \mathrm{d}$. They reported that this rate was similar to those achieved using expensive platinum-catalysed carbon cloth cathodes. A reduction in overpotetnial for hydrogen evolution using this method was observed [115].

Kim et al in a recent project have investigated the production of hydrogen via 3-cell flat-tubular solid oxide electrolysis cell stack. They reported 4.1 lh^{-1} of hydrogen production with the total hydrogen production of 144.32 litres over 37.1 hours of operation time. The active area of a single cell was 30 cm^2 and the cell had an electric efficiency of 97.61%.

Hydrogen gas in an electrolytic process is generated just after the process of electrolysis is started (i.e. decomposition potential). The production of hydrogen is in molecular form occurring through the electrochemical reaction on the surface of cathode. Molecular hydrogen gas nucleates at the cavity of electrode surface [116] to hydrogen gas bubbles at cathode active sites on the surface of electrode, the

hydrogen bubbles then start to grow on the surface of electrode [117]. The Volmer-Heyrovsky-Tafel mechanism occurs at the surface of the electrode. The hydrogen electrode reaction consists of three parts as follows [118]:

$$H_2O + e^- = H_{adsorbed} + OH^- \quad \text{(Volmer Reaction)}$$

$$H_{adsorbed} + H_{adsorbed} = H_2 \quad \text{(Tafel Reaction)}$$

$$H_{adsorbed} + H_2O + e^- = H_2 + OH^- \text{ (Heyrovsky Reaction)}$$

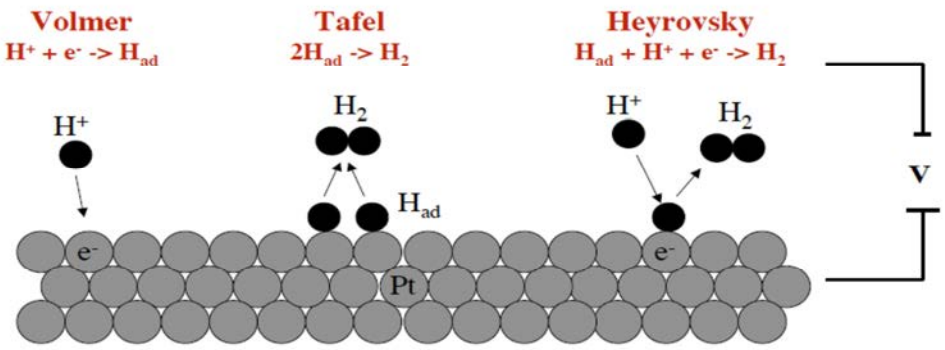

Figure 12 [119]: Elementary Reaction Phases in HER.

The Volmer-Heyrovsky-Tafel mechanism for hydrogen evolution reaction (HER) can be shown in figure 12 for a platinum electrode where subscript 'ad' refers to adsorbed species on the surface of electrode.

In this section the author had a look at the important electrolytic processes mentioned in the literature including alkaline water electrolysis, steam electrolysis, MEC and PEM along with the electrolysis in the presence of the ultrasound. The combination of ultrasound, electrolysis and solar energy could be a successful blend in order to produce sustainable clean energy for future if the energy requirements and capital investment for the equipment and material could be decreased. It may be deduced from the literature that the use of PEM electrolysers are preferred over conventional electrolysis due to less energy consumption and higher efficiency and ease of use however more investigation is required to draw a more comprehensive conclusion.

2.7. Sonoelectrochemistry; a literature survey

This field was born through the marriage of electrochemistry and ultrasound and increasingly gained the interest of electrochemists as well as engineers. The industrial scale-up of the electrochemical processes lacks adequate mass transfer to the electrode surface and also suffer from fouling of the electrode surface. The utilisation of the ultrasound for the electrochemical processes tackles the problem of mass transfer limitation by simply increasing its rate to the electrode, reducing the diffusion layer thickness and elevating the limiting current density [120]. Although escalating the mass transfer, ultrasound can also have some influences in homogenous systems, which engage releasing highly reactive radical species [121] [122].

The start of sonoelectrochemistry was with Morigushi in 1930s who investigated the effect of ultrasound on the water electrolysis, In the 50s an extensive attention was paid to sonic- aided electroplating specifically that of nickel and chromium however methodical applications were used in 1960s. 1980s was the decade when the main focus of sonoelectrochemistry was pulled towards analysis of styrene polymerization, thiophene and organic sonoelectrosynthesis. The active progress of sonoelectrochemistry was flourished in the 90s both in basic know-how as well as the applied studies. Today not only general reviews on sonoelectrochemistry are not hard to find but also unambiguously oriented applications such as organic synthesis [121] and electroanalysis [123] can be found [124]. Varieties of experiments and different set-ups have been carried out as of the first sonoelectrochemical experiments [125];

- The parallel use of ultrasonic tip as electrode and ultrasound emitter
- Combination of voltammetric cell and ultrasonic tip through liquid chamber or glass wall
- Submersion of the electrochemical cell into the ultrasonic bath
- The immersion of electrodes and ultrasonic tip into the liquid, known as sonochemical cell, which is the most widely used configuration

The important effect of ultrasound in chemistry and electrochemistry as the result of cavitation phenomena made this technology popular in the mentioned fields. At the verge of cavitation when the ultrasound irradiation spreads, the occurrence of chemical and mechanical events is evident, this impinges on any heterogeneous process such as electron transfer at the surface of electrode. There are mechanical events corresponding to the ultrasonic field propagation as follows: [126]

- Cavitation and shock waves
- Acoustic streaming and microjetting
- Mass transport promotion from/to the electrode
- Electrode surface cleaning

In 2003 all the mentioned phenomena have been re-examined at high and low frequencies by Compton et al and the conclusion was that at high frequency ultrasound the electrochemical processes are manipulated by different processes than that of low frequencies, for instance micromixing and microjetting are attributed processes to high frequency while acoustic streaming is related to lower frequencies [127].
The cavitation is the result of quick generation and collapse of microbubbles within the medium, which can cause accelerated mass transfer, improved energy transfer and pressure and thermal differentials on a microscopic scale [122].
The sonication in the electrochemical process promotes the following benefits [122]:

1. The ultrasonic agitation via cavitation within the bulk interrupts the diffusion layer and stops the diminution of electro-active species
2. The transfer of ions across the electrode double layer is made available more evenly via ultrasonic agitation
3. Ultrasonic degassing prevent the accumulation of gas bubbles at the electrode
4. The electrode surface is continuously activated and cleaned via ultrasonic irradiation

E. Namgoong et al [128] were among those of first to make an effort towards the analysis of the effect of ultrasound implementation to an electrochemical system; this was the application of ultrasound directly to the cathode rather than the electrolyte throughout the electroplating experiments. The current efficiency of chromium deposits was observed to be reduced by 5%-10% resulted from pressure and temperature increase at the surface of the electrode. This enhancement in temperature and pressure is resulted from the cavitation caused by the ultrasonic field. Reisse et al [129] in a similar pattern reported the idea of a sonoelectrochemical reactor unique design in the literature with different approaches being detailed [130] [131] however the need for additional control was mentioned for some experiments, this type of control was used in order to work with specified potentials on both the working electrode and the titanium sonotrode [132].

Another field being subject of investigation in the area of sonoelectrochemistry is the leverage of medium in the spread of ultrasound. Mediums such as highly resistive ones for the effect of mass transfer [133], acoustically emulsified media [134] and organic solvents [135] have been investigated. Also low (20KHz) and high frequencies in sonoelectrochemical systems in terms of mass transfer and surface effects have been considered, low temperature, high pressure, sonochemical enhancement of electrochemiluminescence and high speed voltammetry are other aspects, which were analysed [124] [136].

T.J.Mason et al. reported that the ultrasound amends the chemistry of reactions at the electrode and significantly increases current efficiencies however the effects of ultrasound on electrochemical processes still needs considerable exploration [122].

The initial work in sonoelectrochemistry emphasised on depolarising effect of the ultrasound, at 280 kHz or 1200 kHz intense ultrasonic field, the investigation resulted to find out that hydrogen or chlorine deposition potentials are influenced by this strong field.

One of the early attempts to measure the amount of hydrogen gas released at the cathode was the work of F. Cataldo in early 90s who investigated the effect of ultrasound on the hydrogen and chlorine production during the electrolysis of aqueous solutions of NaCl and HCl. This was done under 30kHz- ultrasonic field and the electrolytic process included a Hoffman's coulometer submersed in an ultrasonic bath. It was reported that the effect of ultrasound is more evident with chlorine since its solubility is higher in water (i.e. 3150 ml/l) while that of oxygen is 19.6 ml/l at standard pressure and 15°C. In this work a very strong degassing effect of ultrasonic waves was observed, which was attributed to enhanced coalescence of gas bubbles and their mechanical stripping. This phenomenon vividly increased the chlorine gas generated in the presence of ultrasound [9].

F.Cataldo in another work reported the effect of ultrasonic irradiation on the conductivity of aqueous solutions such as KCl, LiCl and KI, it was stated that the ultrasonic irradiation of the aforementioned solutions increased their conductivity however this effect immediately faded away at the moment the ultrasonic filed was turned off. This phenomenon was clarified with collapse of the cavitation bubbles caused by the ultrasound. This was explained as the energy was released in the form of heat and shock waves hence increasing the temperature within the bulk of medium thus generating hot spots and this resulted in an increase in the conductivity [137].

In a study, the effects of the ultrasonic irradiation on the electrochemical reduction were researched employing the electrolysis and cyclic voltammetry at a constant potential. In this work benzaldehyde and benzoquinone electroreduction in different solvents were used as the solution in a sonoelectroreactor having the working electrodes operating as sonotrode as well. The electrode-solution interface and mass transfer were reported to be significantly affected by the ultrasound. It was determined that the ultrasound resulted in a dramatic change in the behaviour of the electroactive species. Alex Durant et al in this work compared mechanical stirring to the ultrasound and suggested that the stirring is almost as efficient as the ultrasound and more study is required to decisively conclude the benefits of the ultrasound over mechanical stirring [138].

The gas bubble collection on the surface of the electrodes is an important phenomenon having an effect on the efficiency of water electrolysis. The behaviour of gas bubbles at the electrodes has been the topic of research for several papers. Electrode surface coverage and bubble dispersion within the electrolyte were reported as two effective factors on the electrolysis of water. The gas bubbles on the surface of electrode

result in an increase in electrical resistance of the cell, stemmed from an increase in current density due to a rise in the number of gas bubbles and reduction in the active surface area of the electrode [105].

The ultrasound can be employed to enhance the efficiency by removal of gas blanketing on the electrode surface, promoting the bubble disengagement from the electrolyte and increased mass transfer. It was reported by Sheng-De Li et al that the ultrasound resulted in an energy saving of about 10-25% for hydrogen production at high current densities [105].

It is suggested by Sheng-De Li et al that the amount of energy that could be saved via the application of the ultrasound is reasonably notable compared to the investment in equipment and energy consumption by an ultrasonic filed. For instance, a 100 kA cell with a bubble-overpotential of 0.3V could save up to 30 kW while an ultrasonic filed uses about 0.05 kW only [105].

Pier Luigi Gentili et al have successfully produced hydrogen via water sonophotolysis in water/ethanol solutions. The highest amount of hydrogen produced in their work was attributed to concentrated suspensions using a catalyst named S: $La_{0.8}Ga_{0.2}lnO_3$. A piezoelectric transducer was responsible for generating 38 kHz ultrasound at 50W power output. A Xe lamp at 35W emitted the light used for this study, which was located on top of the reaction cell. The hydrogen production after 3 hours of treatment time for the samples containing 0.4g of the aforementioned catalyst in 200 mL water/ethanol was reported as follows; in photocatalysis (light) the amount was 4.44 µmol, sonocatalysis (ultrasound) 215.6 µmol and sonophotocatalysis (ultrasound and light) 269.6 µmol. The results consistently agreed on a greater amount of hydrogen being produced when the ultrasound and light are combined in comparison to the single use of the ultrasound and light. The ultrasound was also solely more productive than the light [139].

In a different study the effect of the ultrasound on an aqueous slurry containing alumina and polyacrylic acid was examined at 28, 45 and 100 kHz ultrasound. The results indicated that the viscosity of the slurry was changed by the act of the ultrasound resulted from breaking of hydrogen bonding networks of alumina and the acid. The viscosity was reduced as the output power was increased. The lower ultrasound frequency was also helpful in reducing the viscosity [140].

The ultrasound is considered a helpful tool in many areas such as chemistry, medicine, material sciences and etc. Although variety of works has been carried out with the aid of ultrasound in the field of chemistry and electrochemistry but majority used in chemical labs suffer from inflexibility due to the less control of the parameter. Most works are done in cleaning ultrasonic bath, which does not allow controlling the parameters. The frequency, intensity and irradiation mode could be subject of alteration, which would lead to significant areas of research and opens new windows [141].

Chapter 3: Experimental procedure

In this chapter the experimental procedure will be explained along with the materials and equipment used throughout the research. The experiments and the conditions of use are tabulated in table 3 in section 3.2.

3.1. Material and equipment

The materials used for this project includes sodium hydroxide and potassium hydroxide pellets, which were then solved into the water to produce the electrolyte of required molar concentration. Carbon rods (manufactured by Morganite) and nickel-based electrodes (Rolls Royce electrodes) were used as the electrodes with the diameter of 0.5 cm and 0.6 cm respectively. The electricity was supplied using a power supply (Thurlby PL320 32V-2A). A digital hydrogen flowmeter (Red-y compact flowmeter (L/min)) was in use in order to measure the rate of hydrogen production at the specified voltage and concentration. A magnetic stirrer was also utilised especially for high molar concentration, which stirs the solution using a magnetic bead. The ultrasound was irradiated to the medium using either an ultrasonic bath (Langford Ultrasonics 3.75l Ultrasonic Cleaning Tank, 40 kHz) or an ultrasonic transducer (Sonics Ti Alloy, 47 mm in diameter linked to Vibracell Sonics VCX750 set on 20 kHz). The amplitude of the ultrasound was set on 30% on the ultrasonic equipment. The water was pumped and heated through the external jacket of the cell using a water pump and heater (yellow line ET Basic) illustrated in figure 14. The separation distance between the electrodes was 7.5 cm.

3.2. Experiments

The experiments throughout this research projects were done under silent (unsonicated) and sonicated conditions and the silent results are compared to the case in which the ultrasound was applied to investigate whether the ultrasound has increased the hydrogen production. The experiments were carried out either in a custom glass cell demonstrated in figure 13 with a total volume of 1000 cm^3 ,at the bottom was attached an ultrasonic transducer (frequency used 20 kHz) or in a beaker positioned in an ultrasonic bath with the volume of 800 cm^3.

There were various parameters subject of change including temperature and concentration of the electrolyte, material of electrode and electrolyte, electrode surface area by altering the electrode active length.

The experimental conditions and parameters are reported in table 3. The first six pairs of experiments were done for low concentration (0.1M) and that is considered as the first part of the experiments. The 2nd part belongs to pairs 7 and 8 where higher concentrations were subject of the study. Each pair of experiment includes silent and sonicated conditions. The reason higher concentrations were experimented in this research was the fact that some industrial electrolysers employ this approach [142], [143] where the potential is reduced in comparison to the low concentration case. Having a look at the tables of the results in appendix III provided in the CD, one can see the difference between the potentials. Please refer to the tables 15 (concentration 0.1M) and 90 (concentration 15M) in appendix III for more information. For the experiments tabulated in table 90 the maximum potential applicable was 3.2V while this was 30V for the experiments in table 15.

Table 3: Table of Experiments.

Name	Electrolyte	Concentration	Temperature	Electrode Active surface area (cm^2)	Electrode
Pair 1	NaOH	0.1M	25°C	28.8, 32, 35.1, 38.25, 41.4	carbon rods
Pair 2	KOH	0.1M	25°C	same as above	carbon rods
Pair 3	NaOH	0.1M	25°C	32, 33.5, 35.1, 36.7, 38.25	carbon rods
Pair 4	KOH	0.1M	25°C	Same as above	carbon rods
Pair 5	NaOH	0.1M	No Temperature Regulation	28.8, 32, 35.1, 38.25, 41.4	carbon rods
Pair 6	KOH	0.1M	No Temperature Regulation	same as above	carbon rods
Pair 7	KOH	0.1M, 1M, 5M and 10M	25°C	40.12	RR (Nickel Based)
Pair 8	KOH	15M	25°C, 40°C and 60°C	38.25, 42, 45.8	RR (Nickel Based)

The electrode surface area was changed throughout this research project by varying the electrode active length from 9 cm to 13 cm to see its effect on the hydrogen production. These changes could be justified by pointing to the fact that at higher electrode surface area there are more available active sites for the electrochemical reaction on the surface of the electrode hence more current and hydrogen generation is expected. . The temperature of the electrolyte was increased since at higher temperatures ionic conductivity and the rate of the electrochemical reaction is enhanced [144].

Since the electrolytic process at the potentials higher than thermoneutral potential (1.48V) is exothermic, it was decided to try some experiment (pairs 5 and 6) without temperature control as the temperature of the electrolyte will be increased during the exothermic process with the heat being released [145]. The data sheets of 'no temperature control' experiments can be found in the appendix III (in CD) table 45 onward on page 49.

3.3. Experimental Technique

An electrolytic cell with a total volume of 1000 cm3 was used equipped with an ultrasonic horn (Sonics Ti Alloy, 47 mm in diameter linked to Vibracell Sonics VCX750 set on 20 kHz) at the bottom from which the ultrasonic irradiation can spread to the medium.

An ultrasonic bath (Langford Ultrasonics 3.75l Ultrasonic Cleaning Tank, 40 kHz) was also used which would transduce the ultrasound to the electrolyte at 800 cm^3.

In figure 13 the custom glassware with the volume of 1000 cm^3 is shown.

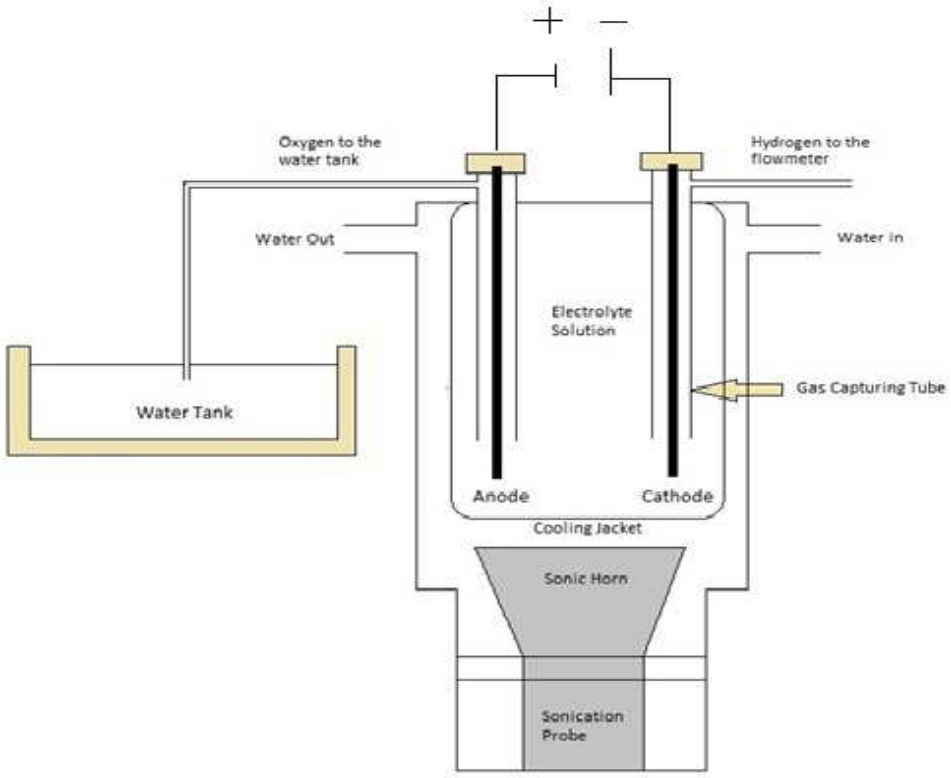

Figure 13: Schematic presentation of electrolytic cell.

Hydrogen gas was evolved at the cathode and oxygen at the anode. The generated hydrogen gas was measured using a digital hydrogen flowmeter (Red-y compact flowmeter (lit/min)).

The efficiency of the hydrogen gas produced may be calculated using the equation presented:

$$\text{Efficiency}(\%) = \frac{V_{Real}}{V_{Ideal}} \times 100\% \qquad (30)$$

This equation (Eqn 30) is the comparison of the actual hydrogen gas produced versus the ideal value. $V_{Real}(cm^3)$ is the hydrogen gas produced per unit of time, which is read by the flowmeter and $V_{Ideal}(cm^3)$ is the ideal volume of hydrogen gas generated, which can be calculated using the ideal gas law equation at the given conditions. The ideal volume may be calculated using the relation below [105]:

$$V_{Ideal}(cm3) = \frac{SIt}{nF} \times \frac{RT}{P} \qquad (31)$$

Where S is the stoichiometric coefficient, I is applied current, t is the time of operation, n is number of electrons transferred, F is Faradic constant (96484 C.mol^{-1}), T is the operating temperature in Kelvin, R is ideal gas constant (8.314 J.K^{-1}.mol^{-1}) and P is the pressure (atmospheric in Pascal).

The hydrogen and oxygen production rates may also be found on a molar basis from the equations below in respective order [72]:

$$N_{H_2} = \frac{JA}{2F} \qquad (32)$$

$$N_{O_2} = \frac{JA}{4F} \qquad (33)$$

Where N_{H_2} and N_{O_2} are the hydrogen and oxygen producing rates (mol.s^{-1}), J is the current density (A cm^{-2}), A is surface are (cm^2) and F is Faraday's constant (96485 C mol^{-1})

In figure 14 the electrolytic cell is shown during the operation for high concentration (15M) KOH electrolysis.

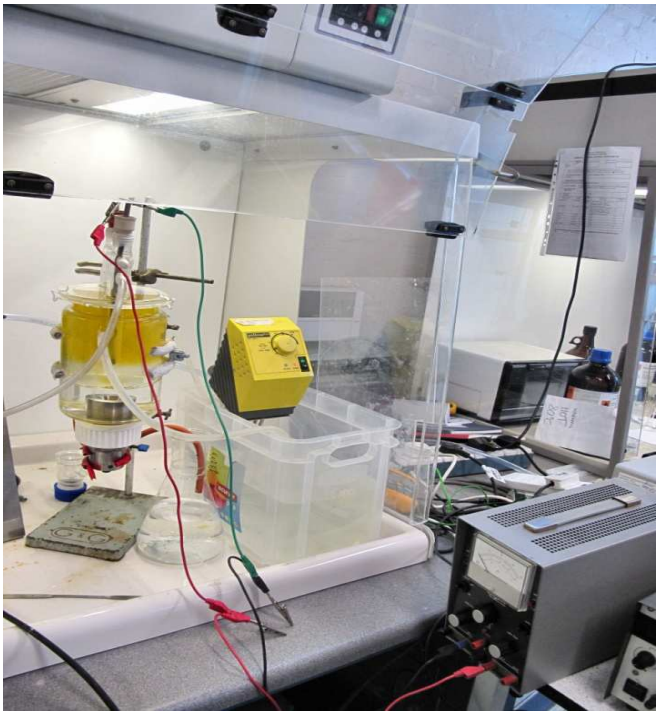

Figure 14: The custom glassware during electrolysis of 15 molar concentration KOH.

3.4. Electrolyte Preparation

In order to obtain the required molar concentration, masses of KOH or NaOH necessary to make the solution are found then dissolved into water to achieve a final volume of one litre. In tables 4 and 5 below various masses, required to have different concentrations, are shown. The electrolytic cell or reaction vessel was entirely filled up with the solution and sealed using three crocodile clips to prevent the escape of gas bubbles from the cell.

Table 4**:** Mass of electrolytes.

Concentration (M)	**Mass of Electrolyte (g) for the final volume of 1000 mL**	
	NaOH	**KOH**
0.1M	4.0	5.61
1M	40	56.10
5M	200	280.5
10M	400	561
15M	600	841.5

The concentrations however for 85% KOH pellet are different as tabulated below in table 5.

Table 5: Mass of electrolytes.

Concentration (M)	Mass of electrolyte (KOH) (g) for final volume of 1000 mL[85% KOH pellet]	Mass of KOH for final volume of 800 mL[85% KOH pellet]
0.1	6.60	5.28
1	66.01	52.81
5	330.06	264.04
10	660.12	528.10
15	990.30	792.13

Chapter 4: Analysis, Interpretations of Results and Discussion

In this chapter the author goes through the analysis of the current and current density generation and explaining the electrical resistance using the current-voltage graph. The decomposition potential and overpotential are then evaluated followed by the hydrogen generation comparison for silent and ultrasound-aided experiments. The effects of ultrasound, temperature and concentration are presented using the graphs and tables staring from sections 4.1 to 4.5. There are separate sections assigned to the energy and the effects of electrode surface area and electrodes on the production of hydrogen namely as 4.6, 4.7 and 4.8.

4.1. Current Generation

In figure 15 a current-voltage graph shows that by increasing the voltage, the current is increased and that the higher the electrode active length (i.e. electrode active surface area), the greater the current is for the given voltage. In the graph shown in this figure it is clear that for KOH the produced currents are higher than NaOH. This is due to fact that potassium hydroxide is a stronger electrolyte than NaOH since it is more electrically conductive and has higher molecular mobility where electrons can move more freely compared to sodium hydroxide thus the current is transferred more readily.

The solutions with smaller ions are generally more conductive compared to the solutions with larger ions since the viscous drag is less in them. The conductivity is inversely proportional to the radius of hydrated ion (i.e. $\lambda \propto 1/\text{radius}$) [146]. Sodium ions have larger solvation shells (known as hydration shell when water is the solvent) than Potassium ions, sodium ions because of their greater charge density attract more water to

become hydrated leading to a greater radius of their hydrated ion hence potassium hydroxide is more conductive than sodium hydroxide [147], [148].

According to Ohm's law $R = \frac{V}{I}$ where R is Ohmic resistance, V (volts) is potential and I is the current (A). If the potential is increased at a greater rate than the current, then the ohmic resistance is increased otherwise a reduction in resistance is observed. During the experiments it was observed that an increase in potential resulted in the current being generated at a greater rate hence resulted in a reduction in resistance. (Tables of data can be found on appendix III page 9 of the document provided on CD)

For instance for 0.1M NaOH silent experiment at the electrode active length 9 cm (surface area: 28.8 cm^2) and 25°C, the resistance started at 1000Ω for 1Volts of potential and 0.001 amperes of current and had a decreasing pattern and at 30V potential and 0.924A current, the resistance was reduced to 32.47 Ω, similar pattern was noted for other active areas. In figure 16 a graph of electrode active length versus resistance shows the pattern.

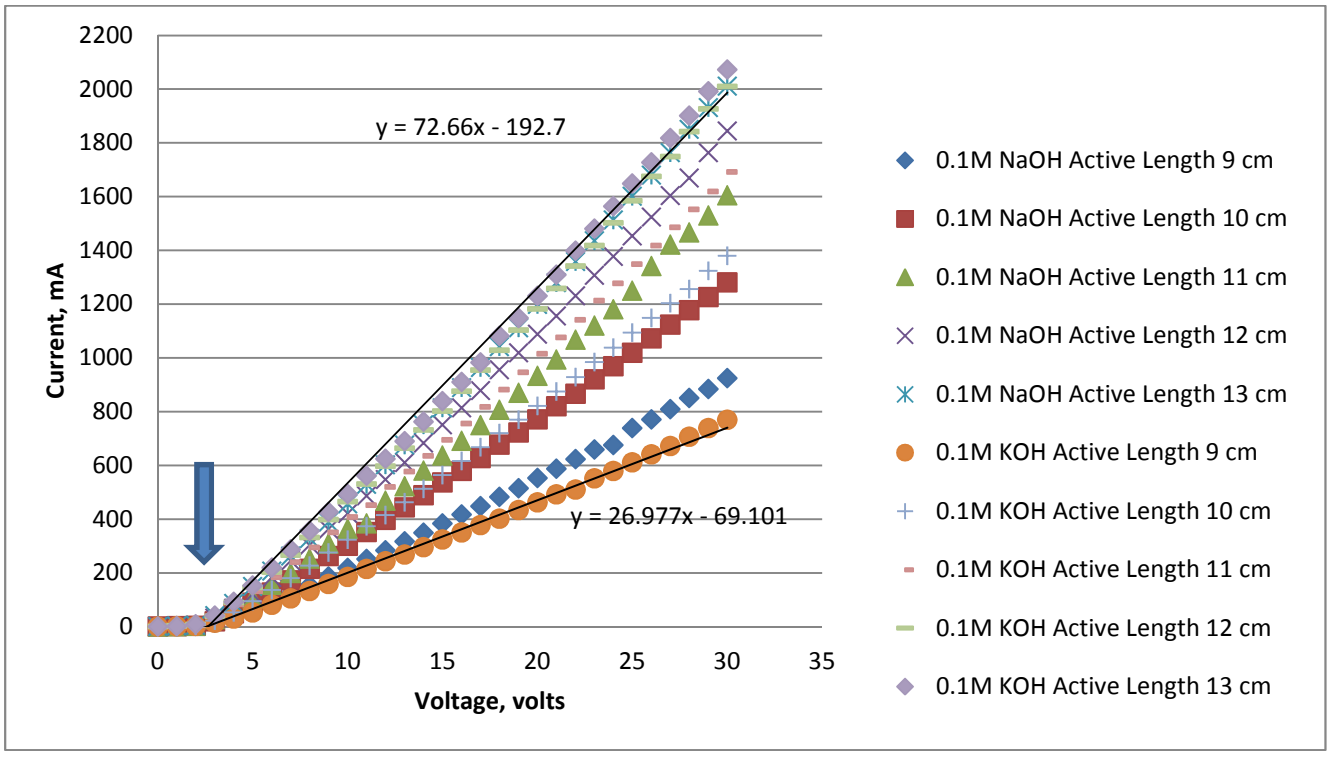

Figure 15: Current-Voltage graph for silent NaOH and KOH at 25° C.

The Current-Voltage curves in this graph (Figure 15) can be used to calculate the decomposition potentials for each curve. Figure 16 demonstrates that the higher the electrode active length (i.e. more surface area), the less the resistance will be. The ohmic resistances are calculated from 0-30V and currents for each applied

surface area for comparison. The lowest resistance for this experiment (Silent condition) was 14.92 Ω belonging to the applied potential of 30 volts and generated current of 2.011 amperes.

In figure 16 it can also be seen that the introduction of ultrasound further decreases the resistance, for this experiment under sonicated condition the lowest resistance was 13.97 Ω at 30V and 2.147A and electrode active length of 13 cm. The ultrasound helps remove gas bubbles at the surface of the electrode and also within the electrolyte. These bubbles are resistance to ionic transfer in the electrolyte and cause of transport-related resistances [104]. This may be compared to the literature work carried out by Sheng-De Li et al [105] who also reported a reduction in the electrolyte resistance when the ultrasonic field is on. The behaviour of gas bubbles has an impact on the electrode surface coverage and void faction of the electrolyte solution, which is proportional to ohmic resistance according to Qian et al [149]. The application of the ultrasonic field results in the removal of bubbles away from the electrodes as well as void fraction of the bulk electrolyte.

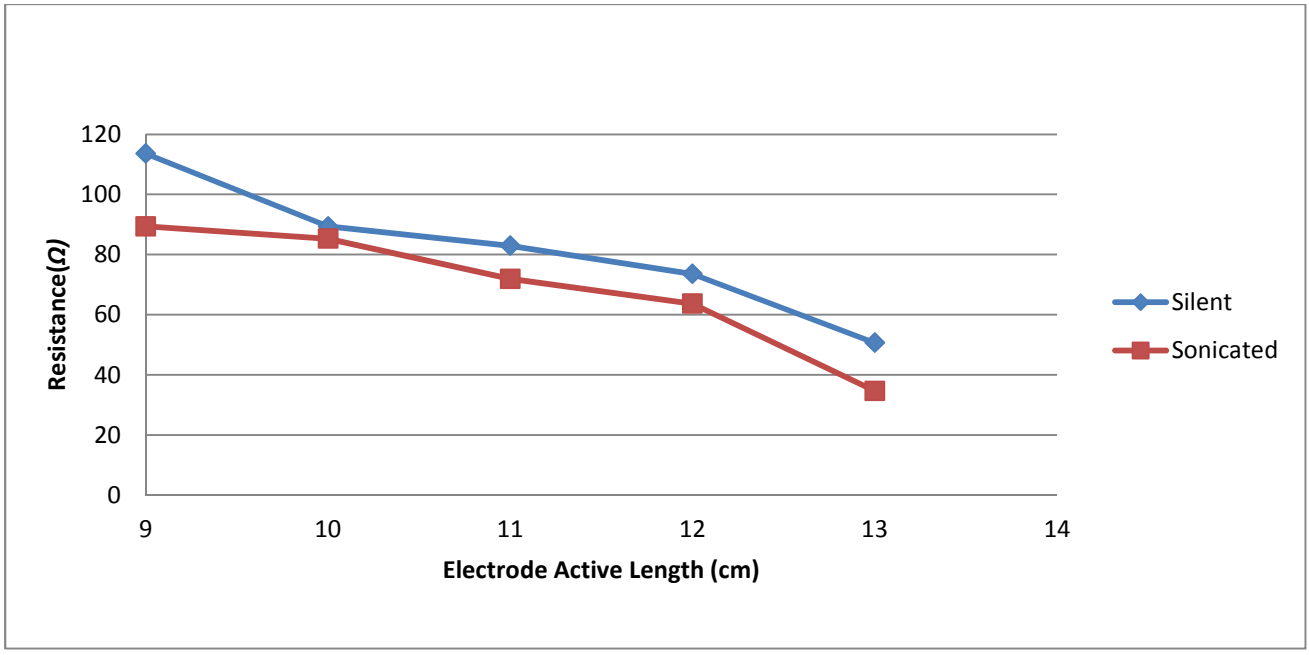

Figure 16: Graph of electrode active length versus Ohmic resistance for 0.1M NaOH at 25°C.

It may be suggested, having a look at figure 15, that the resistance is increased by increasing the voltage considering the equations of the line for individual curves and finding the slope of the line, however it must be noted that the resistance is the voltage divided by the current at a certain point according to ohm's law, not the division of changes in voltage by changes in current ($\Delta V/\Delta I$). Furthermore the gradient of the line on the current-voltage curves does not represent resistance as it gives $\Delta I/\Delta V$, which is-

[Changes in Current/Changes in voltage] . More accurate method is to use ohms law for individual cell voltages applied and generated currents and plot the graph as shown in figure 16.

In the next figure (17) a comparison of current-voltage curves is done for sodium hydroxide and potassium hydroxide electrolytes at 9 cm electrode active length (28.8 cm^2 surface area) for silent and sonicated conditions. In figure 17 it is shown that the ultrasound enhances the current generation through enhanced mass transfer and conductivity.

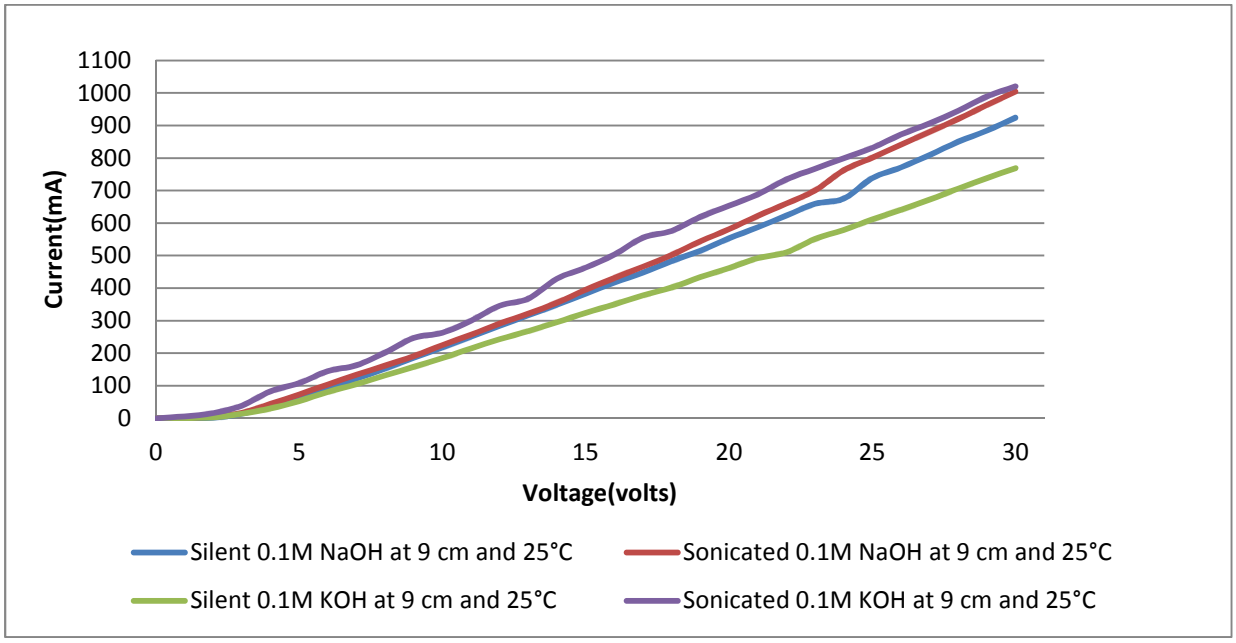

Figure 17: Current-voltage graph comparison for NaOH and KOH at 25°C.

For sodium hydroxide (NaOH) experiment in this figure (17) it was calculated that the ultrasound increased the current by between 20-27.5 mA and current density by 1.90 mA/cm^2 for the individual applied potentials whereas the enhancement in current and current density for potassium hydroxide at 9 cm electrode active length and 25°C were 112-136.5 mA and 9.5 mA/cm^2 respectively.

This shows the ultrasound has been more effective for potassium hydroxide and the reason may be the fact that KOH is a more active electrolyte than NaOH and the ultrasound seems to have boosted the mass transfer and conductivity much better in potassium hydroxide.

In figure 18 the effect of concentration is investigated on the electrolysis where an increase in the generated current can be seen when the concentration of the electrolyte is increased. This is resulted from the augmentation of charge carriers in the solution therefore more current is produced. Higher concentration means there is more H^+ and OH^- ions in the solution hence the electrical current is increased and the resistance is reduced. The ohmic resistance for the experiments at 5M and 10M were reduced down to 2.31Ω (for 4.85V, 104.6 mA/cm^2) and 2.17Ω (for 4.72V, 108.2 mA/cm^2) respectively, which shows that at

higher concentrations the resistance is considerably reduced. This was compared to the resistance calculated for 0.1M for this experiment, which was 30Ω at 30V potential and 49.83 mA/cm^2 of current density.

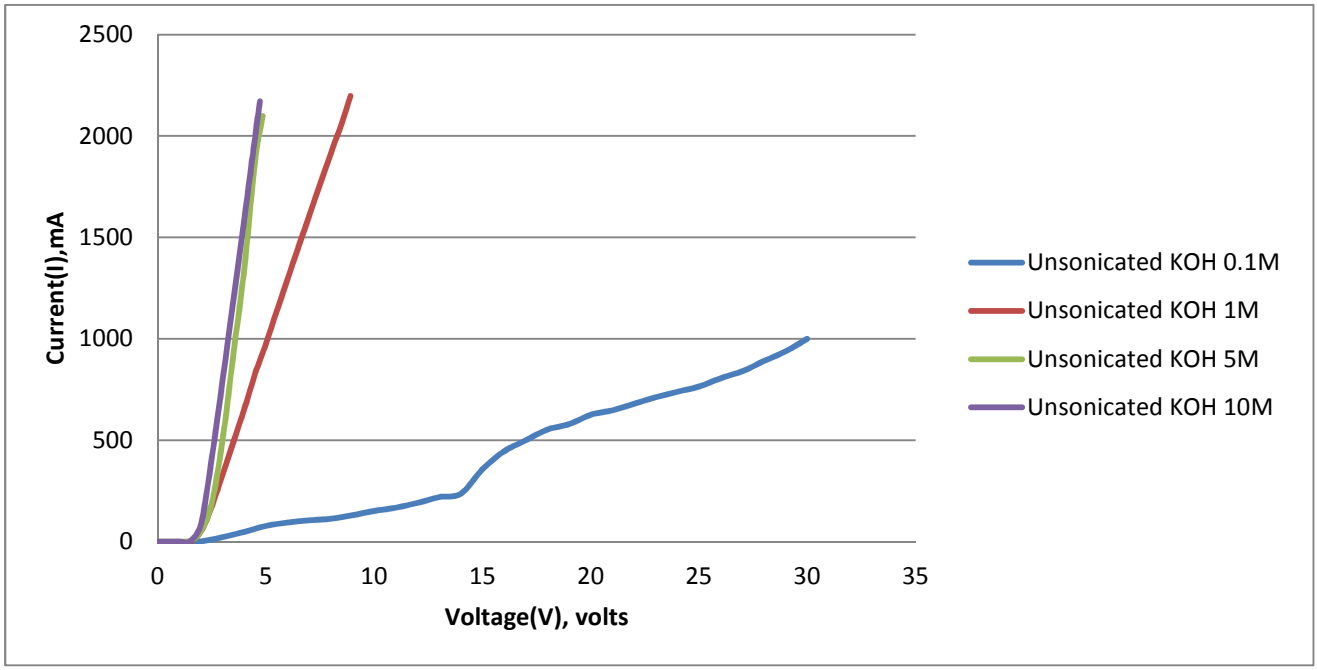

Figure 18: Silent current voltage graph for potassium hydroxide at various concentrations and 10.5 cm electrode active length (surface area: 40.12 cm^2).

The maximum applied voltage for 10M concentration experiment shown in figure 18 was 4.72 volts, which generated 2171 mA of current, at 5M concentration the voltage and current were 4.85V and 2099 mA respectively, for 1M this was 8.9V and 2197 mA and finally for 0.1M concentration the maximum applied voltage was 30V and the current was 1000 mA. It was expected to see a greater difference in current generation between10M and 5M however the graph shows otherwise. At high concentration when the potential is increased the surface of electrodes are covered with the bubbles and the electrodes may have been deactivated hence less current is generated as well as less hydrogen produced. This electrode surface coverage results in a reduction in the active surface area therefore higher current density.

The effect of temperature on the current generation is considered for high concentration experiment at 15M potassium hydroxide where the changes were measured for 3V of applied potential. The graphical demonstration of this is presented in figure 19. According to Jason C. Ganley, at high temperatures the ionic conductivity is increased as well as the rate of electrochemical reactions at the surface of the electrode [144].

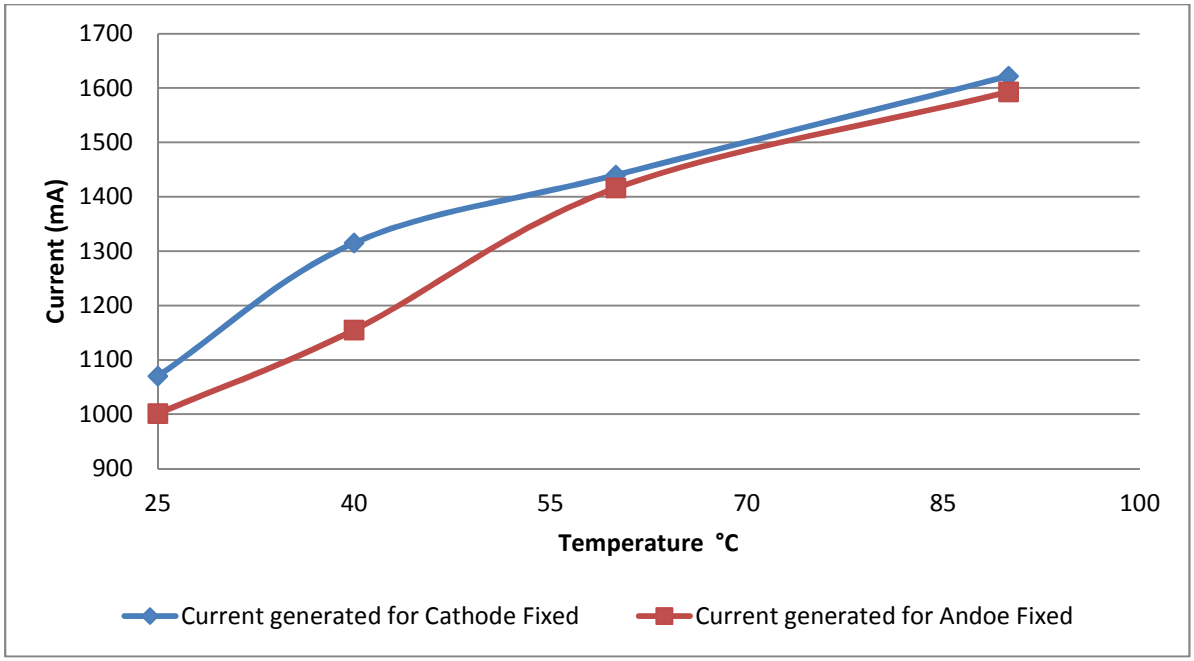

Figure 19: Graph of average current produced for temperature changes at 3V for 15M KOH.

The current generation is increased as the temperature is raised as can be seen in figure 19. The greatest current in this experiment was 1718 mA produced at 90°C and the smallest value was recorded at 25°C, which was 782 mA. The current density was also improved by increasing temperature, for example the current density for anode fixed experiment at 25°C started at 26.4 $\mathrm{mA/cm^2}$ and it was at its peak value (40.15 $\mathrm{mA/cm^2}$) at 90°C.

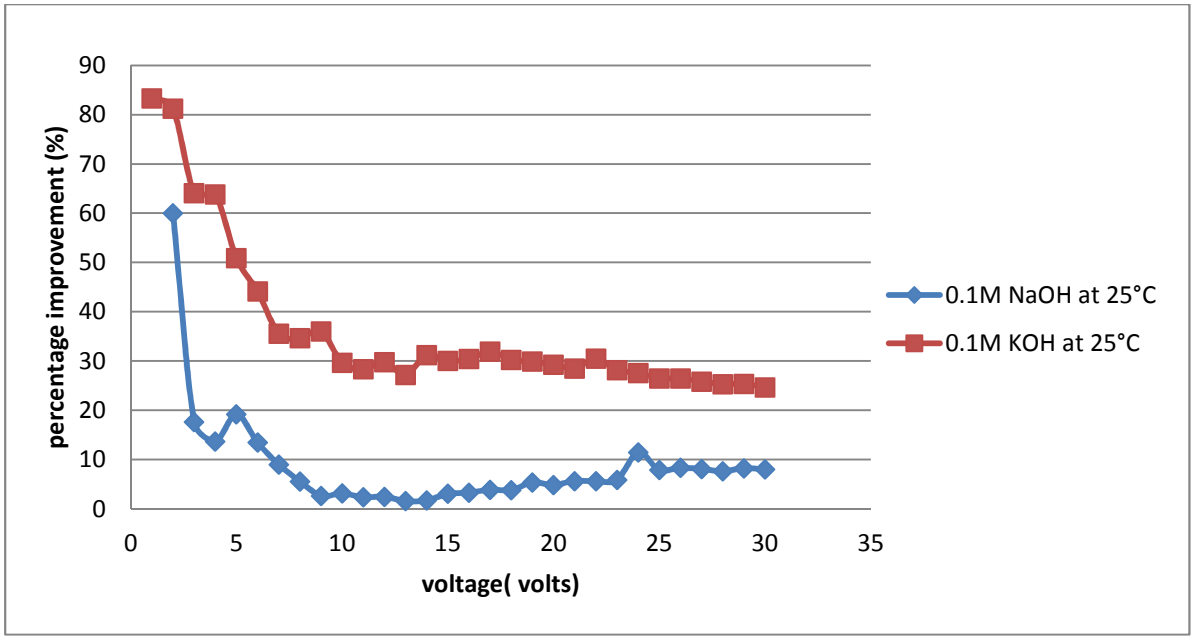

Figure 20: Current enhancement for selected experiments at 28.8 $\mathrm{cm^2}$ active surface area.

The current generation was recorded for silent and sonicated conditions and it was observed that the current is always increased when the voltage is increased. In figure 20 a graph of current enhancement is plotted. The current enhancement for a set of experiment is calculated; the generated current at a voltage under sonicated experiment is subtracted from a current generated under silent condition for the same voltages.

A comparison of two curves on the graph in figure 20 displays a greater enhancement for potassium hydroxide curve (Red curve), that is resulted from the nature of the electrolyte. Not all of the current enhancement graphs followed a similar pattern though, for instance figure 50 on page 144 in appendix V (in CD) shows the pattern for 0.1M KOH at 25°C or figure 49 where the curves display fluctuations. These patterns are resulted from the actual fluctuations in the current generation at each applied potential, which may be resulted from the voltage drop and resistances throughout the cell, the resistances were mentioned in the literature survey by Zeng et al [6].

4.2. Decomposition potential and overpotential determination

4.2.1. Decomposition potential

In 2.4.2.1 it was explained how to calculate decomposition voltages using the current-voltage graph. In order to find the values of decomposition voltage using the graph, the equation of the line is constructed assuming y=0, then one may be able to find the value. In figure 15 on the graph, the blue arrow shows the region of decomposition voltages, this is a representation of the voltages at which the process of electrolyte decomposition starts however these potentials for various curves on the graphs are different and one may be able to see the differences having a look at I-V graph, also the equation for each plotted curve is different.

In figure 21 the effect of surface area on the decomposition potential is shown where it can be seen a reduction in this potential as the surface area is increased. The increase of electrode surface area by varying its active length, means that there are more sites available for the electrochemical reaction at the surface of electrode hence the amount of the minimum potential that must be applied between the electrodes before the current flows, may be reduced (i.e. the decomposition potential is reduced). The lowest decomposition potential calculated for sonicated 0.1M NaOH was 1.71 volts, which was related to the greatest surface area ($41.38\mathrm{cm}^2$) and the lowest value for the other experiment shown in red in figure 21 was also associated with greatest electrode surface area and that was 1.99 volts.

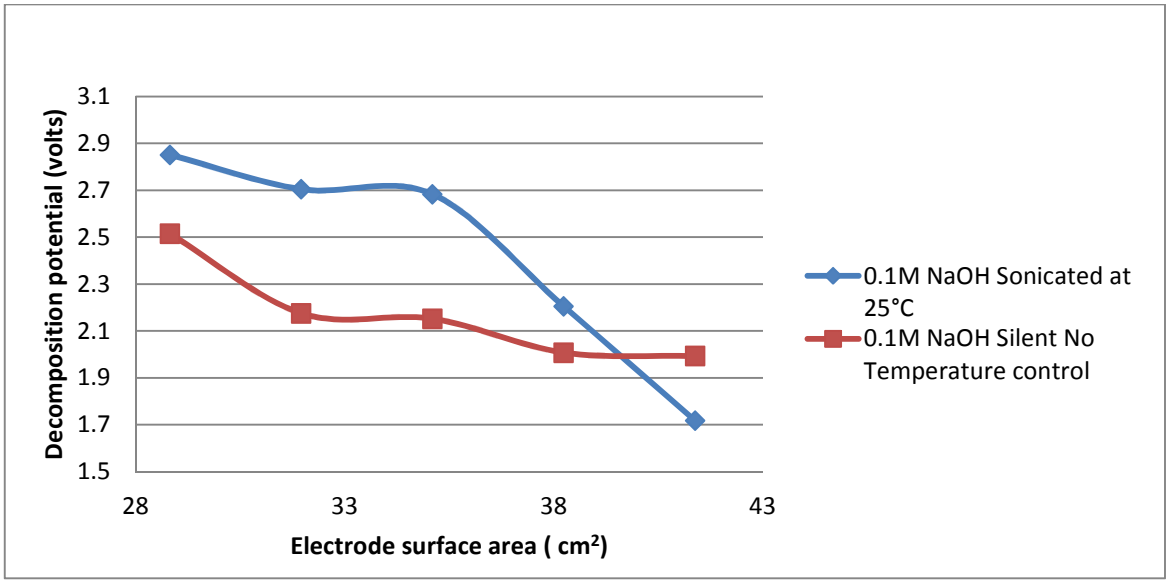

Figure 21: Graph of decomposition potential versus surface area for selected experiments.

According to Vladimir M. Nikolic et al a reduction in cell potential is obtained either by altering the catalytic nature of the overpotetnial for HER or by increasing true surface area of an electrode [74] and above on figure 21 the latter case's effect is shown even though this was not the case for all of the experiments. Further experimentation is required to draw a more comprehensive inference.

Figure 21 also displays that the temperature is another factor effective in the reduction of decomposition voltage. The experiment for which the red curve is plotted on the graph benefited from no temperature control, the starting temperature of the cell was 25°C and the average finishing temperature reached to about 35°C, this was compared to the experiment where the temperature was constant at 25°C.

The increase of temperature inside the cell within the electrolyte is resulted from exothermic electrochemical reactions occurring on the electrodes, which would release heat owing to temperature increase if there is no control.

S.K. Mazloomi et al in their work state the influence of higher temperature in an electrolytic process, that the electrolysis is more efficient when the temperature is raised. The water splitting reaction potential is also said to decrease as the temperature is increased. An increase in temperature also raises the ionic conductivity and surface reaction of an electrolyte [150].

A comparison of silent and sonicated conditions shows that the introduction of the ultrasound reduces the decomposition potential. Table 6 below compares the values at silent and sonicated for selected experiments and proves this. The ultrasound increases mass transfer from one electrode to another, removes the gas bubble from the electrode surface and within the electrolyte and prepares the surface of electrode for electrochemical reaction via electrode surface cleaning.

Table 6: Comparison of decomposition potentials for various experiments under silent and sonicated conditions.

	Decomposition Potential (Volts)	
Experiment	With Ultrasound	Without Ultrasound
0.1M NaOH at 25°C and 13 cm electrode active length	2.74	1.71
0.1M KOH at 25°C and 9 cm electrode active length	2.56	1.83
0.1M KOH Silent without temperature control at 11 cm active length	2.62	1.79
0.1M NaOH without temperature control at 10 cm active length	2.17	1.90
5M KOH at 25°C and 10.5 cm electrode active length	1.05	0.96

Another parameter is the concentration of electrolyte whose effect was considered on the decomposition potential. An increase in concentration of potassium hydroxide from 0.1M to 10M has significantly influenced this potential. The water molecules started to decompose at 3.54V for the experiment done for 0.1M KOH at 25°C and 10.5 cm electrode active length $(\text{surface area: } 40.12\ \text{cm}^2)$ while the decomposition of water molecules for this experiment at 5M and 10M concentration were 1.06V and 0.95V respectively. An increase in the number of charge carriers gives rise to this reduction. The average decomposition potential for various experiments is tabulated in table 7 where a decrease in the potential is observed at high concentration experiments. The potential for 15M KOH in table 7 is 0.83V that is less than that of the reversible potential (1.23V). This may be referred to as underpotential deposition (UPD), which occurs when the species in a medium are electrodeposited. This is usually the case for the reduction of a metal cation to a solid metal. This indicates that the depositing atoms on a crystal surface (adatom) are attached to the foreign metal electrode strongly (nickel electrode in our case). In other words the UPD occurs as a result of strong interaction between the electrodepositing metal in the solution and the substrate (electrode material/ Nickel) [151], [152] however this may hardly be the case as there seems to be no interaction of this kind between nickel electrode and potassium hydroxide other than oxidation of nickel to nickel oxide [153], therefore it may be hard to imagine the potassium metal plates out from the KOH electrolyte and coat the electrode surface. More investigation is required using different electrochemical and surface characterisation techniques such as cyclic voltammetry technique, Fourier transform infrared reflection (FTIR), Surface-enhanced Raman spectroscopy (SERS), scanning tunnelling microscopy (STM) and atomic force microscopy (AFM) [152].

Table 7: Average decomposition potential.

Experiments	Average Decomposition Voltage (volts)
0.1M NaOH (silent and sonicated)	2.44
0.1M KOH(silent and sonicated)	2.33
KOH 10M (silent and sonicated)	0.95
KOH 1M (silent and sonicated	1.22
15M KOH at various Temperatures and Electrode Surface Area	0.83

In table 8 the decomposition potentials for silent and sonicated shown in table 7 are separated and presented where the effect of ultrasound once again can be seen more general compared to table 6.

Table 8: Decomposition potential for different experiments.

		0.1M NaOH	**0.1M KOH**	**KOH at various concentrations**
Decomposition Voltage (V)	**Unsonicated**	2.57	2.52	1.77
	Sonicated	2.31	2.14	1.30

4.2.2. Overpotential

The basic definition of overpotential was explained in 2.4.2.2 and it was stated in 2.4.2.1 that the overpotential can be found using equation 18 and 19. The equations 20 and 21 in 2.4.2.2.1 can be used to separately calculate the overpotential of cathode and anode. Here are the equations 20 and 21 respectively:

$$\eta_{\text{Cathode}} = 2.3\frac{RT}{\alpha F}\log\frac{i}{i_0},\ \eta_{\text{Anode}} = 2.3\frac{RT}{(1-\alpha)F}\log\frac{i}{i_0}$$

In equations 20 and 21 the term exchange current density (i_0) is unknown for our work since our electrolytic cell was 2-electrode system therefore not applicable. A three-electrode system may be required to separately find anode and cathode overpotentials since it allows studying anode and cathode half-cell reactions regardless of one another. In a three electrode system (voltammetry), a reference electrode is used along with a working electrode and an auxiliary electrode. The current and current density is measured for anode and cathode separately with respect to the reference electrode.

Equation 18 is used to determine the overpotential but first the reversible potential must be calculated for various experiments. In order to calculate the reversible potential (E_{Rev}^{Cell}) of a system, equations 10 (2.4.1.1) and 19 (2.4.2.1) can be applied [85] [154].
A sample calculation can be found on the next page to find overpotential for 0.1M NaOH at 25°C where the decomposition potential is 2.68V.The half-cell reactions are balanced with base since sodium and potassium hydroxide were used [155].

Oxygen- water half-cell reaction at the anode is given by [155]**:**

$2H_2O\ (l) + 4e^- + O_2\ (g) \rightarrow 4OH^-(aq)$

Where number of electrons n=4, F= 96485 c/mol, T=298.15K, R= 8.314J.K^{-1}.mol^{-1} and Standard Electrode Potential (SEP) E^0=-1.23V for Oxygen, hence via equation 10:

$$E_{Rev,a} = E° + \frac{RT}{nF}\ln\frac{[OH^-]^4}{[H_2O]^2} \rightarrow E_{Rev,a} = -1.23 + \frac{8.314\times298.15}{4\times96485}\ln\frac{0.1^4}{1} \rightarrow E_{Rev,a} = -1.23 + (-0.0591) = -1.289V$$

Hydrogen half-cell reaction at the cathode is:

$4H_2O\ (l) + 4\ e^- \rightarrow 2H_2\ (g) + 4OH^-\ (aq)$

Where n=4 and E^0 =0 for hydrogen and other values are the same as above thus we can write;

$$E_{Rev,C} = 0 + 6.422\times10^{-3}\ln\frac{0.1^4}{1} \rightarrow E_{Rev,C} = -0.0591V$$

The reversible potential of the cell can be found using equation 19, therefore:

$$E_{Rev}^{Cell} = |\ E_{Rev,C} - E_{Rev,a}\ | = |\ -0.0591 - (-1.289)\ | \rightarrow E_{Rev}^{Cell} = 1.230V$$

Therefore the overpotential can be determined via equation 18:

$$\eta = E_D - E_{Rev}^{Cell} \rightarrow \eta = 2.68 - 1.23 = 1.45V$$

When the concentration and temperature are changed the reversible potential could be calculated by replacing their values into the equations above however equation 10 is applied for low concentration experiments and at high concentrations in which the solution is far from ideal conditions, equation 11 may be used where the activity is applied instead of concentration. In table 9 [147] the activity coefficient for KOH is shown at different concentrations where the activity can be found via $a = \gamma\frac{C}{C_0}$ with C being the concentration of solute,C_0 the standard concentration and γ the activity coefficient [148], [147].

Table 9: activity coefficient for potassium hydroxide.

KOH	Activity coefficient (γ)
0.1M	0.779
1M	0.773
5M	1.697
10M	6.110
15M	19.9

The Cell's reversible potential for 10M KOH at 25°C is calculated using equation 11 and table 9 ($a = \gamma \frac{C}{C_0} = 6.11 \times \frac{10M}{1M} = 61.1$), which is 1.226V. If equation 10 is used for this molarity, the cell's reversible potential will be 1.229V, which is a close value to 1.226V. Therefore it may be okay to use both equations interchangeably since the difference is trivial. Furthermore in equations 10 and 11 (logarithmic term: $\ln \frac{a_O}{a_R}$ or $\ln \frac{C^*_O}{C^*_R}$, the expression before logarithm: $\frac{RT}{nF}$), the change in temperature from 25°C to 90°C and also change in concentration from 0.1M to 15M did not result in major difference in the value of cell's reversible potential since logarithmic term is used and also faraday constant value is large in the denominator and an increase in temperature in our work does not greatly influence the final value of the reversible potential. The water activity was assumed 1 for the calculations.

For instance the reversible potential of the cell for 0.1M KOH at 25°C is 1.23V and its value for 15M KOH at 25°C is also 1.23V. Another example is the reversible potential of the cell for 0.1M KOH at 25°C, which is 1.229V while at 90°C, it is 1.230V. Therefore it is okay to assume that the cell's reversible potential for all experiments is 1.23V. In tables 10 and 11 the overpotentials are calculated using equation 18.

The Nernst equation for concentrated solutions can be defined in terms of activity of species involved in reduction and oxidation or partial pressure of gases, below one can find the Nernst equation using this approach [156] [157]:

Water / hydrogen:

$4H_2O + 4e^- \rightarrow 2H_2 + 4OH^-$ (34)

Water / oxygen (as a reduction half-reaction):

$2H_2O + 4e^- + O_2 \rightarrow 4OH^-$ (35)

Nernst equation for the water / hydrogen electrode (cathode) where ($\mathbf{E^o} = -0.84$) [156] [157]:

$$\mathbf{E = E^o - \frac{RT}{4F} \ln \left(\frac{a_{H_2}{}^2 a_{OH^-}{}^4}{a_{H_2O}{}^4} \right)} \quad (36)$$

Nernst equation for the water / oxygen electrode (Anode) where ($\mathbf{E^o} = 0.39$):

$$\mathbf{E = E^o - \frac{RT}{4F} \ln \left(\frac{a_{OH^-}{}^4}{a_{O_2} a_{H_2O}{}^2} \right)} \quad (37)$$

Overall reaction is Eq. 34 – Eq. 35:

$4H_2O + 4e^- – 2H_2O – 4e^- – O_2 \rightarrow 2H_2 + 4OH^- – 4OH^-$

That gives: $2H_2O \rightarrow O_2 + 2H_2$

Therefore the Nernst equation becomes Eq. 36 – Eq. 37 for the whole cell:

$$\mathbf{E = -0.84 - \frac{RT}{4F} \ln \left(\frac{a_{H_2}{}^2 a_{OH^-}{}^4}{a_{H_2O}{}^4} \right) - 0.39 - \left[- \frac{RT}{4F} \ln \left(\frac{a_{OH^-}{}^4}{a_{O_2} a_{H_2O}{}^2} \right) \right]}$$

$$= -\mathbf{1.23} - \frac{\mathbf{RT}}{\mathbf{4F}} \ln\left(\frac{{a_{H_2}}^2 {a_{OH^-}}^4 a_{O_2} {a_{H_2O}}^2}{{a_{H_2O}}^4 {a_{OH^-}}^4}\right) = -\mathbf{1.23} - \frac{\mathbf{RT}}{\mathbf{4F}} \ln\left(\frac{{P_{H_2}}^2 P_{O_2}}{{a_{H_2O}}^2}\right) \quad (38)$$

Where activity $a = \frac{P}{P^0}$ with P being partial pressure and P^0 is the atmospheric pressure (P^0=1bar)

The negative sign after E^0 in equations 36 and 37 results from the logarithmic term as the reduced species are on top of the fraction and oxidised at the bottom unlike equations 10 and 11. The final expression in equation 38 is based on partial pressure of gases, the term P^0 disappears when the activity is written in terms of partial pressure as it is divided by 1 bar. The term activity remains in the denominator as the system is liquid and water is being used as the solution. The calculation could be carried out using the partial pressure of the gases but since the pressure inside our cell was not measured hence the activity of liquid species can be used to do the calculations at higher concentrations (5M-15M) [157].

Table 10: Overpotential for various experiments.

Experiments	Average Overpotential (volts)
0.1M NaOH (silent and sonicated)	1.24
0.1M KOH(silent and sonicated)	1.10
KOH 1M, 10M (silent and sonicated)	1.03, 0.27
15M KOH at various Temperatures and Lengths	-0.40

Table 11: Overpotential comparison for silent and sonicated.

		0.1M NaOH	0.1M KOH	KOH at various concentrations
Overpotential	**Unsonicated**	1.34	1.30	0.47
	Sonicated	1.09	0.92	0.07

The overpotential for 15M experiments was negative as the average value was demonstrated in table 10. This may be resulted from a faster reaction rate and very low resistive losses in this experiment. More exploration is needed to see the effect of high concentration on the rate of reaction and resistive losses. In the literature [158] though, the negative overpotential is referred to as underpotential (deposition), which is defined as the voltage below the optimum value for a device or component [159]. Underpotential deposition (UPD) was explained in 4.2.1. The decomposition potentials and overpotentials for various experiments can be found in appendix II on page 5.

4.3. Current density

Current density is the current flowing through a conductor per unit cross-sectional area and is measured in amperes per square metre [160]. Figure 22 illustrates the current density changes for the change in surface area of the electrodes for chosen experiments under silent and sonicated conditions. The base of comparison on this graph is to see the effect of surface area at a constant 15V voltage for sodium and potassium hydroxide. Increasing the surface area by $9.45\ \mathrm{cm}^2$ results in an increase in the current density by the following values for the specified experiments at 15 volts:

- Enhancement in current density (relative to the primary value) for 0.1M NaOH Silent: 16.1 mA
- Enhancement in current density for 0.1M NaOH Sonicated: 14.4. mA
- Enhancement in current density for 0.1M KOH Silent: 33.1 mA
- Enhancement in current density for 0.1M KOH Sonicated: 24.2 mA

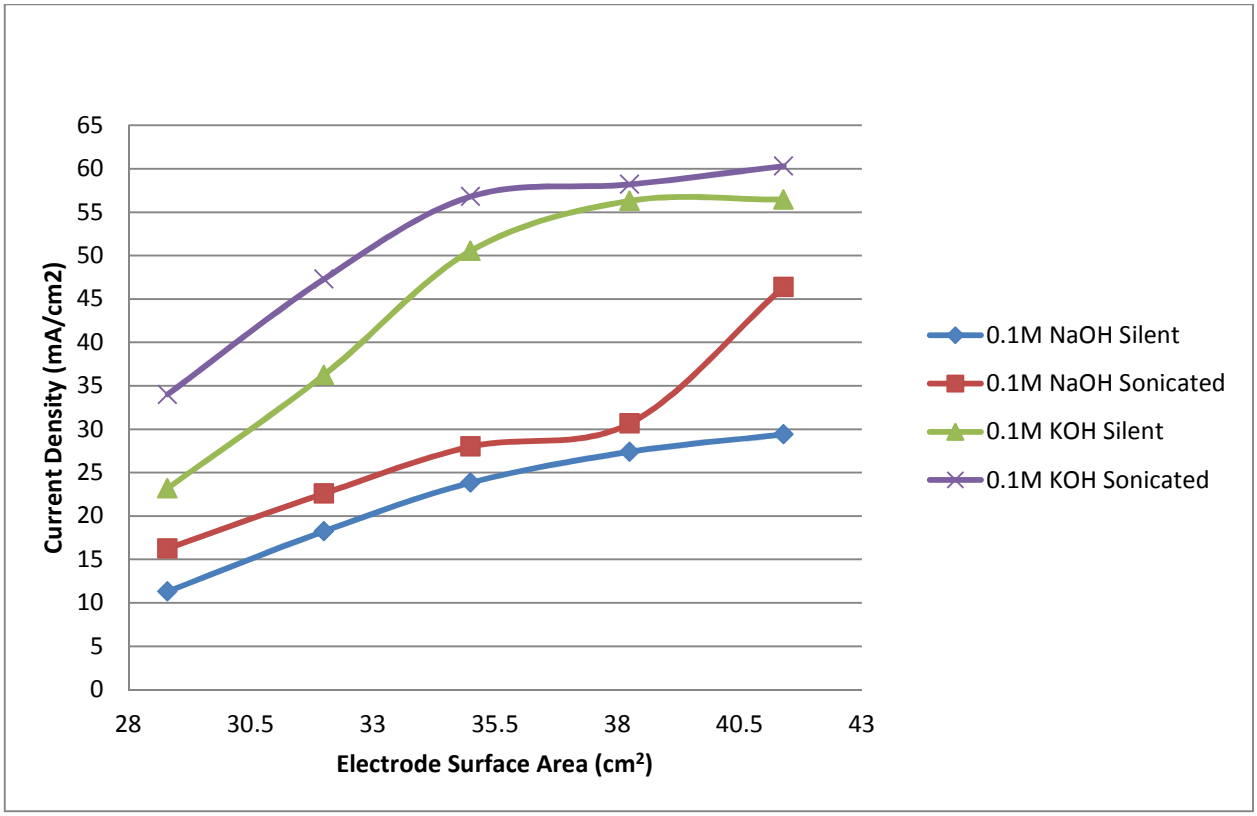

Figure 22: Graph of current density versus surface area for different experiments at 15V, no temperature control.

The ultrasound has increased the current density as can be observed from the graph above in figure 22. This increase was calculated for 0.1M NaOH experiment to be 4.17 mA and for 0.1M KOH to be 7.5 mA. The increase is higher for potassium hydroxide as expected since this electrolyte is more conductive than sodium

hydroxide. A decrease in current density may be expected by an increase in electrode surface area according to the current density and current relation however since an increase in electrode surface area considerably increases the current therefore current density is increased overall.

An increase in voltage also increases the current density, in figure 23 an increase in current density for different experiments is shown using a graph of current density-voltage. This increase is expected as the current density is a function of current and its value is raised when the cell's potential is increased.

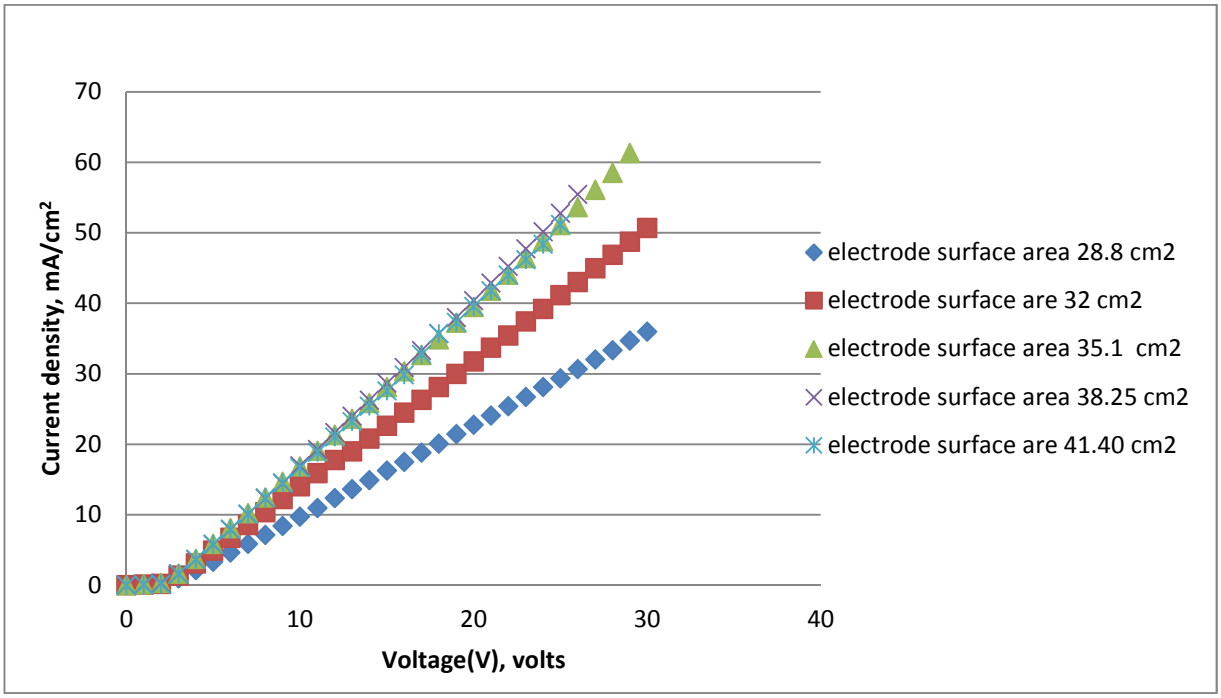

Figure 23: Current density- Voltage graph for sonicated 0.1M NaOH without temperature control.

Figure 24 demonstrates the enhancement in current density when the ultrasound is applied. The enhancement in current density is obtained by finding the difference between sonicated and silent experiments for applied potentials and electrode active lengths (active surface area). On the graph in figure 24, the low active lengths (active surface area) account for highest improvement in current density, which may be resulted from gas blanketing on the surface of electrode that decreases the active surface area hence increases the current density as the current density is Current/Surface Area. The current density-voltage graph for different experiments can be found in appendix V figure 17 onward on page 128.

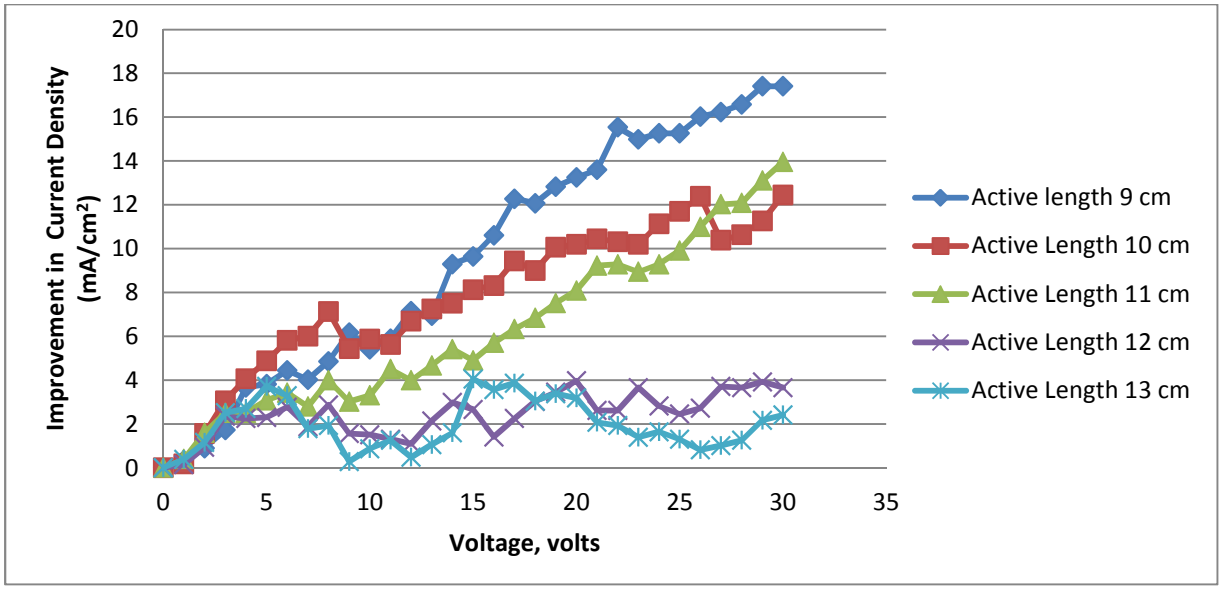

Figure 24: Graph of improvement in current density versus voltage for 0.1M KOH at 25°C.

The curves on the graph in figure 24 fluctuate and do not follow a regular pattern. This was observed for majority of experiments. The current density is a function of current and since the current generation was accompanied by fluctuations resulted from various resistances and potential drop hence the irregularities are expected for the current density as well until the resistances are reduced to minimum. The repetition of the experiments in a different cell with reduced resistances is highly recommended.

4.4. Hydrogen Generation

The hydrogen generation measurement was carried out using a digital hydrogen flow meter. The hydrogen gas was produced at the cathode and captured through a glass tube.

The hydrogen production for silent experiment with 1.0 M concentration KOH at 25°C (40.12 cm^2 electrode surface area, Nickel-based electrode) was 0.31 L/min with the applied voltage of 5.5V and current density of 28.16 mA/cm^2. The volume of the cell was 800 cm^3 for this experiment and the cell was filled with the electrolyte. This may be compared to the literature work carried out by Ebru Önder Kiliç et al who produced hydrogen at a rate of 3.2 mL/min (0.0032 L/min) at 25 mA/cm^2 of current density [108]. The current density values are similar but Ebru et al had a much lower rate produced compared to our work. They used 3.0 M HCOOH and 2.5 M NaOH solution as the electrolyte but our electrolyte was 1.0M KOH.

The voltage requirement is decreased by increasing the electrolyte concentration. The highest voltage applied for 0.1M NaOH and KOH experiment is 30 volts, however this is significantly reduced at 10M KOH

and 15M KOH to 3.72V and 3.2V respectively. The highest hydrogen generation was recorded 0.72 $\mathrm{L/min}$ (12 cm^3/second) for sonicated 10M KOH at 25°C and 4.65V potential.

Another literature work by W.L. Guo et al reported hydrogen generation at a rate of 53 $\mu\mathrm{mol/hr}$ for 3.0 M HCOOH and 2.5 M NaOH solution at a current density of 8.0 $\mathrm{mA/cm^2}$ [110]. An initial electrolysis voltage as low as 0.30V was used when the concentration of the formic acid was larger than 0.8×10^{-9}M.

The best comparison to W.L.Guo et al may be the experiment done for 1.0M KOH at 25°C and electrode surface area of 40.1 $\mathrm{cm^2}$, the rate of recorded hydrogen production was 0.6 $\mathrm{litre/min}$ for the applied voltage of 8.5 volts. This is equal to $8.69 \times 10^{-4}\,\mathrm{gram/second}$ that is a better value compared to that of W.L.Guo (53 $\mu\mathrm{mol/hr}$ equal to 2.96×10^{-8} $\mathrm{gram/second}$) however their applied potential was very low compared to our work and the current density in our experiment was about 20 mA/cm^2, which was larger than theirs. Therefore the carry-out of the experiments at low potential and high electrode surface area and high concentration is recommended.

Figure 25 shows a graph of enhancement in hydrogen generation for potassium hydroxide at different applied voltages.

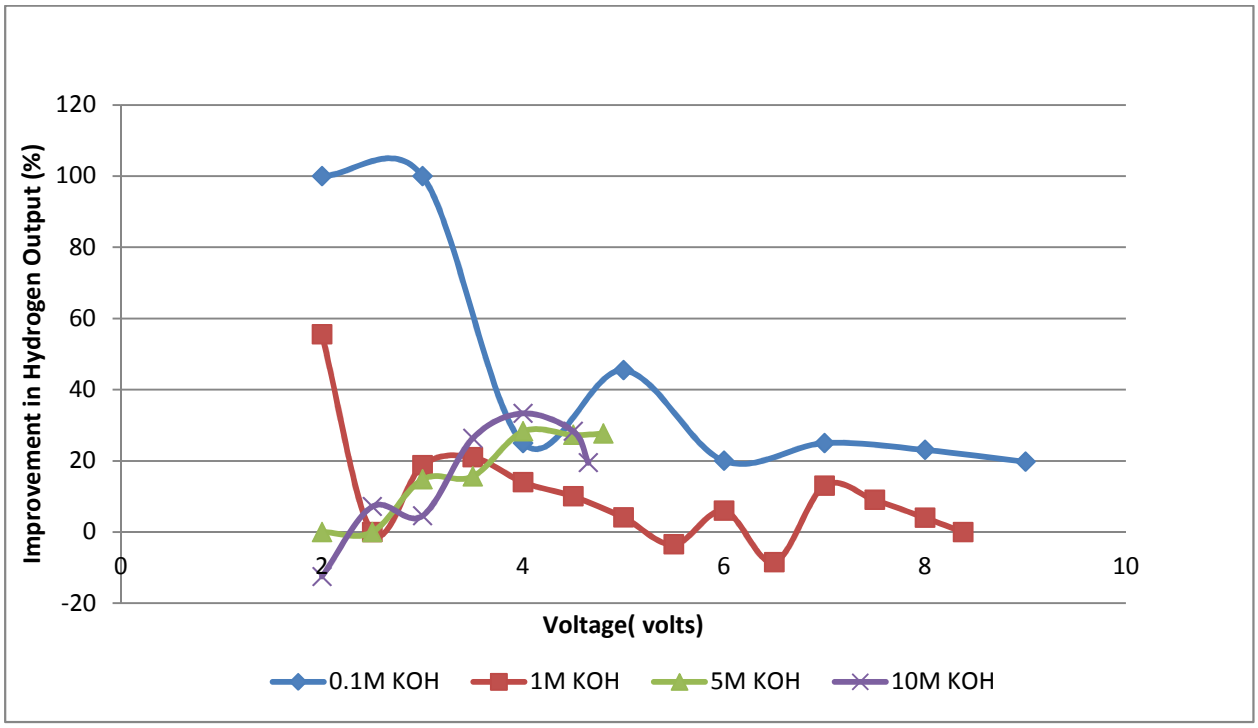

Figure 25: Enhancement in hydrogen production at 25°C, electrode surface area: 40.1 $\mathbf{cm^2}$ (electrode active length 10.5 cm)

The greatest improvement in hydrogen generation occurs for 10M experiment, which was 0.17 $\mathrm{L/min}$ at an applied potential of 4.65V while this was 0.18 $\mathrm{L/min}$ for 5M at 4.8V. The curves on the graph in figure 25 do

not follow a regular pattern, which is originated from the cell deign, resistances in the production of hydrogen such as transport-related resistances, electrical resistances of the DC supplier and voltage drop therefore variation in the hydrogen production for silent and sonicated experiment leading to a graph such as the one presented in figure 25.

Increasing the potential does not seem to result a steady improvement in hydrogen generation either (Figure 25), for instance at 5.5V, the improvement for 1M is -0.01 $\mathrm{L/min}$, even though it is 0.04 at $\mathrm{L/min}$ at 5V and 0.02 $\mathrm{L/min}$ at 6V potential. This pattern is resulted from the aforementioned reasons.

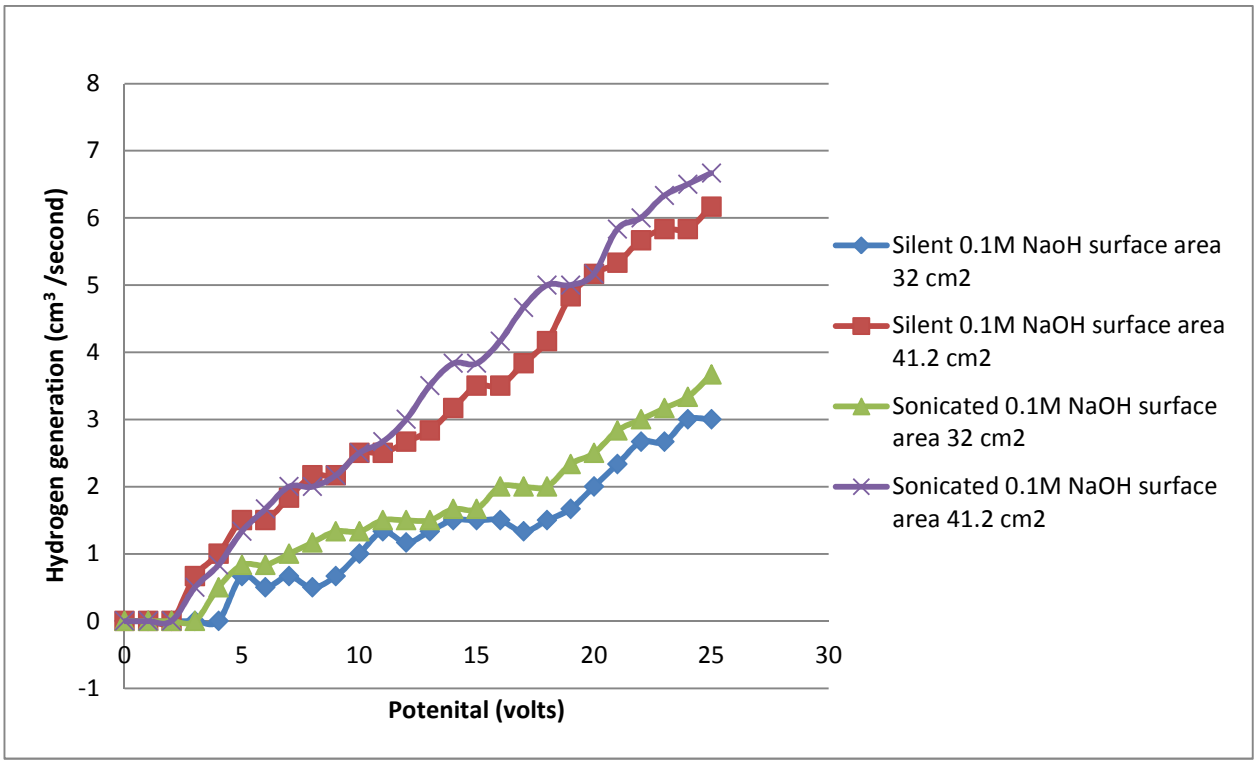

Figure 26: Hydrogen generation rate for selected experiments at 25°C.

Figure 26 above shows rate of hydrogen generation in cubic centimetre per second as the cell potential is increased. The greatest rate of hydrogen was generated at higher potentials applied as can be seen in this figure. For the presented experiments, the lowest applied voltage at which the hydrogen generation was recorded, belonged to silent and sonicated experiments at 3V and electrode surface area of 41.2 cm^2. It is expected that the experiments with ultrasound lead to higher hydrogen generation and that was the case. The results can be seen in tables 12 and 13. More graphs on hydrogen production can be found in appendix V (located in the CD) figure 33 onward on page 136.

Table 12 below demonstrates the improvement in hydrogen production for selected potentials. This improvement is the difference between the produced values for sonicated and silent experiments. The negative improvements are errors emanated from the cell design and different resistances throughout the cell including electrical, electrochemical and transport resistances.

Table 12: Improvement in hydrogen production for different experiments.

Experiments	Improvement in Hydrogen production (%)		
	3V	15V	25V
0.1M NaOH Various electrode surface areas	22.22%	6.33%	7.75%
0.1M KOH various electrode surface areas	33.33%	17.9%	21.7%
0.1M NaOH fixed anode, various cathode surface area	28.6%	-9.2%	1.46%
0.1M KOH fixed anode, various cathode surface area	0.0%	5.62%	-1.42%
0.1M NaOH various surface area without Temperature control	-36.6%	5.88%	18.8%
0.1M KOH various surface area without temperature control	0.0%	4%	25%

In table 13 the average values of enhancement for hydrogen production is displayed for various experiments where the highest improvement is attributed to the potassium hydroxide at 0.1M concentration.

Table 13: Enhancement in hydrogen production for different experiment. * Electrode surface area.

Experiments at 25°C unless otherwise mentioned	Improvement in Hydrogen production (percentage)
0.1M NaOH Various electrode surface area (*e.s.a)	13.82%
0.1M KOH various e.s.a	25%
0.1M NaOH fixed anode, various cathode e.s.a	7.5%
0.1M KOH fixed anode, various cathode e.s.a	13%
0.1M NaOH various e.s.a No Temperature Regulation	7.8%
0.1M KOH various e.s.a No temperature Regulation	19.2%
KOH various molar concentration e.s.a. 40.1 cm^2	18.5%
15M KOH Silent various temperatures	8.0%

The ultrasound has improved the hydrogen generation for most of the applied potentials, it was expected to see greater enhancement in production at higher potentials but that was not the case. The hydrogen gas bubbles did not always go through the capturing tube at the cathode, especially for higher potentials and electrode surface area. This is resulted from the diameter of capturing tube as it was not large enough to allow all hydrogen gas bubbles in, hence caused invalid reading at high potentials such as 20V and above. The other factors, which may have influenced the hydrogen generation, are electrode coverage by gas bubbles, electrode deactivation as a result of high gas concentration on the electrode surface and different

resistances as mentioned in section 2.6. The hydrogen production was improved by about 65% when the electrode surface area was increased by about 45%. This was calculated finding the increase in surface area and increase in the hydrogen production over that surface area increase then finding the percentage. For instance the increase from 28.8 cm^2 to 41.4 cm^2 is 12.6 cm^2 and the percentage increase in surface area can be found as follows: $[(41.4 - 28.8)/\ 28.8] \times 100$ = 43.75%. The same method is used to find the percentage increase in hydrogen production.

The hydrogen production was enhanced by about 11% when the ultrasound was applied, this could be calculated having a look at tables 12 and 13 and using the same technique mentioned above.
For example the improvement in hydrogen generation for the first experiment on table 13 is 0.024 L/min. The hydrogen production for this experiment was 0.146 L/min (calculated from the table of data, Appendix III table 5 onward), which gives the percentage increase as $[0.024/\ 0.146] \times 100\% = 16.44\%$ meaning that the ultrasound has improved the hydrogen generation by 16.44% for this experiment.

4.5. Hydrogen generation efficiency

The hydrogen production efficiency may be found using the equations 30 and 31 in 3.3, here are the equations again:

$$\text{Efficiency}(\%) = \frac{\text{V}_{\text{Real}}}{\text{V}_{\text{Ideal}}}$$

$$\text{V}_{\text{Ideal}}(\text{cm3}) = \frac{\text{SIt}}{\text{nF}} \times \frac{\text{RT}}{\text{P}}$$

The hydrogen production efficiency for the electrolysis cell was calculated for each potential applied and every electrode surface area employed. The data sheets in appendix III (CD provided) deliver the information regarding to the efficiency calculated for each potential, hydrogen generation, current density and etc.

The efficiency was plotted against the applied potential for sodium hydroxide at the specified operating conditions in figure 27. The efficiency curves do not follow a steady shape with increase or decrease in the potential. This may be explained by referring to equation 31 in 3.3 for the ideal volume calculations. In the stated equation, time and current are the numerator and since the time of hydrogen generation for every applied potential was different, as was the current generated, hence the variations on the graph in figure 27 could be justified. For 18V potential as an example, the time of hydrogen generation with the ultrasound was 36 seconds leading to the production efficiency of about 88% at this voltage, however this was 42 seconds for the silent case and the production efficiency was nearly 74%.

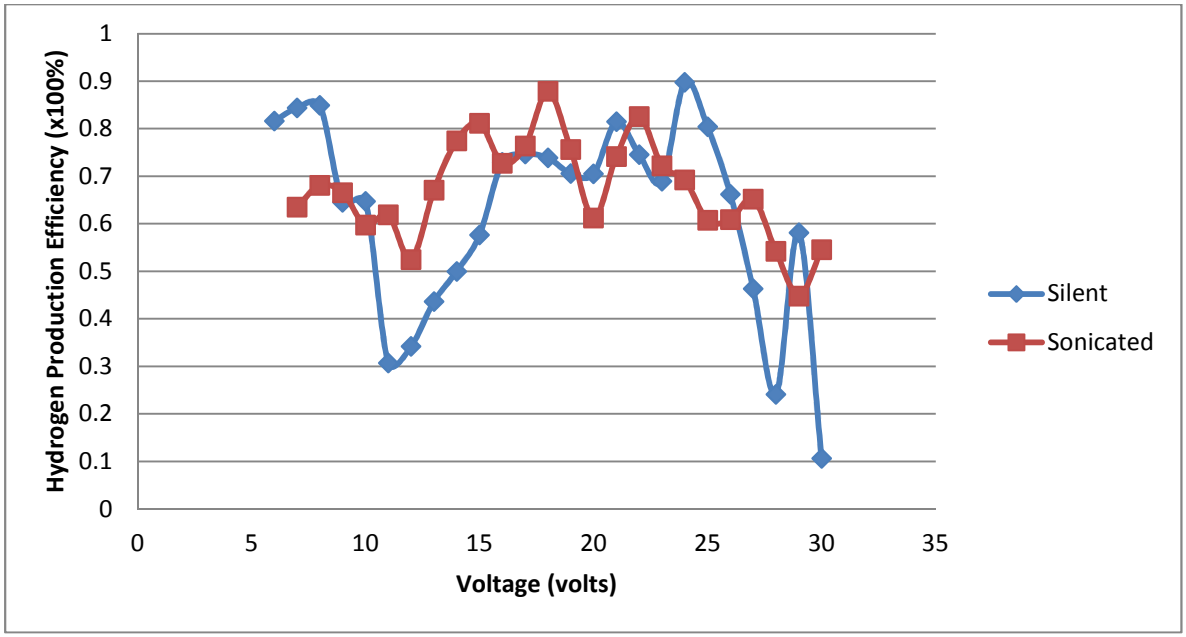

Figure 27: Graph of production Efficiency Vs. Voltage for NaOH at 25°C, 35.1 $\mathbf{cm^2}$electrode surface area.

The efficiencies of up to 96% have been mentioned in the literature by some researchers employing electrodes such as low carbon steel [74] and 10 vol% 1-butyl-3-methyl-imidazolium-tetrafluoroborate (MBI.MF4)in water as electrolyte under current density of 44 $\mathrm{mA/cm^2}$ [150] while commercial and industrial electrolysers are usually less than 73% efficient [76]. Therefore our study could be compared with the literature work [74, 76 and 150] done since our efficiencies were similar in value as they are reported in table 15.

The enhancement in efficiency for numerous experiments was calculated and tabulated in table 14 below. This enhancement is the difference of the efficiency for sonicated and silent conditions.

Table 14: Improvement in production efficiency.

Experiments at 25°C unless otherwise mentioned	Improvement in Efficiency (%)
0.1M NaOH Various electrode surface area (A)	5.31
0.1M KOH various electrode surface area (A′)	3.26
0.1M NaOH fixed anode, various cathode surface area (B)	1.70
0.1M KOH fixed anode, various cathode surface area (B′)	5.20
0.1M NaOH various electrode surface area No Temperature Regulation (C)	-4.47
0.1M KOH various electrode surface area No temperature Regulation (C′)	4.03
KOH various molar concentration and 40.1 $\mathrm{cm^2}$ surface area	25.60
15M KOH Silent various temperatures	5.24

The improvement in efficiency could be compared for potassium hydroxide and sodium hydroxide electrolytes using table 14 for the denoted experiments on the table. A comparison of (A) and (A′) shows that at 0.1M concentration sodium hydroxide had a better production efficiency (2.05% better) however the opposite was expected since KOH solution is more conductive [161]. For B-B' and C-C' cases, potassium hydroxide is more efficient for hydrogen production with better improvements of 3.5% and 8.5% respectively.

The efficiency of hydrogen production in another experiment was calculated for the case in which the potential was constant at 2.5V and the effect of electrode surface area was considered for 1M KOH at 25°C (Nickel-Based Electrode). The comparison was done for both silent and sonicated conditions, the result is reported in figure 28. The increase in surface area results in a raise in the efficiency for both silent and sonicated cases, additionally the ultrasound further increases the efficiency for this experiment.

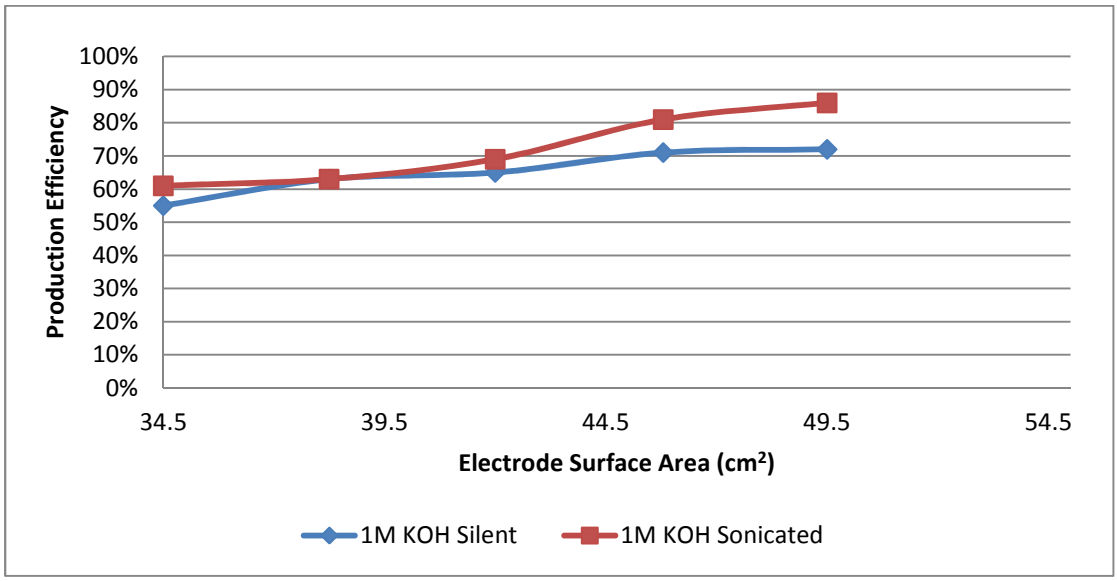

Figure 28: Graph of efficiency versus electrode surface area for 1M KOH at 25°C, Nickel-Based electrodes, 2.5V Potential.

It was observed that the increase of electrode surface area results in higher rate of current being generated whilst the time of hydrogen generation is slightly reduced as a result of this increase, since time and current are main influencing factors in order to find the ideal volume (Eqn. 31 in 3.3.), hence the efficiency (Eqn. 30 in 3.3.) is indirectly related to the electrode surface area and directly to the time and current. Figure 28 clarifies these changes in production efficiency. Equations 30 and 31 can be again found below respectively:

$$\text{Efficiency}(\%) = \frac{V_{Real}}{V_{Ideal}}$$

$$V_{Ideal}(cm3) = \frac{SIt}{nF} \times \frac{RT}{P}$$

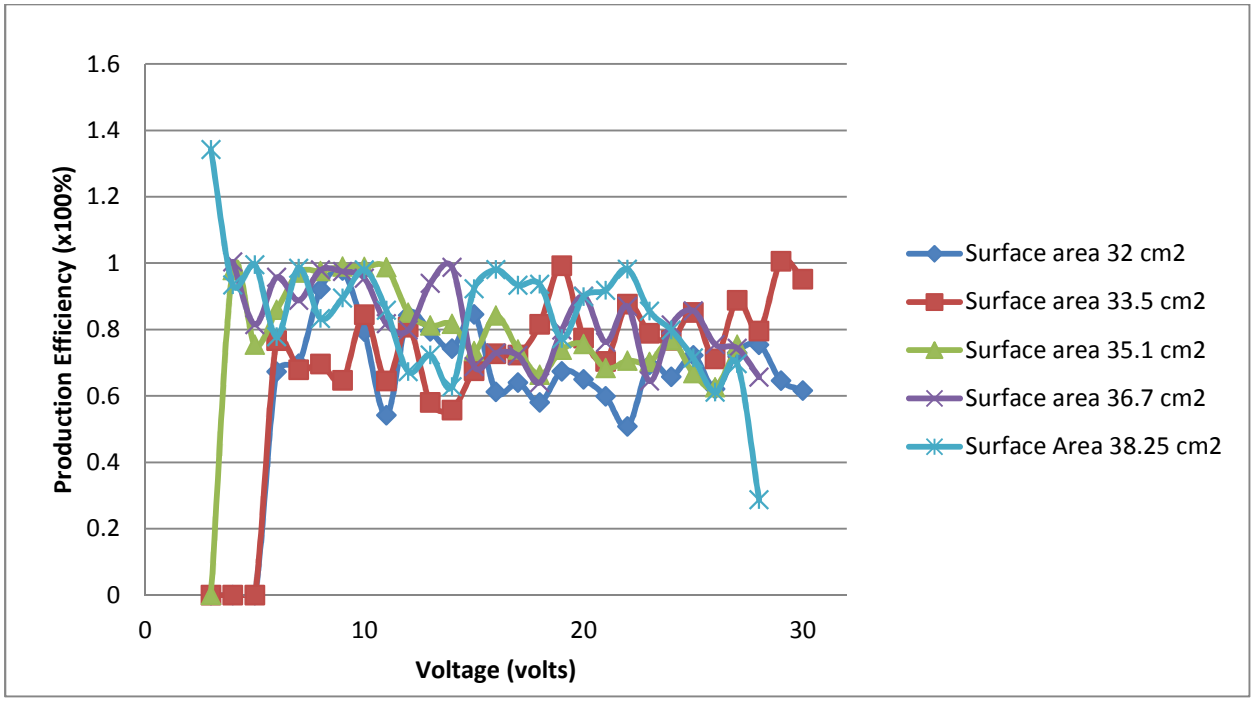

Figure 29: Production efficiency for 0.1M NaOH at 25°C.

Figure 29 displays the production efficiency behaviour with the increase in the potential for a selected experiment. The efficiency is between 60-90% for majority of applied voltages and as seen above there is no linear increase in efficiency with an increase in voltage. The efficiencies above 100% may be errors, which may be resulted from malfunction of DC supplier for a certain voltage or errors in reading by the digital hydrogen flowmeter. The graphs for the improvement in efficiency for various experiments can be found in appendix V figure 65 and onwards on page 152. In table 15 below the production efficiency for different experiments is demonstrated.

Table 15: Production Efficiency for different experiment silent and sonicated.

Experiment	Production Efficiency (%)
0.1M NaOH at 25°C	78.44
0.1M KOH at 25°C	77.1
0.1M NaOH without Temperature Control	68.92
0.1M KOH without Temperature Control	66
15M KOH	70.55

The overall efficiency of the electrolytic cell could be averaged using table 15 efficiencies, which would give the average value of about 72%.

4.6. Energy

The energy balance on a system demonstrates how efficient a process is in terms of energy consumption when the produced energy is compared to the consumed amount of energy. An energy balance on the electrolytic system shows how much energy is used to produce a certain amount of energy in the form of hydrogen.

The amount of electrical energy consumption for hydrogen production can be found using the relation described below in equation 39 and ultrasonic power consumption via (Eqn.40) [74] [162]

$$P = V \times I \text{ And } Energy = P \times t \qquad (39)$$

Where P is power (watt or Joule/s), V and I are overall voltage (volts), t is time (s) and current (amperes) through the cell respectively.

The energy consumed for the sonicated experiments may be found via equation 40 assuming that the losses are negligible and all the ultrasound goes to the temperature increase (i.e. heat):

$$Q \text{ (joules)} = mC_p\Delta T \qquad (40)$$

Where ΔT is the change in the temperature of electrolyte, m (grams) is the mass of electrolyte solution and C_p is the specific heat capacity of the solution (electrolyte) (j/kg.K).

The material properties and the ultrasonic power of materials can be seen in appendix IX tables 134 and 135 on page 162. The value of dT/dt (change in temperature over time) was calculated for each electrolyte by measuring the temperature changes over a period of time at 30% (sonication amplitude) and 5 second time intervals. The temperature rise with time for the ultrasound applied can be found on table 136 in the appendix IX.

The energy efficiency for various experiments can then be calculated using the equation below:

$$\textbf{Energy Efficiency}: \frac{\textbf{Enrgy Produced}}{\textbf{Energy Consumed}} \times 100\% \qquad (41)$$

Another way to find the energy efficiency is to find the energy losses during the process including the losses at the circuit, electrode and within the electrolyte, then using equation 42 [6].

$$\eta_{net} = 1 - \frac{E_{Loss}}{E_{Input}} \qquad (42)$$

Energy loss at the electrode includes the loss due to the partial coverage of electrode by gas bubbles resulting in bubble overpotential both at the anode and cathode. The energy loss at the circuit is resulted from connections and wiring at the anode and cathode. The resistance to ion transfer within the electrolyte is the reason to another form of energy loss [6].

The energy efficiency can be calculated for various experiments using equations 41 and 42. For instance, the efficiency for the case in which 0.35 kW of energy (electrical and ultrasound) was used and 10 cm^3/s of hydrogen was produced is given by (hydrogen density: 0.000089 g/cm^3):

$$10\ (\mathrm{cm}^3/\mathrm{S}) \times 0.000089(\mathrm{g}/\mathrm{cm}^3) = 0.00089\ \mathrm{g}/\mathrm{S}$$

$$\frac{0.00089}{1000} = 0.00000089\,\mathrm{Kg}/\mathrm{S}$$

$$\text{The calorific value of hydrogen is } 141790\ \mathrm{KJ}/\mathrm{Kg}$$

$0.00000089\,\mathrm{Kg}/\mathrm{S} \times 141790\,\mathrm{KJ}/\mathrm{Kg} = 0.1261931\,\mathrm{KJ}/\mathrm{S}$ or KW Amount of energy produced in the form of hydrogen. The energy efficiency:

$$\frac{0.1261931}{0.35} = 0.360 \times 100\% = 36.0\%$$

The literature equation [163] [164] of energy efficiency for an electrolysis system is given by [165]:

$$\boldsymbol{\eta} = \frac{\dot{\mathbf{N}}_{\mathbf{H_2,Out}}\ \mathbf{HHV}}{\mathbf{E}+\mathbf{Q_{Cell}}\left(\mathbf{1}-\frac{\mathbf{T_0}}{\mathbf{T_s}}\right)+\mathbf{Q_{H_2O}}\left(\mathbf{1}-\frac{\mathbf{T_0}}{\mathbf{T_s}}\right)} \qquad (43)$$

Where $\dot{\mathrm{N}}_{\mathrm{H_2,Out}}$ is the hydrogen outlet flow rate, HHV is the higher heating value of hydrogen, E is the electric energy input, $\mathrm{Q}_{\mathrm{Cell}}$ is the redundant heat from the cell , $\mathrm{Q}_{\mathrm{H_2O}}$ is the thermal energy input to raise the temperature of water, T_0 and T_S are the temperatures of the environment and the external heat source, respectively.

The equation 43 could be broken down in order to see its constituents and how they can be calculated. For this reason the overall reaction in water electrolysis can be written in thermodynamics language:

$$\mathrm{H_2O} + \mathrm{Heat} + \mathrm{electricty} \rightarrow \mathrm{H_2} + \frac{1}{2}\mathrm{O_2}$$

The theoretical energy needed to produce hydrogen through electrolysis at a certain temperature is given by:

$$\boldsymbol{\Delta H = Q + \Delta G} \qquad (44)$$

Where Q=TΔS and ΔG is the change in Gibbs free energy. The value of ΔH for water formation at 1atm and 298°K is given by $\Delta H = -285.8\ \mathrm{KJ/mol\ of\ H_2}$

(Standard Gibbs free energy) $\Delta G° = -RT\ln K$ hence (equilibrium constant) $k = e^{\frac{-\Delta G°}{RT}}$ where k can be used to calculate Gibbs free energy (ΔG) at different temperatures.

In an electrolytic cell there are various resistances as mentioned in section 2.6, there resistances resulting from the overpotetnial needed to overcome activation energy of oxygen and hydrogen formations, resistances due to wiring and connection at the electrodes, resistance to ion transfer within the electrolyte and resistance due to electrode surface covered by the gas bubbles. Therefore for energy efficiency calculations it is required to define a term, which encapsulates theses resistances. The cell usually operates at a higher potential than the equilibrium potential, hence the term overpotential is introduced, which can represent the internal resistances in an electrolysis cell. The following equation may be presented for joules heating based on joules law per unit time [165] [166]:

$$\mathbf{Q_j = I^2 R_e = I V_{overpotential}} \quad (45)$$

Where I is the current and R_e is the internal resistance and $V_{Overpotential}$ is the overpotential or overvoltage for different experiments, which was explained and calculated in sections 2.4.2.2 and 4.2.2.

The lost heat or redundant heat (Q_{cell}) mentioned in equation 43 can be found using the equation 46 below:

$$\mathbf{Q_{cell} = T\Delta S - Q_J} \quad (46)$$

Where ΔS is the change in entropy and can be found by Q/T.

In table 16 the energy efficiency is calculated for various experiments along with the energy saving when the ultrasound is applied. The energy efficiency demonstrated on table 16 can be compared to the energy efficiency mentioned in the literature, which is said to be between 40%-60% [74], [75] for the electrolysis [6], [76]. This is higher than the majority of experiments presented on the table however the last experiment had energy efficiency above 40%, which is within the aforementioned range. Our energy efficiencies nevertheless are much lower than that of PEM electrolyser mentioned by Frano Barbir with coupling energy efficiency of 93% (solar cell/PEM electrolyser) [112] [111].

Table 16: Energy efficiency for different experiments.

Experiment	Energy efficiency Range (%)	Energy saving via Ultrasound
0.1M NaOH, electrode surface area cm^2 (28.8, 32, 35.1, 38.25, 41.4) at 25°C	Silent: 6.8-7.83 Sonicated: 6.6-7.54	-0.29%
0.1M KOH, electrode surface area same as above at 25°C	Silent: 8.1-8.4 Sonicated: 9.0-9.57	1.17%
0.1M NaOH fixed anode, various cathode surface area cm^2 (32, 33.5,35.1, 36.7,38.25) at 25°C	Silent: 7.95-8.53 Sonicated: 7.5-9.15	0.62%
0.1M KOH fixed anode, various cathode surface area same as above at 25°C	Silent: 7.77-8.26 Sonicated: 7.81-8.53	0.27%
0.1M NaOH various surface area(28.8, 32, 35.1, 38.25, 41.4) without Temperature control	Silent: 9.2-9.72 Sonicated: 9.5-10.4	0.68%
0.1M KOH various surface same as above without temperature control	Silent: 8.3-9.7 Sonicated: 8.0-10.60	0.90%
KOH at 25°C concentrations (0.1M, 1M, 5M, 10M)	Silent: 12.5-42.8 Sonicated: 11.3-48.6	5.8%

The energy saving using the ultrasound was not significant during the experiments as shown on table 16. This was compared to 10-25% energy saving mentioned by Sheng-De Li. The highest energy saving is attributed to the experiment using potassium hydroxide at various concentration, which was 5.8%. This also had the highest energy efficiency for both silent and sonicated experiments reaching 48.6% for the sonicated experiment.

The energy efficiency can be increased by reducing the potential requirement for the electrolysis, enhancing the cell design, electrode surface and reducing the resistances throughout the cell. Sheng-De Li et al suggested the amount of energy that could be saved via the application of the ultrasound is significant compared to the investment in equipment and energy consumption by an ultrasonic field. They set an example referring to a 100 kA cell with a bubble-overpotential of 0.3V , which could save up to 30 kW while an ultrasonic field consumes about 0.05 kW only [105] however in our work the energy saving using the ultrasound was not satisfactory having it compared to the mentioned range by Sheng-De Li et al.

4.7. Effect of electrode surface area

The electrode active surface area is the area in contact with the electrolyte at which the electrochemical reactions occur however the meaning of real surface area is defined according to different traits, and further experimentation may be needed in order to determine the real surface area of the electrode. This depends on factors such as electrode surface heterogeneity and homogeneity, surface topography (i.e. macro/micro roughness) and dispersion of active materials within the electrolyte [167].

The techniques with which the real surface area can be found are divided into in-situ and ex-situ methods. The in-situ includes procedures such as voltammetry, hydrogen and oxygen adsorption from the solution, ion exchange capacity, drop weight, capacitance ratio, Parsons-Zobel plots and negative adsorption. The ex-situ method contains X-ray diffraction, Porosimetry, microscopy, adsorption of probe molecules from the gas phase and etc. [167]. Please note that not all of the aforementioned methods are applicable for solid electrode, for instance drop weight (volume) technique is applied for liquid metal electrodes such as Hg and Ga in dynamic or static conditions.

Adsorption processes and capacitance ratio are the most commonly used methods applied for solid electrodes, which are based on diffusion controlled mass transfer when the current is homogeneously distributed. In the 2nd method the differential capacitance is evaluated in the electrical double layer area using Gouy-Chapman theory [168]. The electrical double layer is a region near the surface of the electrode where the first layer includes adsorbed ions and the second has ions attached to surface charge (i.e. positive and negative charges in the layer as a whole) [169].

The active electrode surface area in our work is assumed equal to the geometrical electrode surface area in contact with the electrolyte, the fluctuations in the level of the electrolyte inside the capturing tube at the time of the experiments were not recorded.

4.7.1. Increase of electrode surface area

In this part, the effect of electrode surface area for numerous experiments is evaluated where unlike 4.7.2 the anode and cathode active lengths are the same and their increase is studied on the hydrogen generation. In previous sections, figures 21, 22 and 28 considered the effect of surface area on decomposition potential, current density and production efficiency, this section's focus is to quantify the changes for the current and hydrogen production.

Figures 30 and 31 demonstrate the effect of electrode surface area on the current generation and hydrogen production for selected potentials. The trend shows the current and hydrogen generation are both increased by increasing electrode surface area. In figure 30 increasing the surface area by 12.6 cm^2 from 28.8 cm^2 to 41.4 cm^2 increases the current generation by:

- 1087 mA for silent 0.1M NaOH
- 1143 mA for sonicated 0.1M NaOH
- 1303 mA for silent 0.1M KOH
- 1102 mA for sonicated 0.1M KOH

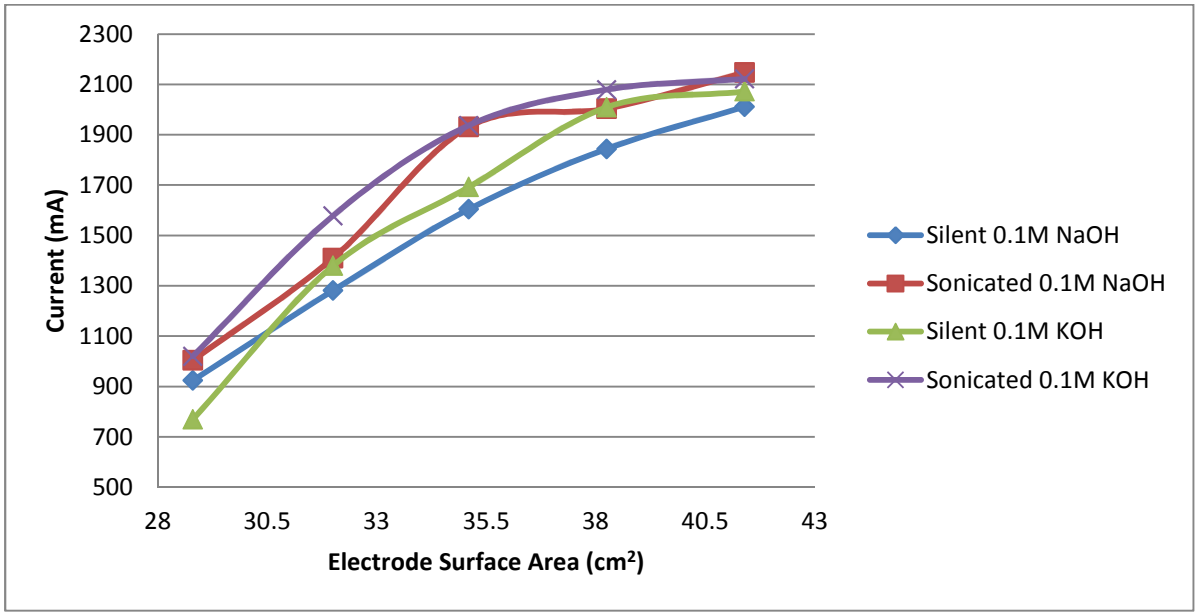

Figure 30: Current vs. surface area for different experiments at 30V and 25°C.

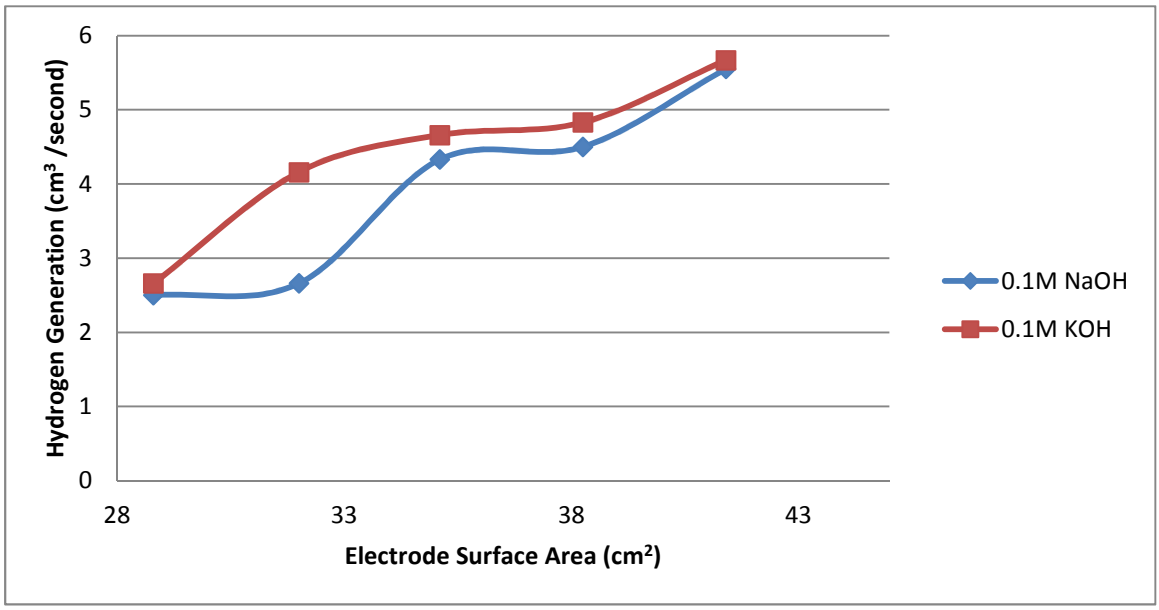

Figure 31: Hydrogen production versus electrode surface area silent experiment at 25°C and 22V.

In figure 31 increasing the electrode surface area by 12.6 cm^2 results in an enhancement in hydrogen generation by:

- 3.05 $\mathrm{cm}^3/\mathrm{second}$ for 0.1M NaOH or 122% increase
- 3.01 $\mathrm{cm}^3/\mathrm{second}$ for 0.1M KOH or 113% increase

Having compared the current generated for various experiments at different electrode surface areas (Appendix III on page 9 onward), it was calculated that increasing the electrode surface area by about 45% increased the current by 2-2.5 times its initial value. This was done by finding the differences between the current generation at active length 9 cm (Electrode surface area: 28.8 cm^2) and active length 13 cm (Electrode surface are: 41.4 cm^2) at different potentials for various experiments. This means that 43.75% increase in the electrode surface area results in 70-150% increase in the current generation.

The enhancement in hydrogen generation by increasing the electrode surface area did not follow a steady trend and negative improvements were spotted for numerous experiment, the reasons to the fluctuations in hydrogen production (errors or negative improvements) come from the cell design (gas capturing tube), resistances to mass transfer and bubble accumulation on the surface of electrode. The enhancement trend however may be found having a look at the consistent results obtained for different potentials such as the data plotted in figure 31. In this figure the hydrogen generation was increased by 113% for 0.1M KOH and 122% for 0.1M NaOH when the electrode surface area was increased by 43.75%.

The improvement in the hydrogen generation, by about 45% increase in surface area, was evaluated to be between 50-130% for the consistent results. The improvement was evaluated by finding the difference between hydrogen production at 28.8 cm^2 (initial electrode surface area) and 41.4 cm^2 (final electrode surface area) for different potentials and experiments, which would give us the range. The low percentage belongs to low applied potentials such as 2-5 volts.

4.7.2. Fixed-anode/Fixed Cathode Electrode Active Length

The first comparison in this section will be made for the experiments carried out at high concentration (15M) electrolyte and variable anode and cathode electrode active length (surface area). The current generation along with hydrogen production are compared for similar surface areas but different electrode configurations in figures 32 and 33. The fixed length of electrode was

set at 11 cm and variable length was changed. Figures 32 and 33 may demonstrate that the cathode-fixed experiment resulted in slightly more current being generated hence more hydrogen production however the overall results were not conclusive and irregular patterns were observed. (Additional information regarding to the results can be seen in appendix III table 73 onward on page 75)

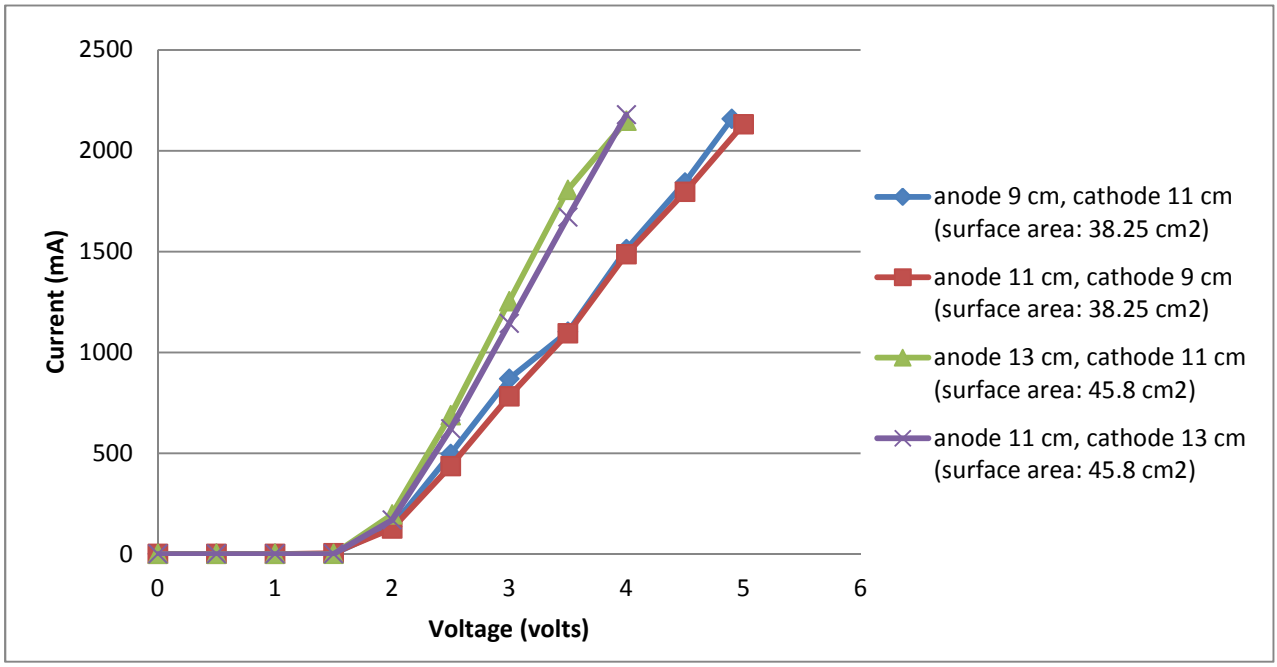

Figure 32: Current-Voltage comparison between anode-fixed and cathode-fixed for 15M KOH at 25°C.

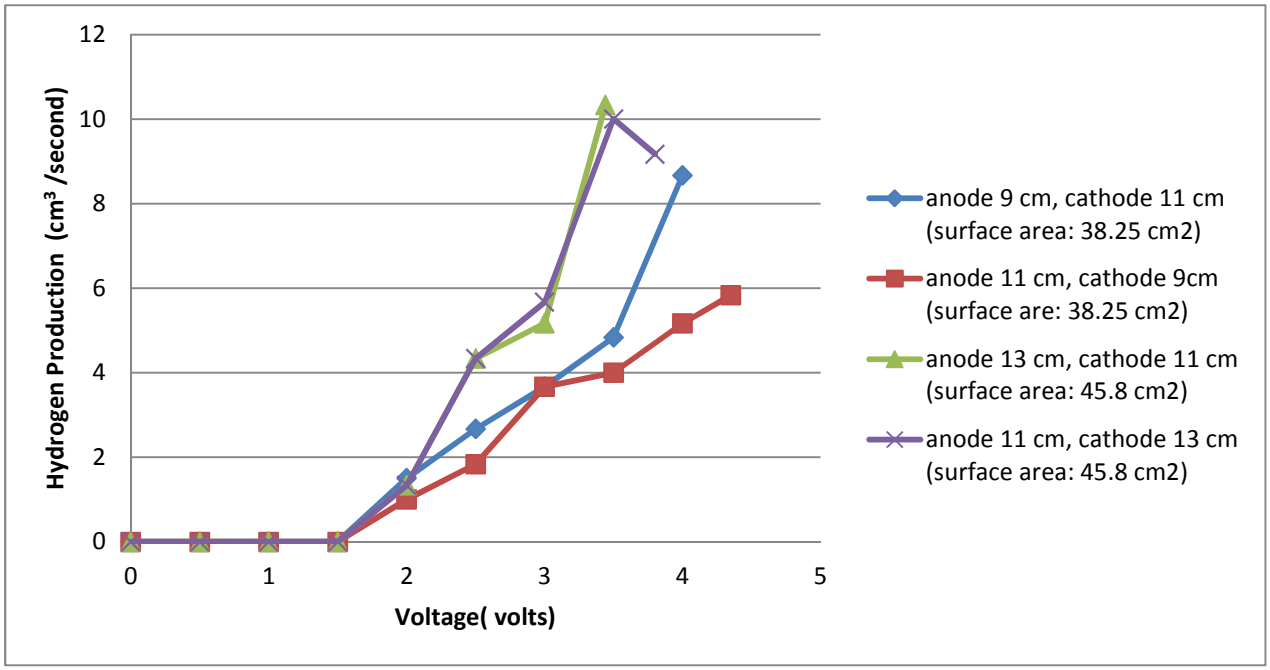

Figure 33: Hydrogen Production comparison between anode-fixed and cathode-fixed for 15M KOH at 40°C.

The aim here was to see whether an increase in the cathode surface area has any influence on the current generation and the production of hydrogen compared to the opposite electrode arrangement. Douglas F. Call et al in a work investigated the effect of high surface area of stainless steel cathode on the generation of hydrogen in a microbial electrolysis cell. It was reported that using a stainless steel brush cathode the hydrogen generation was similar to the rate achieved via platinum-catalysed cathodes. Moreover a reduction in overpotetial for hydrogen evolution was obtained [115].

Hydrogen generation for the experiment shown in figure 33 at 2V for instance, exhibited 0.12 cm^3/s increase for both cathode-fixed electrode arrangements relative to anode-fixed, the current was enhanced by 11 mV (anode 9 cm, cathode 11 cm) and 28 mV (anode 13 cm, cathode 11 cm) however at 4V (anode 13 cm, cathode 11 cm), the current was reduced by 31 mA and the hydrogen production was also reduced by $0.3\mathrm{cm}^3/\mathrm{S}$.

As one can see from the figures 32 and 33 and the data sheet in appendix III, the increase or decrease in current, current density and hydrogen production for cathode-fixed configuration is not decisive and the fluctuations are a barrier on the interpretation of the results. The reason to such indecisive results in this section may be raised from the fact that there was not a large cathode surface area as opposed to the anode and vice versa hence similar results with fluctuations were obtained. It may be suggested to carry out a similar experiment for very large cathode surface area as opposed to a small anode one in order to obtain more reasonable data.

4.8. Effect of electrode

The recorded hydrogen generation for 0.1M potassium hydroxide using carbon electrodes was greater compared to that of nickel-based electrodes. This can be seen from the graph below in figure 34.

Nickel is the most widely used electrode for the electrolysers because of its stability and activity (activation overpotential: -0.28V for hydrogen and +0.56V for oxygen) [6]. The nickel electrode throughout the experimentation showed more resistance to corrosion in comparison to carbon electrode particularly for potassium hydroxide solution. The carbon electrodes (activation overpotential : +0.95 V for oxygen and -0.62V for hydrogen) after operation time of about 90 minutes (low concentration such as 0.1M NaOH or KOH) eroded into the electrolyte solution and changed the colour to black while this erosion was noted for nickel electrode at above 60°C. The

nickel electrode was worn away and altered the colour of the electrolyte solution to yellow at the above-mentioned temperature and an operation time of nearly 60 minutes (high concentrations such as 10M and 15M KOH). The rate of corrosion was not measured.

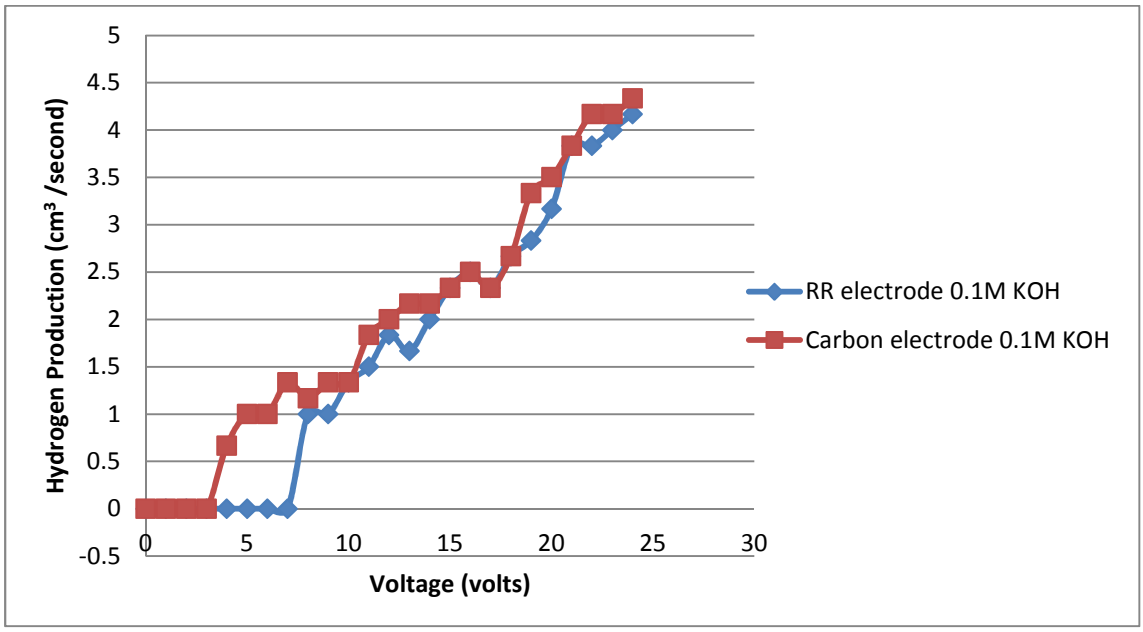

Figure 34: Hydrogen production comparison for carbon electrode and nickel electrode.

At temperatures between 60-90°C for 15M KOH, a dull-brown layer was removed from the surface of the nickel electrodes. This may be resulted from the fact that the exposure of nickel to corrosive materials such as KOH or molten carbonate salts leads to rapid oxidisation of nickel to nickel oxide (NiO), which suffers from electrical conductivity. This oxidisation at the anode side may increase the power requirement for the cell since it polarises the electrolytic cell in an irreversible fashion [153]

It was expected to see higher production rates when the nickel electrode was used because of its activity however figure 34 suggests otherwise. The current generation for the similar experiments showed the same trend. The reason to this trend maybe the deactivation of nickel electrode, which may be caused by the formation of nickel hydride phase at the surface of the electrode, resulted from high concentration of hydrogen. This has been widely discussed in the literature [6], [170], [171]. The deactivation occurs at a certain hydrogen gas pressure and adequate cathodic current density (10 mA/cm^2) when the hydrogen absorbs into the nickel forming a bond with nickel hence changing the outer electron orbital of the nickel. The solution to this problem is the iron coating of the electrode, which avoids the electrode deactivation or dissolution of vanadium species in the alkaline electrolyte that is said to reactivate nickel cathode during the evolution of hydrogen [172].

Another reason to the trend on the graph in figure 34 may be the result of electrode surface. The electrode surfaces are usually amended by pores, cuts and slits to increase bubble detachment from the surface however the size of these amendments must not cause gas trapping [6].

The following factors may be the cause of less current and hydrogen produced for the nickel electrodes:

I. The deactivation of nickel electrode through the development of nickel hydride phase as a result of high concentration of hydrogen.
II. The surface of the nickel electrode may have inhibited the bubble detachment hence resulted in bubble accumulation at the surface, resistance to mass transfer and increase in current density since the bubble blanketing reduces the active surface area of the electrode.
III. Formation of NiO (Nickel oxide) on the surface of the electrode, which reduces the electrical conductivity.

Although nickel is a popular material in the industry for the electrolysers but a careful look at the surface of electrode and material of electrode coating could make a considerable difference in the production and energy efficiency. The electrode surface could be improved using coating materials as well as modification of the surface structure via creation of perforations and apertures.

Chapter 5: Concluding remarks, Recommendations and Future work

5.1. Concluding Remarks

- The electrolytic cell during this research project had the average production efficiency of about 72% and energy efficiency of about 14.5%. The production efficiency is similar to the literature values mentioned between 70-96% [74], [113] however the energy efficiency is far behind the literature range, which is between 40%-60% [114]
- The ultrasound increased the production efficiency by about 6% and energy efficiency by about 1.3%. This means that the energy saving via the ultrasound was only 1.3% that was considerably lower than 10%-25% range mentioned in the literature [105].
- A 45% increase in the electrode active surface area enhanced the current generation by about 70% whilst the hydrogen production was not improved in a regular fashion however

more experimentation is required to achieve an orderly pattern and draw a decisive conclusion.

- Dissimilar electrode configurations has not resulted in a definite increase or decrease in current and hydrogen generation, this may be caused by small variance between anode and cathode surface areas. Further experiment is required employing a very large cathode surface area against a small anode surface area and vice versa in order to investigate the effect of dissimilar electrode configurations.
- The nickel electrode throughout the experiments at high concentrations such as 5M-15M may have undergone deactivation. The nickel electrode deactivation is broadly mentioned in the literature and is a common occurrence [6], [170], [171]. The iron coating could be used to prevent the electrode deactivation. The electrode surface could also be enhanced by creating cuts, slits and perforations in order to ensure a good performance by the electrode.
- Increasing the concentration and temperature of the electrolyte solution resulted in a decrease in the decomposition potential and overpotetnial. The decomposition potential at molar concentrations of 5M-15M had an average value below 1.23V, which may be interpreted as underpotential deposition (UPD) however more study is needed employing electrochemical and surface characterisation techniques such as FTIR, SERS, STM and etc.

5.2. Recommendations and Future Work

The first recommendation is to design a new cell and do the repetition for the similar experiments since the absence of reliability and a definitive conclusion can be seen from some of the experiments. The limited time available to the author did not allow a new cell design. In a new design it is suggested to reduce the resistances by decreasing the gap between the electrodes, reduce wiring at the electrodes and enhance the electrode surface using coating materials.

The cell design could be altered in such a way to enhance the gas capturing by allowing reasonably sized diameter for the capturing tubes. In figure 35 the author's recommended design is depicted. The total volume of the cell may also be differed, at smaller volumes the ultrasound's effect could be studied better since more of the solution will be in the proximity of the ultrasound.

In order to enhance the production rate, the ultrasonic transducer could be removed and instead an ultrasonic tip replaces the cathode/anode or both, which would act as both electrode and an ultrasonic irradiator. In this way there will be a localised ultrasonic field at the electrodes hence the

gas bubble removal from the surface of the electrode and within the electrolyte would be much more effective.

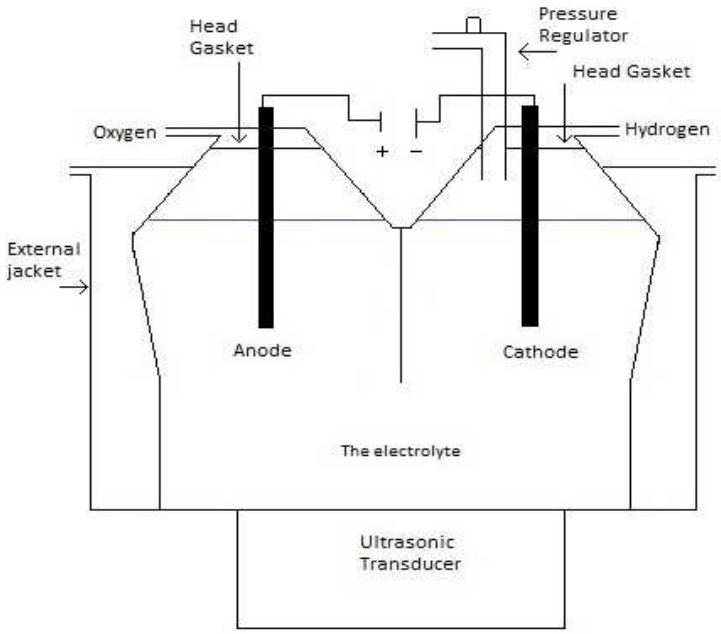

Figure 35: Recommended cell design by the author.

The gap between the electrodes in our study was 7.5 cm, this gap could be reduced and its effect could be studied on the electrochemical reactions, a smaller gap means less distance for ions to travel between the electrodes and may lead to less ohmic and ionic resistances.

The electrode surface can be modified using slit, cuts and perforations in order to maximise the contact with the electrolyte solution. The electrode active surface is increased using this method hence more active sites available for the electrochemical reaction. The nickel electrodes can be coated with the materials such as iron in order to prevent the electrode deactivation at high concentration of hydrogen.

The use of three electrode system (voltammetry) is recommended for future work in order to calculate the anodic and cathodic overpotentials separately as the half-cell reactions in this way can be studied separately irrespective of the other half. This method employs a reference electrode, working electrode and counter electrode [173].

The sonication distance from the electrolyte and also the power of sonication could be subject of alteration for future work. The enhancement in sonication amplitude may also further increase the mass transfer hence productivity of hydrogen.

The electrolyte solution could be purged with argon or nitrogen gas for a specified period of time throughout the experiments to remove the air from the cell. The resistance to mass transfer may be reduced using this technique.

More exploration on the effect electrode surface area on the electrochemical production of hydrogen is recommended, our results in this area were not entirely conclusive hence a repetition in this area is suggested along with the investigation on the effect of large cathode surface area in comparison to a small anode surface area and vice versa. For instance the cell's internal wall may be made from nickel alloy material acting as the cathode while a platinum wire or steel could be placed into the electrolyte as the anode.

The application of a magnetic field in the electrolysis could be studied using ferromagnetic electrode materials and potassium hydroxide as electrolyte solution, this could be coupled with an ultrasonic field in order to enhance the production of hydrogen. The direction of magnetism will determine the direction of gas bubble motion and the convection of electrolytic solution as reported by Ming-Yuan et al in their work who displayed the direction of the electrolyte flow field under the magnetic force effect. Therefore the direction of the ultrasonic irradiation should be set in the direction of magnetism for maximum impact [174].

Urine could be used as the electrolyte material in order to produce hydrogen. Urine has 4 hydrogen atoms per molecule as opposed to water with 2 hydrogen atoms per molecule. Furthermore the hydrogen atom bonds in urine are weaker than that of water therefore less energy may be needed to decompose the urine molecules. Park et al in a recent work studied the electrolysis of Urea and Urine for solar hydrogen production using BiOx–TiO2 anode and stainless steel cathode [175]. The electrolysis of Urine/Urea could be carried out using the ultrasonic field, magnetic field or mechanical stirring in the absence of external electrolyte added to the urine and urea contrary to the work of Park et al in which NaCl, $LiClO_4$or Na_2SO_4 (50 mM, 60 mL) were added to urine solution.

Bibliography

[1] S. International, “Shell energy scenarios to 2050: An era of Volatile Transtions,” Shell International BV, 2011.

[2] B. E. Outlook, “BP Energy Outlook 2030,” BP, London , 2011.

[3] EIA, “unpublished file data of the Coal Reserves Data Base,” U.S Energy Information Administration , Washington, 2004.

[4] A. Steinfeld, “Solar hydrogen production via a two-step water-splitting thermochemical cycle based on Zn/ZnO redox reactions,” *International Journal of Hydrogen Energy,* vol. 27, no. 6, p. 611–619, June 2002.

[5] J. A. Turner, “A Realizable Renewable Energy Future,” vol. 285, pp. 687-689 , July 1999.

[6] K. Z. Dongke Zhang, “Recent progress in alkaline water electrolysis for hydrogen production and applications,” *Process in Energy and Combustion Science ,* vol. 36, pp. 307-326, 2010.

[7] N. Moriguchi, *Journal of The Chemical Society,* vol. 55, pp. 749-751, 1934.

[8] G. S. a. L. E. Z., *Elektrochem,* vol. 43, pp. 408,597, 1937.

[9] F. Cataldo, “Effects of ultrasound on the yield of hydrogen and chlorine during electrolysis of aqueous solutions of NaCl or HCl,” *Journal of Electroanalytical Chemistry,* vol. 332, no. 1-2, pp. 325-331, August 1992.

[10] H. H. N. Elsayed Elbeshbishy, “Hydrogen production using sono-biohydrogenator,” *International Journal of Hydrogen Energy,* vol. 36, no. 2, p. 1456–1465, January 2011.

[11] P. S. R. P. M. B. G. Z. Y. K. a. M. V. Stefania Marini, “Advanced alkaline water electrolysis,” *Electrochimica Acta,* vol. In Press, no. Corrected proof, May 2012.

[12] D. R. Lide, “The Elements,” in *Handbook of Chemistry and Physics*, 82nd ed., Boca Raton, Florida: CRC Press, 2001-2002.

[13] U. D. O. Energy, “Hydrogen Production,” US Department Of Energy , 2006.

[14] K. K. P. a. R. B. Gupta, “Section I: Production and Use of Hydrogen, Chapter 1:Fundamentals and Use of Hydrogen as a Fuel,” in *Hydrogen Fuel; Production, Transport and Storage*, Boca Raton, Florida: CRC Press, Taylor & Francis Group, 2009.

[15] N. Muradov, “Hydrogen from fossil fuels without CO2 emissions,” in *Advances in Hydogen Energy*,

Kluwer Academic Publishers, 2002.

[16] R. D. D.A.J. Rand, “Chapter 1: Why Hydrogen Energy?,” in *Hydrogen Energy; Challenges and Prospects*, Cambridge, Royal Society Of Chemistry , 2008.

[17] F. C. Team, “2007 annual progress report; Fuel Cells Sub-Program Overview,” Washington, 2007.

[18] U. D. o. Energy, “Hydrogen Production,” EERE (Energy Efficiency and Renewable Energy), 2009. [Online]. Available: http://www1.eere.energy.gov/hydrogenandfuelcells/production/current_technology.html?m=1&. [Accessed 08 August 2011].

[19] R. D. D.A.J. Rand, “Chapter 2 Hydrogen from Fossil Fuels and Biomass,” in *Hydrogen Energy: challenges and prospects*, Cambridge , The Royal Society of Chemistry, 2008.

[20] R. D. D.A.J. Rand, “2.3. Reforming of Natural Gas,” in *Hydrogen Energy: challenges and prospects*, Cambridge, The Royal Society of Chemistry,, 2008.

[21] R. D. D.A.J. Rand, “2.4. Partial Oxidation of Hydrocarbons,” in *Hydrogen Energy: challenges and prospects*, Cambridge, The Royal Society of Chemistry, 2008.

[22] R. D. D.A.J. Rand, “2.5. Other Processes,” in *Hydrogen Energy: challenges and Prospects*, Cambridge, The Royal Society of Chemistry, 2008.

[23] B. F. T. a. M. F. David A Bell, “Chapter 4: Gasifiers,” in *Coal Gasification and its Application* , Oxford , Elsevier Inc, 2011.

[24] R. D. D.A.J. Rand, “2.7 Coal and Other Fuels,” in *Hydrogen Energy: challenges and prospects* , Cambridge , The Royal Society of CHemistry , 2008.

[25] D. R. a. R. Dell, “Chapter 4: Hydrogen from Water,” in *Hydrogen Energy: challeneges and prospects*, Cambridge , The Royal Society of Chemistry, 2008.

[26] C. Meyers, “Google invests $168m in world's largest solar power tower plant,” Eco Worldly for Guardian News , 15 April 2011. [Online]. Available: http://www.guardian.co.uk/environment/2011/apr/15/google-solar-mojave-ivanpah. [Accessed 2011 08 09].

[27] S. H. Antonio Luque, “what is photovoltaics,” in *Handbook of photovoltaic science and engineering*, West Sussex, John Wiley and Sons Ltd, 2005.

[28] S. H. Zadeh, *Renewable Energy Systmes,* Birmingham, 2011.

[29] S. Baykara, “Experimental solar water thermolysis,” *International Journal of Hydrogen Energy,* vol. 29, no. 14, p. 1459–1469, November 2004.

[30] B. F. T. M. F. David A Bell, “Chapter 7: Hydrogen Production and Integrated Gasification Combined Cycle (IGCC),” in *Coal Gasification and its application* , Oxford, Elsevier Inc, 2011 .

[31] D. R. a. R. Dell, “Chapter 2.8 Biomass,” in *Hydrogen Energy; Challenges and prospects* , Cambridge, The Royal Society of Chemistry , 2008.

[32] C. C. E. a. R. J. E. Thomas A. Milne, “Hydrogen from Biomass; State of the art and research challenges,” NREL, Golden, Colorado .

[33] S. L. L. G. X. Z. Youjun Lu, “Hydrogen production by biomass gasification in supercritical water over Ni/gAl2O3 and Ni/CeO2-gAl2O3 catalysts,” *Internation Journal of Hydrogen Energy,* vol. 35, no. 13, p. 7 1 6 1 – 7 1 6 8, 2010.

[34] H. J. L. G. X. Z. C. C. X. G. Y.J. Lu, “Hydrogen production by biomass gasification in supercritical water with a fluidized bed reactor,” *Internation Journal of Hydrogen Energy ,* vol. 33, no. 21, p. 6 0 6 6 – 6 0 7 5, 2008.

[35] M. A. Rosen, “Exergy analysis of hydrogen production by thermochemical water decomposition using the Ispra Mark-10 Cycle,” *International Journal of Hydrogen Energy ,* vol. 33, no. 23, pp. 6921-6933, 2008.

[36] R. H. Xing L. Yan, “Chapter 2: Nuclear Hydrogen Production; An overview,” in *Nuclear Hydrogen Production Handbook*, Boca Raton, Florida: CRC Press; Taylor & Francis Group, 2011.

[37] U. D. o. energy, “Hydrogen Storage,” The US Department of Energy , 2011.

[38] M. Klell, “Chapter 1: Storage of Hydrogen in the Pure Form,” in *Handbook of Hydrogen Storage; New Materials for Future Energy Storage*, Weinheim, WILEY-VCH Verlag GmbH & Co. KGaA,, 2010.

[39] X. L. P. X. P. L. Y. Z. J. Y. Jinyang Zheng, “Development of high pressure gaseous hydrogen storage Technologies,” *International Journal of Hydrogen Energy,* vol. xxx, 24 February 2011.

[40] T. K. S. Y. K. K. a. T. N. K. Matsumoto, “Hydrogen Liquefaction by Magnetic Refrigeration,” *Journal of Physics: Conference Series 150 (2009) 012028,* 2009.

[41] B. P. a. M. Hirscher, “Chapter: Physisorption in Porous Materials,” in *Handbook of Hydrogen Storage; New Materials for Future Energy Storage*, Weinheim, WILEY-VCH Verlag GmbH & Co. KGaA, 2010.

[42] J. R. A. v. D. K. d. J. M.G. Nijkamp, “Hydrogen storage using physisorption –materials demands,” *Applied Physics A,* vol. 72, p. 619–623, 2001.

[43] D. S. a. S. Deng, “Hydrogen Adsorption on Metal-Organic Framework MOF-177,” *Tsinghua Science & Technology,* vol. 15, no. 4, pp. 363-376, 2010.

[44] S. R. a. C. J. P. Alireza Shariati, “Chapter 3: Clathrate Hydrates,” in *Handbook of Hydrogen Storage;New Materials for Future Energy Storage*, Weinheim, 2010 WILEY-VCH Verlag GmbH & Co. KGaA, 2010.

[45] N. T. e. al, ""Hybrid hydrogen storage vessel", a novel high-pressure hydrogen storage vessel combined with hydrogen storage material," *International Journal of Hydrogen Energy,* vol. 28, no. 10, p. 1121–1129, October 2003.

[46] S. N. S. S. B. Indranil Ghosh, "Cryosorption storage of gaseous hydrogen for vehicular application – a conceptual design," *International Journal of Hydrogen Energy,* vol. 35, no. 1, p. 161–168, 2009.

[47] X. L. P. X. P. L. Y. Z. J. Y. Jinyang Zheng, "Development of high pressure gaseous hydrogen storage technologies," *International Journal of Hydrogen Energy,* vol. 37, no. 1, p. 1048–1057, 2011.

[48] A. S. C. W. D. S. J. Yang, "High capacity hydrogen storage materials: attributes for automotive applications and techniques for materials discovery," *Chem Soc Rev,* vol. 39, no. 2, 2010.

[49] CPi, "Standard ASME Vessel Designs," CP Industries; producer of large seamless pressure vessels, [Online]. Available: http://www.cp-industries.com/asmecht.html. [Accessed May 2012].

[50] L. L. R. C. P. X. F. K. J. Zheng, "High-Pressure Storage Vessels Used in Hydrogen Refueling Station," *ASME Conference Proceeding,* vol. 5, pp. 23-29 , 2006.

[51] G. Z. Z. H. J. Zheng, "The optimum design of ribbon wound pressure vessel by using adaptive random search method(I)," *Journal of Zhejiang University(Engineering Science),* vol. 25, no. 6, p. 673–680, 1991.

[52] M. G. a. R. Krishnamurthy, "Hydrogen Transmission in Pipelines and Storage in Pressurized and Cryogenic Tanks," in *Hydrogen Fuel; production, transport and storage* , Boca Raton, Florida: CRC Press; Taylor & Francis Group, 2009.

[53] D. R. a. R. Dell, "Chapter 7: Hydrogen-fuelled Transportation," in *Hydrogen Energy; Challenges and Prospects*, Cambridge , The Royal Society of Chemistry,, 2008.

[54] D. W. J. J. Alexander E.Farrell, "A strategy for introducing hydrogen into transportation," *Energy Policy,* vol. 31, no. 13, pp. 1357-1367, October 2003.

[55] G. Hookers, "Chapter 1: Introduction," in *Fuel cell technology handbook*, Boca Raton , Florida : CRC Press, 2003.

[56] D. A. B. ,. J. J. S. Dushyant Shekhawat, "Chapter 1: Introduction to Fuel Processing," in *FUEL CELLS: Technologies for Fuel Processing* , Elsevier , 2011.

[57] G. M. Masters, "4.6.2. Basic Operation Of Fuel Cells," in *Renewable and Efficient Electric Power Systems* , Hoboken, New Jersey: John Wiley & Sons, Inc., 2004.

[58] M. C. Williams, "Chapter 2: Fuel Cells," in *Fuel Cells: Technologies for Fuel Processing* , Elsevier, 2011.

[59] G. M. Masters, "4.6.3. Fuel Cell Thermodynamics: Enthalpy," in *Renewable and Efficient Electric Power Systems* , Hoboken, New Jersey: John Wiley & Sons, Inc, 2004.

[60] E. Chen, “Chapter 3: Thermodynamics and Electrochemical Kinetics,” in *Fuel Cell Technology Handbook*, Boca Raton, Florida: CRC Press, 2003.

[61] D. R. Lide, “DEFINITIONS OF SCIENTIFIC TERMS,” in *CRC Handbook of Chemistry and Physics*, CRC Press, 2001-2002.

[62] M. A. B. Yunus A. Cengel, “Chapter 7: Entropy,” in *Thermodynamics: An Engineering Approach*, 5th ed., McGraw-Hill , 2005.

[63] G. M. Masters, “3.4.2 Entropy and the Carnot Heat Engine,” in *Renewable and Efficient Electric Power Systems* , Hoboken, New Jersey: John Wiley & Sons Inc, 2004.

[64] G. M. Masters, “4.6.4 Entropy and the Theoretical Efficiency of Fuel Cells,” in *Renewable and Efficient Electric Power Systems* , Hoboken, New Jersey: John Wiley & Sons Inc, 2004.

[65] G. M. Masters, “4.6.5 Gibbs Free Energy and Fuel Cell Efficiency,” in *Renewable and Efficient Electric Power Systems*, Hoboken, New Jersey: John Wiley & Sons Inc, 2004.

[66] G. S. Karl Kordesch, “Chapter 4: Fuel Cell Systems,” in *Fuel Cells and Their Applications* , Weinheim, VCH, 1996.

[67] S. H. Zadeh, “Developing a stack of SOFC,” Unpublished , Birmingham, 2011.

[68] T. U. D. o. Defense, “Fuel Cell Basics: Zinc-Air Fuel Cells (ZAFC),” 2011. [Online]. Available: http://www.fctec.com/fctec_types_zafc.asp. [Accessed 24 07 2011].

[69] D. R. Lide, “Definition of Scientific Terms,” in *CRC Handbooks of Chemistry and Physics*, 90th ed., CRC Press/ Taylor and Francis, 2010.

[70] S. S. Zumdahl, “Chapter 17.7; Electrolysis,” in *Chemistry*, 7th ed., Boston, Houghton Mifflin Company, 2007.

[71] G. D. Berry, “Hydrogen Production: Electrolysis of Water and Steam,” in *Encyclopedia of Energy*, Vols. 1-6, Oxford , Elsevier , 2004.

[72] N. B. Y. D. K. S. Muzhong Shen, “A concise model for evaluating water electrolysis,” *International Journal of Hydrogen Energy,* vol. 36, no. 22, pp. 14335-14341, November 2011.

[73] G. D. BERRY, “ Hydrogen Production, 5. ELECTROLYSIS OF WATER,” in *Encyclopedia of Energy*, Vols. 1-6, San Diego, Elsevier, 2004, pp. 259-260.

[74] G. S. T. A. D. M. D. P. S. M. M. M. P. M. K. Vladimir M. Nikolic, “Raising efficiency of hydrogen generation from alkaline water-Energy Saving,” *International Journal of Hydrogen Energy,* vol. 35, no. 22, p. 12369–12373, November 2010.

[75] S. P. S. Š. S. M. Dragica Lj. StojićMilica P. Marčeta, “Hydrogen generation from water electrolysis—

possibilities of energy saving," *Journal of Power Sources,* vol. 118, no. 1-2, pp. 315-319, May 2003.

[76] M. J. S. C. Y. L. C. S. G. Y. P. S. a. S. C. Z.D. Weia, "Water electrolysis on carbon electrodes enhanced by surfactant," *Electrochimica Acta,* vol. 52, no. 19, pp. 3323-3329 , 2007.

[77] encyclopedia, "Electrorefining," Online Encyclopedia, [Online]. Available: http://www.encyclo.co.uk/define/electrorefining. [Accessed May 2012].

[78] U. Department Of MS, "Aluminium Production," University Of Cambridge, Department of Materials, Science and Metallurgy, [Online]. Available: http://www.doitpoms.ac.uk/tlplib/recycling-metals/aluminium_production.php. [Accessed 2011 03 06].

[79] H.-G. SCHWARZ, "Aluminum Production and Energy," in *Encyclopedia of Energy*, Boston, Elsevier, 2004.

[80] M. Data, "Cryolite," Surrey.

[81] D. T. Sawyer, "Introduction and Fundamentals," in *Electrochemistry For Chemists* , New York, John Wiley and Sons, 1995.

[82] A. M. Christopher M.A. Brett, "Introduction," in *Electrochemistry; Principles, Methods and Applications*, Oxford, Oxford Press Incorporation, 1994.

[83] Z. Nagy, "An Introduction-What is Electrochemistry," University Of North Carolina, May 2008. [Online]. Available: http://electrochem.cwru.edu/encycl/art-i02-introduction.htm. [Accessed 06 03 2011].

[84] J. P. M. L. K. a. D. E. C. Madalina Ciobanu, "Chapter 1: Fundamentals," in *Handbook Of Electrochemistry*, Amsterdam, Elseveir , 2007.

[85] J. P. W. M. L. K. D. E. C. Madalina Ciobanu, "1.3. Fundamental Equations," in *Handbook of Electrochemistry*, Amsterdam, Elsevier, 2007.

[86] S. Higson, "10.2. The Nernst equation and electrochemical cells," in *Analytical Chemistry* , New York, Oxford University Press, 2004.

[87] D. Pollet, *Fundamental of Electrochemistry,* Birmingham: University Of Birmingham , 2010.

[88] J. P. W. L. K. a. D. E. C. Madalina Ciobanu, "Part one, Chapter one : fundamentals," in *Handbook of Electrochemistry*, Oxford, Elsevier B.V., 2007.

[89] E. I.-T. a. A. V. Virkar, "Chapter 9: Electrode Polarisations," in *High Temperature Solid Oxide Fuel Cell; Fundamentals, Designs and Applications* , Oxford , Elsevier Ltd, 2003.

[90] J. M. a. D. Ziegler, "The oxygen electrode reaction in acid solutions on RuO2 electrodes prepared by the thermal decomposition method," *Thin Solid Films ,* vol. 163, pp. 301-308, 1988.

[91] D. L. R. P. G. a. J. R. S. Richard L. S. Thomas, "Trap-governed hydrogen diffusivity and uptake capacity in ultrahigh-strength AERMET 100 steel," *Metallurgical and Materials Transactions A,* vol. 33, no. 7, pp.

1991-2004, 2002.

[92] E. B. G. D. Short, “Concentration Overpotentials on Antimony Electrodes in Differential Electrolytic Potentiometry,” vol. 37, no. 8, p. 962–967, July 1965.

[93] L. Shreir, R. Jarman and G. Burstein, “Electrochemical cells and Cell corrosion; Resistance Overpotential,” in *Corrosion*, 3rd ed., Vols. 1-2, Elsevier , 1994.

[94] G. Prentice, “Electrochemical Engineering, Glossary,” in *Encyclopedia of Physical Science and Tehcnology* , 3rd ed., Tarzana, California: Elsevier Science Ltd, 2001.

[95] E. K.-E. E. Gileadi, “Some observations concerning the Tafel equation and its relevance to charge transfer in corrosion,” *Corrosion Science,* vol. 47, no. 12, p. 3068–3085, December 2005.

[96] H. Kies, “Coulometry,” *Journal of Electroanalytical Chemistry ,* vol. 4, no. 5, p. 257–286, November 1962.

[97] S. K. a. M. Ashokkumar, “Chapter 1: The Physical and Chemical effect of Ultrasound,” in *Ultrasound Technologies for Food and Bioprocessing* , New York , Springer Science+Business Media, LLC, 2011.

[98] B. D. a. N. Riley, “Cavitation microstreaming,” *Journal of Sound and Vibration,* vol. 15, no. 2, pp. 217-233, 22 March 1971.

[99] M. K. a. F. H. S. Li, “Acoustic emulsification, Part 1; The instability of the oil-water interface to form the initial droplets.,” *Journal of Fluid Mechanics,* vol. 88, no. 3, p. 499–511, 1978.

[100] S. G. G. a. A. B. Pandit, “Ultrasound emulsification: Effect of ultrasonic and physicochemical properties on dispersed phase volume and droplet size,” *Ultrasonics Sonochemistry,* vol. 15, no. 4, pp. 554-563, April 2008.

[101] K. S. Suslick, Ultrasound; its Chemical, Physical and Biological Effects, New York, NY: VCH Publishers, 1988.

[102] E. W. S. S. B. K. J. W. Y. G. E. S. Jonathan Mbah, “Low voltage H2O electrolysis for enhanced hydrogen production,” *Energy,* vol. 35, no. 12, p. 5008–5012, December 2010.

[103] Z. W. Z. G. Mingyong Wang, “Water electrolysis enhanced by super gravity field for production of hydrogen,” *International Journal of Hydrogen Energy,* vol. 35, no. 8, pp. 3198-3205.

[104] A. M. b. K. R. L Barreto, “The hydrogeneconomy in the 21st century: a sustainable development scenario,” *International Journal of Hydrogen Energy,* vol. 28, no. 3, p. 267–284, 2003.

[105] C.-C. W. a. C.-Y. C. Sheng-De Li, “Water electrolysis in the presence of an ultrasonic field,” *Electrochimica Acta,* vol. 54, no. 15, pp. 3877-3883, 2009.

[106] A. C. a. F. C. Chenghao Yang, “High temperature solid oxide electrolysis cell employing porous structured (La0.75Sr0.25)0.95MnO3 with enhanced oxygen electrode performance,” *International*

Journal of Hydrogen Energy, vol. 35, pp. 3221-3226, 2010.

[107] H. G. N. Y. A. N. H. M. a. E. S. T. Ohmori, "Photovoltaic water electrolysis using the sputter-deposited a-Si/c-Si solar cells," *International Journal of Hydrogen Energy,* vol. 26, no. 7, pp. 661-664, 2001.

[108] A. S. K. Ü. B. Ö. Ebru Önder Kiliç, "Hydrogen production by electrochemical decomposition of formic acid via solid polymer electrolyte," *Fuel Processing Technology,* vol. 90, no. 1, p. 158–163, January 2009.

[109] A. S. S. T. N. K. P. A. O. S. P.K. Dubey, "Hydrogen generation by water electrolysis using carbon nanotube anode," *International Journal of Hydrogen Energy,* vol. 35, no. 9, p. 3945–3950, May 2010.

[110] L. L. L. L. S. T. S. L. Y. W. W.L. Guo, "AuguHydrogen production via electrolysis of aqueous formic acid solutions," *International Journal of Hydrogen Energy,* vol. 36, no. 16, p. 9415–9419, August 2011.

[111] F. Barbir, "PEM electrolysis for production of hydrogen from renewable energy sources," *Solar Energy,* vol. 78, no. 5, p. 661–669, may 2005.

[112] A. B. H. B. W. S. H.A. Steeb, "Operation experience of a 10 kW PV-electrolysis system in different power matching modes," in *Hydrogen Energy Progress VIII*, vol. 2, New York, Pergamon Press, 1990, p. 691–700.

[113] V. B. N. B. G. B. A. D. B. A. S. R. O. E. T. V. A. A. A. S. Siracusano, "An electrochemical study of a PEM stack for water electrolysis," *International Journal of Hydrogen Energy,* vol. 37, no. 2, p. 1939–1946, January 2012.

[114] Y. F. H. L. Hongqiang Hu, "Hydrogen production in single-chamber tubular microbial electrolysis cells using non-precious-metal catalysts," *International Journal of Hydrogen Energy,* vol. 34, no. 20, p. 8535–8542, October 2009.

[115] M. ,. a. B. E. Douglas F.Call, "High Surface Area Stainless Steel Brushes as Cathodes in Microbial Electrolysis Cells," *Environmental, Science and Technology,* vol. 43, no. 6, p. 2179–2183, 2009.

[116] R. d. J. S. v. S. H.F.A. Verhaart, "Growth rate of a gas bubble during electrolysis in supersaturated liquid," *International Journal of Heat and Mass Transfer,* vol. 23, no. 3, p. 293–299, March 1980.

[117] F. H. M. K. A. M. a. A. S. C. Gabrielli, "Potential drops due to an attached bubble on a gas-evolving electrode," *Journal of ELectrochemistry,* vol. 19, no. 5, pp. 617-629, 1989.

[118] K. T. a. 0. Yoshinari, "Hydrogen-Metal Systems: Electrochemical Reactions (Fundamentals and Applications)," in *Encyclopedia of Materials - Science and Technology*, Elsevier , 2001.

[119] E. Skúlason, *Hydrogen Evolution Reaction: Density Functional Theory,* Nano.DTU and CAMd.

[120] J. C. E. F. M. Richard G. Compton, "Sonoelectrochemical processes: A review," *Electroanalysis,* vol. 9, no. 7, pp. 509-522, April 1997.

[121] A.-M. W. H. H. L. a. P.-L. F. P.Cognet, “Ultrasound in Organic Synthesis,” *Ultrasonics Sonochemistry ,* vol. 7, no. 4, pp. 163-167, 2000.

[122] M. L. a. D. W. T.J.Mason, “Sonoelectrochemistry,” *Ultrasonics,* vol. 28, 1990.

[123] R. C. C.E. Banks, “Ultrasonically enhanced voltammetric analysis and applications: an overview,” *Electroanalysis,* vol. 15, pp. 329-346, 2003.

[124] V. S. M. E. P. B. Y. V. L. G. J. Gonzalez Garcia, “Relevant developements and new insights on sonoelectrochemistry,” *Physics Procedia,* vol. 3, no. 1, pp. 117-124, January 2010.

[125] J. F. a. D. W. R.G. Compton, “Electrode Processes at the surfaces of sonotrodes,” vol. 41, no. 2, pp. 315-320, 1996.

[126] M. D. E. P. B. Y. V. H. L. G. C. a. V. S. Jose Gonzalez Garcia, “Current Topic on Sonoelectrochemistry,” *Ultrasonics,* vol. 50, no. 2, pp. 318-322, 2010.

[127] B. C. F. R. a. E. F.Javier Del Campo, “High frequency Sonoelectrochemical processes: mass transport, thermal and surface effects induced by cavitation in a 500 KHz reactor,” *Ultrasonics Sonochemistry,* vol. 6, no. 4, pp. 189-197, 1999.

[128] E. N. a. J. S. Chun, “effect of ultrasonic vibration on hard chromium plating in a modified self-regulating high speed bath,” *Thin Solid Films,* vol. 120, no. 2, pp. 153-159, October 1984.

[129] H. F. J. V. O. F. A. K.-d. M. C. M. a. J.-L. D. J. Reisse, “Sonoelectrochemistry in aqueous electrolyte: A new type of sonoelectroreactor,” *Electrochimica Acta,* vol. 39, no. 1, pp. 37-39, January 1994.

[130] F. M. D. N. W. a. R. G. C. John C. Eklund, “Voltammetry in the presence of ultrasound: a novel sono-electrode geometry,” *Electrochimica Acta,* vol. 41, no. 9, pp. 1541-1547, 1996.

[131] J. P. L. S. S. P. T. J. M. a. J. -Y. H. B. G. Pollet, “A novel angular geometry for the sonochemical silver recovery process at cylinder electrodes,” *Ultrasonics Sonochemistry ,* vol. 10, no. 4-5, pp. 217-222, 2003.

[132] F. M. a. R. G. Compton, “Electrochemistry in the presence of ultrasound: the need for bipotentiostatic control in sonovoltammetric experiments,” *Ultrasonics Sonochemistry,* vol. 3, no. 2, pp. S131-S134, 1996.

[133] D. a. R. C. F.Marken, “Eonoelectrochemistry in highly resistive media; Mass trasport effect,” *Electroanalysis ,* vol. 10, pp. 562-566, 1998.

[134] N. V. R. a. R. G. C. Craig E. Banks, “Sonoelectrochemistry in acoustically emulsified media,” *Journal Of electroanalytical Chemistry ,* vol. 535, no. 1-2, pp. 41-47, 2002.

[135] C. B. a. C. D. Jiri Klima, “Sonoelectrochemistry: transient cavitation in acetonitrile in the neighborhood of a polarized,” *Journal of Electroanalytical Chemistry,* vol. 399, no. 1-2, pp. 147-155, 1995.

[136] M. S. D. M. ,. P. S. Allen J. Bard, Encyclopedia of Electrochemistry; Electrochemical Engineering, vol. 5, Wiley , 2007.

[137] F. Cataldo, “Effects of ultrasound on the electrolytic conductivity of simple halide,” *Journal of Electroanalytical Chemistry,* vol. 431, no. 1, pp. 61-65, 1997.

[138] H. F. J. R. A. K.-D. Alex Durant, “Sonoelectrochemistry: The effects of ultrasound on organic electrochemical reduction,” *Electrochimica Acta,* vol. 41, no. 2, p. 277–284, 1996.

[139] M. P. F. O. F. C. F. R. F. E. Pier Luigi Gentili, “Synergistic effects in hydrogen production through water sonophotolysis catalyzed by new La2xGa2yIn2(1−x−y)O3 solid solutions,” *International Journal of Hydrogen Energy,* vol. 34, no. 22, p. 9042–9049, November 2009.

[140] K. T. Ngo Le Ngoc, “Ultrasound stimulus effect on hydrogen bonding in networked alumina and polyacrylic acid slurry,” *Ultrasonics Sonochemistry,* vol. 17, no. 1, p. 186–192, 2010.

[141] T. C. C. D. O. F. J. V. J. D. R. W. J. Reisse, “Quantitative sonochemistry,” *Ultrasonics Sonochemistry,* vol. 3, no. 3, pp. S147-S151, November 1996.

[142] J. L. Jongsik Jeong, “Electrochemical oxidation of industrial wastewater with the tube type electrolysis module system,” *Separation and Purification Technology,* vol. 84, p. 35–40, 2012.

[143] M. P. D. H. O. R. C. T. K.S. Agbli, “Multiphysics simulation of a PEM electrolyser: Energetic Macroscopic Representation approach,” *International Journal of Hydrogen Energy,* vol. 36, no. 2, p. 1382–1398, 2011.

[144] J. C. Ganley, “High temperature and pressure alkaline electrolysis,” *International Journal of Hydrogen Energy,* vol. 34, no. 9, p. 3604–3611, May 2009.

[145] D. Y. G. Frank Kreith, Handbook of Energy Efficiency and Renewable Energy, Boca Raton : CRC Press: Taylor and Francis Group, 2007.

[146] W. R. L. Stancy L. Gelhaus, “19. Measurement of The Electrolytic Conductance,” in *Ewing's Analytical Instrumentation Handbook*, Marcel Dekker , 2005.

[147] J. d. P. Peter Atkins, Atkin's Physical Chemistry, Oxford University Press, 2006.

[148] D. R. Lide, “5. Thermochemistry, Electrochemsitry, and Kinetics,” in *CRC Hanbook of Chemistry and Physics* , 87th ed., CRC Press, 2006.

[149] Z. D. C. a. J. J. J. C. K. Qian, “Bubble coverage and bubble resistance using cells with horizontal electrode,” *Journal of applied electrochemistry,* vol. 28, no. 10, pp. 1141-1145, 1998.

[150] N. S. S.K. Mazloomi, “Influencing factors of water electrolysis electrical efficiency,” *Renewable and Sustainable Energy Reviews,* vol. 16, no. 6, p. 4257–4263, August 2012.

[151] A. K. R. M. E. G.-A. John O'M. Bockris, Modern Electrochemistry 2A: Fundamentals of Electrodics, 2nd ed., vol. 2A, New York: Kluwer Academic/Plenum Publishers, 2000.

[152] V. S. a. M. Sangaranarayanan, "Underpotential deposition of metals – Progress and prospects in modelling," *Journal of Chemical Sciences ,* vol. 117, no. 3, p. 207–218, 2005.

[153] ,. Y. M. T. W. M. K. J. S. Yoshiyuki Izaki, "Direct observation of the oxidation nickel in molten carbonate," *Journal of Power Sources,* vol. 75, no. 2, p. 236–243, October 1998.

[154] T. J. O. a. P. Yu, "Pourbaix Diagrams; Nernst Equation," in *Encyclopedia of Materials - Science and Technology*, Elsevier, 2001.

[155] L. Pauling, "15. Oxidation-Reduction Reactions. Electrolysis," in *General Chemistry*, Mineola, Dover Publications, 1988.

[156] B. R. Eggins, "2.2 Potentiometry and Ion-Selective Electrodes: The Nernst Equation," in *Chemical Sensors and Biosensors*, John Wiley & Sons, 2002.

[157] A. D. James Larminie, "2.5.1 The Nernst Equation," in *Fuel Cell Systems Explained* , 2nd ed., west sussex, John Wiley & Sons, 2003.

[158] D. K. A. W. G. S. I.A. Schneider, "Effect of inert gas flow on hydrogen underpotential deposition measurements in polymer electrolyte fuel cells," *Electrochemistry Communications,* vol. 9, no. 7, p. 1607–1612, July 2007.

[159] S. M. Kaplan, Wiley Electrical and Electronics Engineering Dictionary, Hoboken: Wiley - IEEE Press, 2004.

[160] E. M. John Daintith, "Current Density," in *Dictionary of Science*, 6th ed., Market House Books Ltd, 2010.

[161] D. S. D. Berndt, "Batteries," in *Ullmann's Encyclopedia of Industrial Chemistry*, Wiley-VCH, Weinheim, 2005.

[162] L. S. Lerner, "27.6. Joule's law," in *Physics for scientists and engineers* , vol. 2, Sudbury , MA: Jones and Bartlett, 1996.

[163] M. K. L. D. Y. L. Meng Ni, "Energy and exergy analysis of hydrogen production by solid oxide steam electrolyzer plant," *International Journal of Hydrogen Energy,* vol. 32, no. 18, p. 4648–4660, December 2007.

[164] M. Rosen, "Energy and exergy analyses of electrolytic hydrogen production," *International Journal of Hydrogen Energy,* vol. 20, no. 7, p. 547–553, July 1995.

[165] G. L. J. C. Houcheng Zhang, "Evaluation and calculation on the efficiency of a water electrolysis system for hydrogen production," *International Journal of Hydrogen Energy,* vol. 35, no. 20, p. 10851–10858, October 2010.

[166] C. O. J. C. Yingru Zhao, “A new analytical approach to model and evaluate the performance of a class of irreversible fuel cells,” *International Journal of Hydrogen Energy,* vol. 33, no. 15, p. 4161–4170, August 2008.

[167] S. a. O.A.Petrii, “Real Surface Area Measurement in Electrochemistry,” *International Union of Pure and Applied Chemistry ,* vol. 61, no. 5, pp. 711-734, 1991.

[168] G. J. a. Z. Borkowsk, “On the real surface area of smooth solid electrodes,” *Electrochimica Acta,* vol. 42, no. 19, p. 2915–2918, 1997.

[169] M. J. Sparnaay, The electrical double layer, Pergamon Press, 1972.

[170] D. W. K. S. J. T. Anne E. Mauer, “The role of iron in the prevention of nickel electrode deactivation in alkaline electrolysis,” *Electrochimica Acta,* vol. 52, no. 11, p. 3505–3509, 2007.

[171] A. R.M., K. D.W., T. S.J. and G. J.W., “Reactivation of nickel cathodes by dissolved vanadium species during hydrogen evolution in alkaline media,” *Electrochimica Acta,* vol. 47, no. 4, pp. 613-621(9), 2001.

[172] D. K. S. T. J. G. R.M Abouatallah, “Reactivation of nickel cathodes by dissolved vanadium species during hydrogen evolution in alkaline media,” *Electrochimica Acta,* vol. 47, no. 4, p. 613–621, November 2001.

[173] L. a. C.A.C.Sequeira, “10.4. The voltammetric Techniques,” in *Microbial Corrosion: Proceedings of the 2nd EFC Workshop*, The Institute of Materials, 1992.

[174] L.-W. H. C.-W. K. Ming-Yuan Lin, “The effect of magnetic force on hydrogen production efficiency in water electrolysis,” *International Journal of Hydrogen Energy,* vol. 37, no. 2, p. 1311–1320, 2012.

[175] W. J. K. C. J. C. M. R. H. H. P. Jungwon Kim, “Electrolysis of urea and urine for solar hydrogen,” *Catalysis Today,* pp. In Press, Corrected Proof, 2012.

[176] K. S. M. S. P. L. Jaroslaw Milewski, “Chapter 1: Introduction,” in *Advanced Methods of Solid Oxide Fuel Cell Modelling*, London, Springer, 2011.

[177] K. K. Subhash C. Singhal, “Introduction to SOFCs,” in *High Temperature Solid Oxide Fuel Cells; Fundamentals, designs and applications*, Oxford, Elsevier, 2003.

[178] E. Chen, “2.5.2 Bacon (1954, 1969, 1979),” in *Fuel Cell Technology Handbook* , Boca Raton , Florida : CRC Press LLC.

[179] V. S. BAGOTSKY, “Chapter 2: THE LONG HISTORY OF FUEL CELLS,” in *Fuel Cells : solutions and Problems* , Hoboken, John Wiley & Sons, Inc, 2009.

[180] F. S. J.M. Andu´ jar, “Fuel cells: History and updating. A walk along two centuries,” vol. 13, no. 9, pp. 2309-2322, 2009.

[181] J. S. J. X. Shiming Liu, “Effects of surface overpotential at the La1−xSrxCo1−yFeyO3-yttria stabilized zirconia interface in a model solid oxide fuel cell cathode,” *International Journal of Hydrogen Energy,* vol. 33, no. 21, p. 6322–6326, November 2008.

[182] S. J. Pearton, Processing of wide bandgap semiconductor, Norwich : Noyte Publication/William Andrew Publishings , 2000.

[183] G. D. BERRY, “Hydrogen Production: Section 5. Electrolysis of Water and Steam,” in *Encyclopedia of Energy*, San Diego, Elsevier , 2004.